

Universidade de Vigo

Escola Internacional de Doutoramento

Laura Rodríguez Díaz

TESE DE DOUTORAMENTO

*A particle tracking model to analyze
transport in ocean*

Dirixida polos doutores:

Ramón Gómez Gesteira

Francisco José Santos González

2018

“Mención internacional”

Universidade de Vigo, Campus de Ourense, Departamento de Física Aplicada,
Environmental Physics Laboratory (Ephyslab).

Laura Rodríguez Díaz (larodriguez@uvigo.es).

A particle tracking model to analyze transport in ocean.

Ourense, 14 de marzo de 2018.

Universidade de Vigo

Escola Internacional de Doutoramento

Dr. Ramón Gómez Gesteira, catedrático do Departamento de Física Aplicada da Universidade de Vigo e **Dr. Francisco Jose Santos González**:

FAN CONSTAR que o presente traballo, titulado “**A particle tracking model to analyze transport in ocean**”, que presenta Laura Rodríguez Díaz para a obtención do título de DOUTORA POLA UNIVERSIDADE DE VIGO CON MENCIÓN INTERNACIONAL, foi elaborado baixo a súa dirección no programa de doutoramento **Marine Sciences, Technology and Management (Campus do Mar)**.

Ourense, 14 de marzo de 2018.

Os directores da tese doutoral



Dr. Ramón Gómez Gesteira



Dr. Francisco Jose Santos González

Agradecementos/Acknowledgments

Os meus primeiros agradecementos son para Maite e Moncho que me deron a oportunidade de unirme a Ephyslab e empezar esta etapa que por fin chega o seu fin con esta tese doutoral. Dende aquí quero darlles as gracias pola súa paciencia e a súa axuda.

Tamén quero agradecerlle a Fran que como codirector desta tese, axudoume a iniciar esta aventura. Gustaríame estender tamén o meu agradecemento a Inés por todas as horas que me dedicou axudándome a corrixir os artigos que hoxe forman os capítulos desta tese. Algúns días roubándolle as poucas horas libres que tiña, que ata me daba reparo molestala máis, pero ela sempre estivo dispoñible para axudarme en todo o que fixera falta. Moitas gracias.

A miña familia, somos unha piña non hai quen diga o contrario. Se un de nós necesita algo aparecemos o resto en manada para o que faga falta. Cada un de vós aportou o seu grao de area para formarme como a persoa que son hoxe en día. Principalmente, meus pais José Manuel e Marisol que se des viviron para que tanto a min como a miña irmá Rosita non nos faltara de nada. A miña irmá que me deu o seu apoio cando mais me fixo falta. A meus tíos Javi e Manolo, miñas tías Eli e Amelia e a meus primos Víctor e Isa. Teño que incluír nestes agradecementos á familia, a Macu que xa é unha tía máis. Que podo dicir dela se ata me deixou o seu piso para escribir esta tese. Familia, foron moitas horas escoitándome, moitas horas aconsellándome, moitas risas, moitas xuntanzas, bos momentos, outros non tanto pero sempre estivestes o meu lado. Sodes os mellores!. Quérovos!.

A ti meu rei. Xa son dez anos. Quen o ía dicir!. Todo o que vivimos xuntos e o que nos queda por diante. Non teño dúbidas de que será fantástico. Somos un equipo. Moitas grazas por estar o meu lado nos bos momentos pero tamén nos malos. Sen o teu apoio, Rubén non houbera chegado ata aquí.

A Lorena. A miña pichurriña. Máis ca unha amiga. Non recordo un momento importante da miña vida que non compartira contigo. Xunto coa miña irmá somos as tres mosqueiteiras, unhas coidamos das outras. Pode que non nos vexamos tanto como quixéramos pero sei que o deixariades todo por axudarme se vos necesito.

Por ultimo, quero darlle as gracias a todas as persoas que estiveron comigo todos estes anos universitarios. Especialmente a Diego e David cos que empecei a carreira e compartín moi bos momentos. Tamén quero agradecer o resto do grupo Ephyslab Orlando, Alex, Ángel, Curro, Andrés, Nieves... que en maior ou menor medida me axudaron nesta etapa. Como mención especial, quero agradecerlles os membros do laboratorio perico: Marisela, Manolo, Susana, Miki, Xurxo, Santi e Lucía porque sen vós cada día non sería o mesmo. Somos algo ruidosos pero pasámolo moi ben xuntos, entre risas, cartas, serenatas, cenas... Moitas gracias por axudarme cando o necesito e sabedes que sempre poderedes contar comigo.

Este traballo foi financiado pola Xunta de Galicia a través do Plan galego de investigación, innovación e crecemento 2011-2015 (Plan I2C) en colaboración co Campus de Excelencia Internacional Campus do Mar (PRE/2013/474).

Resumen

La circulación oceánica es el movimiento a nivel global de las masas de agua en las cuencas oceánicas. Por un lado, las corrientes oceánicas redistribuyen el calor desde el ecuador hacia las regiones polares y, por otro lado, transportan todo tipo de materias como la basura marina y organismos como nutrientes o larvas desde su origen hasta prácticamente cualquier región del planeta.

La posición de la Tierra respecto al Sol y a la Luna, el viento y las propiedades físicas del agua como la temperatura y la salinidad, son los factores que influyen en la circulación oceánica. En cuanto a la atracción gravitacional que ejerce el Sol y la Luna sobre el planeta Tierra, esta da lugar a las mareas. Este tipo de corrientes ocurren a lo largo de la costa y arrastran una gran cantidad de sedimentos hacia áreas costeras como estuarios. Las mareas tienen una particularidad frente a las otras corrientes marinas, y es que son predecibles debido a que se conoce en profundidad el movimiento y la posición del Sol, la Tierra y la Luna. Por su parte el viento es el factor que afecta en mayor medida a la circulación oceánica. La interacción atmosfera-océano genera la circulación oceánica superficial. El patrón global del viento, integrado por los vientos alisios, los vientos del oeste y los vientos del este, al entrar en contacto con la capa superficial del océano, le transfiere parte de su momento dando lugar a las corrientes superficiales. A su vez, estas corrientes superficiales debidas al viento, se ven afectadas por la fuerza de Coriolis de manera que se mueven hacia la derecha de la dirección del viento en el Hemisferio Norte y hacia la izquierda en el Hemisferio Sur. La fuerza de Coriolis también afecta a los vientos que al entrar en contacto con los océanos generan en ambos hemisferios los giros oceánicos. En total existen cinco grandes giros: dos giros en el océano Atlántico (Norte y Sur), dos en el océano Pacífico (Norte y Sur) y uno en el océano Índico. En cuanto a las propiedades físicas, la radiación solar es el causante de las variaciones de temperatura, salinidad y por tanto de densidad de las masas de agua. Por un lado, el ecuador recibe mayor radiación solar que los polos debido a la curvatura del planeta lo que provoca que la distribución del calor no sea homogénea. Por otro lado, la salinidad se modifica por el ciclo de precipitación-evaporación, por el derretimiento de hielo, la congelación del agua oceánica y la descarga de los ríos ya que todo ello altera el aporte de agua dulce. Cualquier variación en la temperatura y/o salinidad altera la densidad del agua. Cuando el agua profunda se acerca a la región del ecuador empieza a calentarse y a volverse menos densa dando lugar a un movimiento vertical de agua hacia la superficie. Este proceso es conocido como la circulación termohalina. Este tipo de circulación se caracteriza por su lento movimiento pero que ocurre a escala global. Es el responsable de la contribución de los nutrientes necesarios para el desarrollo de la vida en los océanos.

El objetivo de esta tesis es el estudio del transporte de partículas en el océano y su patrón de dispersión a través de simulaciones usando un modelo lagrangiano. Estos modelos utilizan un grupo de partículas virtuales para obtener las trayectorias que seguirían en el océano al ser arrastradas por las corrientes. Para ello la principal variable para ejecutar el

modelo lagrangiano es el campo de velocidades de las corrientes que se obtienen de bases de datos. En concreto en esta tesis hemos usado las bases de datos Simple Ocean Data Assimilation (SODA) o HYbrid Coordinate Ocean Model (HYCOM). Por un lado, de la base de datos SODA hemos usado el campo de velocidades de dos versiones distintas (v. 2.2.4 y v. 2.1.6) las cuales se han aplicado a los casos de estudio de capítulo 3 y del capítulo 5 respectivamente. Esta dos versiones de SODA tienen 40 niveles de profundidad a una resolución horizontal de $0.5^{\circ} \times 0.5^{\circ}$. La diferencia entre ambas reside en la resolución temporal. En el caso de la versión 2.2.4, el periodo de datos disponible es 1871-2010 a escala mensual. En el caso de la versión 2.1.6, el periodo temporal es 1958-2010 a escala de 5 días. Por otro lado, el campo de velocidades de HYCOM tiene datos desde 1992 hasta la actualidad para 40 niveles de profundidad a una resolución horizontal de $1/12^{\circ} \times 1/12^{\circ}$ a escala diaria. Estos datos de HYCOM se utilizaron en los casos de estudio desarrollados en los capítulos 3, 4 y 6.

Como ya hemos mencionado, la característica común a todos los casos particulares desarrollados en esta tesis es que el modelo lagrangiano necesita un campo de velocidades para poder calcular las trayectorias de dispersión de las partículas virtuales. Sin embargo, también son necesarios otros tipos de datos que dependerán del objetivo de cada capítulo. Así, en esta tesis se han utilizado variables como la temperatura superficial del agua (SST) de datos de satélite, la radiancia, datos de viento, de salinidad, de la temperatura de la columna del agua, de las descargas de los ríos y los valores de dos índices de teleconexión: North Atlantic Oscillation (NAO) y Atlantic Multidecadal Oscillation (AMO). En la siguiente tabla se recogen todas estas variables con información de la base de datos de donde se obtuvieron, así como su resolución temporal y espacial y el caso de estudio de esta tesis en el que se utilizaron.

Variable	Base de datos	Resolución espacial	Resolución temporal	Caso de estudio
U, V velocidad	SODA v. 2.2.4	$0.5^{\circ} \times 0.5^{\circ}$	1899-2010	Capítulo 3
U, V velocidad	SODA v. 2.1.6	$0.5^{\circ} \times 0.5^{\circ}$	1958-2008	Capítulo 5
			1996-2009	Capítulo 3
U, V velocidad	HYCOM	$1/12^{\circ} \times 1/12^{\circ}$	1996-2012	Capítulo 4
			1993-2015	Capítulo 6
Índice AMO	NCAR/UCAR	---	1899-2010	Capítulo 3
Índice NAO	NCAR/UCAR	---	1899-2010	Capítulo 3
SST	OISST _{1/4}	$0.25^{\circ} \times 0.25^{\circ}$	1982-2015	Capítulo 6
Radiancia	MODIS	1 Km	2003-2015	Capítulo 6
Viento	CFSR	$0.3^{\circ} \times 0.3^{\circ}$	1982-2015	Capítulo 6

Descarga fluvial	Mississippi	Tarbert Landing station	---	1982-2015	Capítulo 6
	Atchafalaya	Simmesport			
	Salinidad	HYCOM	1/12°x1/12°	1993-2015	Capítulo 6
	Temperatura del agua	HYCOM	1/12°x1/12°	1993-2015	Capítulo 6

Tabla 1. Resumen de los datos usados en esta tesis. La resolución temporal hace referencia a los periodos usados en los diferentes casos de estudio.

Los primeros estudios con modelos lagrangianos se remontan a 1980 (Awaji et al., 1980; Imasato et al., 1980), pero desde entonces se han aplicado a un gran número de temas como el análisis de masas de agua en diferentes océanos (Imasato and Qiu 1987, Döös 1995), la circulación termohalina (Drijfout et al. 1996), o las conexiones interoceánicas (Blanke et al., 2001, van Sebille et al., 2012, Paris et al., 2013); la dispersión y acumulación de basura en torno a los cinco giros oceánicos lo que permite detectar el origen de los mismos y plantear medidas de contención y estrategias de limpieza (Lebreton et al. 2012) e incluso dispersión de basura en regiones concretas y a menor escala (Gomez-Gesteira et al., 1999, Dias et al., 2001, Neumann et al., 2014, Mansui et al., 2015, Politikos et al., 2017); el estudio de la dispersión larval a través de diferentes áreas considerando parámetros biológicos de las especies (Kettle and Haines 2006, Pous et al. 2010, Young et al. 2012, Pacariz et al. 2014) o la dispersión de pequeñas partículas como nutrientes (Chenillat et al. 2015) o microorganismos (Hellweger et al. 2014).

Los estudios desarrollados durante esta tesis doctoral pretenden contribuir al conocimiento previo de la dispersión de partículas en los diferentes océanos usando simulaciones lagrangianas. Para ello se han recogido en este manuscrito estructurado de la siguiente manera:

El capítulo 1 incluye la introducción general. En el primer apartado se describe el objetivo principal de este manuscrito. También recoge información acerca de la circulación oceánica, los principales factores que la influyen, así como una clasificación de la misma. Finalmente se describen los modelos lagrangianos y se aportan ejemplos de estudios previos como contextualización para los casos de investigación desarrollados en el resto de los capítulos.

El capítulo 2 incluye una descripción detallada de todas las bases de datos utilizadas y del modelo lagrangiano desarrollado para hacer las simulaciones de partículas virtuales en cada caso de estudio.

En el capítulo 3 se aplica el modelo lagrangiano para analizar las trayectorias de partículas pasivas, usando el campo de velocidad de la base de datos SODA, con el fin de determinar cambios en la probabilidad de cruzar el océano Atlántico Norte durante el periodo 1899-2010 para las larvas con una vida larval superior a 1 año. Para ello las partículas fueron

liberadas dos veces al año y en cuatro profundidades en el Estrecho de Florida donde la Corriente del Golfo es la principal fuerza impulsora de la dispersión. Los meses de liberación (mayo y octubre) fueron elegidos para que coincidiesen con las épocas de desove de varias especies del área de estudio. Además, se consideró una etapa larval de 18 meses siguiendo el ejemplo de estudios previos. En primer lugar, se compararon los datos de velocidad de SODA con los de HYCOM obteniendo que la baja resolución temporal y espacial de SODA no es un impedimento para utilizar su campo de velocidades en este estudio de dispersión y además la longitud de su serie de datos es una gran ventaja. Los primeros resultados de este capítulo mostraron que las partículas virtuales se dispersaron describiendo las características macroscópicas de la Corriente del Golfo en todas las profundidades y estaciones consideradas salvo en la capa más superficial. Al igual que en estudios previos se detectaron picos de concentración en torno a 33°N y 54.5°N. El análisis del porcentaje de partículas que cruzaron el Atlántico mostró un aumento significativo desde el inicio del siglo 20. Este resultado se relacionó con los cambios en la energía cinética de los remolinos la cual se ha intensificado a lo largo de la trayectoria de la Corriente del Golfo. A mayores el tiempo mínimo de migración para la partícula más rápida en alcanzar el meridiano 25°W fue de 6-7 meses con una tendencia negativa significativa. Estos resultados son comparables a los obtenidos en estudios previos basados en el análisis de la microestructura de los otolitos de las anguilas. La tendencia obtenida para este tiempo mínimo de migración indica que las partículas se están moviendo más rápido que al inicio del siglo 20. Debido a la extensa serie de datos de SODA se han relacionado los resultados con los patrones de teleconexión Oscilación del Atlántico Norte (NAO) y Oscilación Multidecadal del Atlántico (AMO). Sin embargo, no se obtuvieron correlaciones significativas para ninguna de los casos simulados.

En el capítulo 4 se aplica el modelo lagrangiano para determinar si es posible obtener tiempos de migración de la anguila europea similares a los obtenidos del análisis de la microestructura de los otolitos, pero a través de modelos numéricos. Para ello, se ha usado el campo de velocidades de HYCOM para el periodo 1996-2012 y se han considerado diferentes estrategias de migración: (i) migración pasiva donde las partículas son horizontalmente advectadas por las corrientes a una profundidad fija; (ii) migración pasiva horizontalmente con una migración vertical diaria (DVM) donde las partículas se fijaron a 50m durante la noche y a 300m durante el día; y (iii) migración con camino aleatorio (random walk) añadido que puede ser totalmente aleatorio (fully random) o localmente orientado siguiendo las corrientes (downstream swimming). Inicialmente las partículas se liberaron en el mes de abril en un área en el Mar de los Sargazos para que coincidiera con el pico y área de desove de la anguila europea. Además, se consideró una etapa larval de 18 meses siguiendo el ejemplo de estudios previos y grabando la posición de las partículas cada día. Con el fin de calcular los tiempos de migración y comparar con estudios previos, se consideraron los meridianos 20°W y 15°W como las líneas de meta de la migración transatlántica de la anguilla. Los primeros resultados, considerando el meridiano 20°W mostraron dos picos de concentración consistentes con estudios previos y debido a la circulación oceánica del océano Atlántico Norte. Además, se analizó el origen de esas

partículas que alcanzaron el meridiano 20°W y se observó que aquellas liberadas en la parte más al oeste de la región del Mar de los Sargazos alcanzaron preferentemente las costas del norte de Europa mientras que las liberadas más al este alcanzaron las costas del norte de África. El siguiente paso fue analizar la dependencia de la migración con la profundidad. Para ello se consideraron ambas líneas de meta y las estrategias de migración (i) pasiva y (ii) DVM. Para el primer caso (i) el principal resultado obtenido es que la migración más rápida (243 días para el meridiano 15°W y 201 días para el meridiano 20°W) se alcanzó cuando las partículas son liberadas en la capa superficial. Para el segundo caso (ii) la estrategia de migración vertical diaria implicó un aumento del tiempo de migración lo cual demuestra su ineficiencia. Finalmente se analizó si el efecto del movimiento activo de las larvas reducía el tiempo de migración. Para ello se consideró el meridiano 15°W y la migración con camino aleatorio fully random y downstream swimming. En el primer caso el tiempo mínimo de migración obtenido fue 20 días más largo que en el caso base (243 días). En el segundo caso se obtuvieron varias realizaciones donde el tiempo mínimo de migración fue más corto que en el caso base (204 días) lo que implica que esta estrategia (downstream swimming) es la más eficiente de las consideradas en este estudio. A mayores estos valores de aproximadamente 7 meses son comparables a los obtenidos del estudio de la microestructura de los otolitos de la anguila.

En el capítulo 5 se aplica el modelo lagrangiano para analizar la conectividad entre las poblaciones de la langosta espinosa *Panulirus penicillatus* en el océano Índico durante el periodo 1958-2008. Para ello se ha utilizado el campo de velocidades de la base de datos SODA y se han considerado las partículas virtuales como trazadores pasivos horizontalmente advectados por las corrientes oceánicas. Puesto que el estudio se centra en una especie concreta fue necesario incluir características biológicas de la misma como la migración vertical diurna (DVM) que varía desde los 100 m de profundidad durante el día hasta los 5 m durante la noche, la duración larval de 9 meses y los periodos de desove que ocurren de noviembre a marzo en el hemisferio sur y de marzo a septiembre en el hemisferio norte. Las áreas de lanzamiento (Mar Rojo, Madagascar, Maldivas, Aceh y Java) se eligieron de acuerdo a las descritas por [Abullah et al. \(2014\)](#) en su estudio genético sobre la misma especie, con el fin de determinar si sus resultados podrían ser explicados por la conectividad debida a la circulación oceánica del océano Índico. El primer paso en este capítulo fue estudiar en profundidad y a escala estacional las corrientes en la capa superficial y a 100 m. En general se ha observado que las corrientes a 100 m no tienen unas variaciones estacionales tan marcadas como la capa superficial y son más débiles. En cuanto a la dispersión de partículas desde cada área de lanzamiento el primer resultado obtenido es que el área del Mar Rojo está completamente aislada del resto de áreas puesto que el Estrecho de Mandeb actúa como barrera impidiendo la dispersión de los trazadores pasivos. De hecho, el 93% de las partículas liberadas en el Mar Rojo quedaron retenidas. En cuanto a las partículas liberadas en Madagascar, ninguna pudo alcanzar el resto de áreas consideradas en el estudio. Esto fue debido a la circulación oceánica alrededor de la isla que obligó a las partículas a dispersarse en dirección opuesta a la posición del resto de las áreas. El caso de Java es parecido al de Madagascar. Java tiene un alto porcentaje de retención (35.2%) debido a la respuesta de

las corrientes a los vientos del monzón. A mayores las partículas liberadas en esta área no alcanza ninguna otra de las consideradas dentro del océano Índico puesto que la mayoría son dispersadas hacia Australia y el océano Pacífico. Los casos de Maldivas y Aceh produjeron resultados diferentes. En cuando a las partículas liberadas en Maldivas, el 28.2% fue capaz de llegar a Aceh y <5% a Java a través de una dispersión directa. Por otro lado, en estudios previos se encontró una conexión genética entre Maldivas y Madagascar que en este capítulo sólo se pudo explicar a través de una migración por etapas entre ambas áreas de la siguiente manera: desde Maldivas a las islas Seychelles y de estas hasta Madagascar. En cuanto a las partículas liberadas en Aceh, estas fueron capaces de llegar a Maldivas (13.1%) y Java (5.7%). Finalmente se encontraron dos tendencias positivas significativas que indicaron que las partículas que llegaron hasta Aceh desde Maldivas aumentaron un 6.5% por década y las que alcanzaron Java desde Aceh aumentaron un 1.4% por década.

En el capítulo 6 se aplica el modelo lagrangiano para analizar las corrientes en la región de la plataforma continental de Texas-Luisiana influenciada por la pluma de los ríos Atchafalaya y Mississippi. El objetivo principal es encontrar una explicación plausible al patrón de temperatura detectado en esa área el cual muestra una tendencia al enfriamiento, $-0.5\text{ }^{\circ}\text{C}$ por década durante los meses de noviembre a febrero, muy diferente al calentamiento observado en las áreas oceánicas adyacentes. Estas diferencias entre costa y océano pueden deberse a diferentes forzamientos entre ellos la entrada de agua dulce debido a la descarga de los ríos. Para comprobar si la pluma formada por los ríos Atchafalaya y Mississippi es el forzamiento que modula la temperatura en esta región del Golfo de Mexico, se liberaron partículas durante el periodo 1993-2015 en la desembocadura de cada río diariamente durante esos meses de enfriamiento. Se permitió que las partículas se dispersaran durante 90 días grabando su posición a diario. Las partículas, desde cada desembocadura, se dispersaron mayoritariamente en dirección oeste. Con el fin de detectar cambios en las corrientes en esta área se calculó la diferencia en el porcentaje de ocupación entre dos periodos de 10 años (2005-2015 y 1993-2003) y se observó que el transporte en dirección oeste se redujo debido al descenso del aporte de agua dulce por parte de los ríos. La descarga de los ríos se redujo $1.265\text{ m}^3\text{s}^{-1}$ por década durante los meses de enfriamiento (noviembre-febrero) para el periodo 1993-2015. Este resultado unido a la reducción de los vientos del este, explica la pérdida de flotabilidad en el área ocupada por la pluma que forman los ríos Atchafalaya y Mississippi. La flotabilidad fue calculada usando los datos de temperatura y salinidad de HYCOM para detectar cambios en la estratificación de la columna de agua. Esta pérdida de flotabilidad provoca a su vez una mayor mezcla vertical que favorece la entrada de agua más fría en la capa de mezcla creando esa franja de menor temperatura detectada a lo largo de la plataforma continental de Texas-Luisiana.

Como cierre a esta tesis, se incluye un apartado final en el que se recogen las conclusiones generales de la misma.

Abstract

The ocean circulation is the global movement of water, which occurs in the ocean basins. On the one hand, the ocean currents distribute heat from the equator to the poles and on the other hand, they transport all kind of materials like debris and organisms like nutrients or larvae from their origin to almost anywhere in the planet. Ocean circulation can be classified into density driven deep ocean circulation and wind driven surface ocean circulation. The first one act like a conveyor belt moving warm surface water and forcing an upward movement of cold water. The second one is due to the effect of the global wind pattern and originate oceanic gyres at both hemispheres.

The aim of this thesis is to contribute to the knowledge of the drift of particles into different ocean currents using lagrangian simulations. Lagrangian models are a useful tool to analyze pathways in the ocean by using a set of virtual particles, which are transported by the ocean currents. The main variable to run the lagrangian model is the velocity field provided by different databases. Here, we will use velocity data from SODA and HYCOM along with other variables like sea surface temperature (SST), radiance, Mississippi and Atchafalaya river discharge, wind, salinity, water temperature and the teleconnection NAO and AMO indices.

The changes in the probability of larvae crossing the North Atlantic Ocean over the period 1899-2010 was analyzed in the first study case using lagrangian trajectories of passive tracers. Virtual particles were released in the Strait of Florida where the main driving forcing is the Gulf Stream. An increase in the chances of crossing the Atlantic was obtained considering species with long planktonic larvae duration. In addition, a minimum travel period around 6-7 months was calculated. The increase was related with the intensification of the changes in eddy kinetic energy along the Gulf Stream path.

In the second study case, the minimum migration duration of the European eel was analyzed in order to obtain similar results than those from the microstructure of eel otoliths, which are around 7-9 months. The lagrangian simulations were tested under different conditions like spatial and time resolution, depth, release area and also initial distribution. Overall, the results showed faster migration when increasing the resolution of the model and also when decreasing the release depth. In addition, the fastest migration was obtained when the virtual particles were passive tracers horizontally advected by the currents. However, the migration strategy with downstream swimming resulted in faster migrations.

The continuous displacement of water masses due to ocean currents contributes to larval dispersion allowing connectivity among populations from different geographic areas. In the third study case, the connectivity among five populations (Red Sea, Madagascar, Maldives, Java and Aceh) of spiny lobster *Panulirus penicillatus* in the Indian Ocean was analyzed using numerical simulations of passive tracers over the period 1858-2008. Biological parameters of the spiny lobster as release depth and areas, larval duration and spawning season were selected and used in the lagrangian model. The results showed how the *Panulirus penicilatus* larvae moved among different regions in the Indian Ocean, favoring the genetic connectivity among them. Specially, two significant positive trends

were obtained for particles that reached Aceh from Maldives and for particles that reached Java from Aceh.

Finally, the sea surface temperature pattern in the Texas-Louisiana shelf as well as the influence of the plume formed by the Mississippi-Atchafalaya (MA) river system on it were investigated. The lagrangian model was one of the methods applied in this study case to analyze the current in the area under scope. Passive particles were released at each river mouth over the period 1993-2015. The results showed a buoyancy lost in the area occupied by the MA river system turbid plume due to the reduction of westward transport of freshwater, the reduction of river discharge and the decrease in the frequency of easterly winds. This buoyancy lost causes a higher vertical mixing favoring the entrainment of colder water, which explain the coastal SST decrease in the area under study.

In conclusion, this thesis not only proves the interest of lagrangian models to describe transport of larvae into ocean currents or connectivity among different areas but also proves that they constitute a complementary tool for climate studies.

Table of contents

Chapter 1: Introduction

1.1. The aim	1
1.2. Ocean circulation	1
1.2.1. Influential factors in ocean circulation	2
1.2.1.1. <i>The Earth-Sun-Moon interaction</i>	2
1.2.1.2. <i>The wind</i>	2
1.2.1.3. <i>Physical properties</i>	3
1.2.2. Classification	4
1.2.2.1. <i>Density driven deep ocean circulation</i>	4
1.2.2.2. <i>Wind driven surface ocean circulation</i>	5
1.3. Lagrangian models	6

Chapter 2: Data and Methodology

2.1. Data	10
2.1.1. Oceanographic database and River discharge data.....	10
2.1.1.1. <i>Simple Ocean Data Assimilation (SODA)</i>	10
2.1.1.2. <i>HYbrid Coordinate Ocean Model (HYCOM)</i>	10
2.1.1.3. <i>Daily 1/4° Optimum Interpolation SST (OISST_{1/4})</i>	11
2.1.1.4. <i>Moderate Resolution Imaging Spectroradiometer (MODIS)</i>	11
2.1.1.5. <i>River discharge data</i>	11
2.1.2. Atmospheric database	12
2.1.2.1. <i>Climate Forecast System Reanalysis (CFSR)</i>	12
2.1.3. Climate indices	12
2.1.3.1. <i>The North Atlantic Oscillation (NAO)</i>	12
2.1.3.2. <i>The Atlantic Multidecadal Oscillation (AMO)</i>	13
2.2. Eddy Kinetic energy (EKE)	14
2.3. Particle tracking model	14
2.3.1. Initial release configurations	14
2.3.2. Interpolation process	15

Chapter 3: Has the probability of larvae crossing the North Atlantic changed over the twentieth century?

3.1. Motivation----- 20
 3.1.1. The North Atlantic Ocean ----- 20

3.2. Material and methods ----- 22
 3.2.1. Data ----- 22
 3.2.2. Lagrangian models ----- 23
 3.2.3. Selecting the release point ----- 25
 3.2.4. Dependence on the number of particles ----- 37

3.3. Results and discussion ----- 28
 3.3.1. Comparison with a high resolution model ----- 28
 3.3.2. Distribution of particles ----- 32
 3.3.3. Particles crossing the Atlantic ----- 34
 3.3.4. Variability and trends ----- 36
 3.3.5. Minimum travel period ----- 37
 3.3.6. Eddy kinetic energy ----- 38
 3.3.7. Influence of atmospheric forcing ----- 39

3.4. Conclusions ----- 39

Chapter 4: The migration time of European eel

4.1. Motivation----- 42

4.2. Material and methods ----- 43
 3.2.1. Data ----- 43
 3.2.2. Lagrangian models ----- 43

4.3. Results and discussion ----- 46
 3.3.1. Characterization of larval migration ----- 46
 3.3.2. Dependence on depth ----- 49
 3.3.3. Effect of the initial distribution ----- 50
 3.3.4. Random walk effect ----- 51

4.4. Conclusions ----- 53

Chapter 5: On the connectivity of *Panulirus penicillatus* populations in the Indian Ocean

5.1. Motivation----- 55
 5.1.1. The Indian Ocean ----- 55

5.2. Material and methods ----- 57
 5.2.1. Data ----- 57
 5.2.2. Lagrangian models ----- 57

5.3. Results and discussion ----- 59
 5.3.1. Indian Ocean surface current system ----- 59
 5.3.2. Red Sea ----- 61
 5.3.3. Madagascar ----- 61
 5.3.4. Java ----- 62
 5.3.5. Maldives ----- 63
 5.3.6. Aceh ----- 64

5.4. Conclusions ----- 66

Chapter 6: On the use of Lagrangian to identify drivers in SST warming

6.1. Motivation----- 68
 6.1.1. The Mississippi-Atchafalaya River System ----- 69

6.2. Material and methods ----- 71
 6.2.1. Data ----- 71
 6.2.2. Lagrangian models ----- 71

6.3. Results and discussion ----- 73

6.4. Conclusions ----- 83

General Conclusions ----- 85

Acronym and Abbreviation List ----- 88

List of Figures ----- 91

List of Tables ----- 99

Bibliography ----- 102

Chapter 1

Introduction

1.1. The aim

It is a well-known fact that both ocean and atmospheric currents influence the Earth's climate and can play a key role in climate change (Trenberth and Caron, 2001). Ocean currents, which are the main topic of this thesis, move large water masses from equatorial to Polar Regions, which redistributes the heat content and affects the global climate (Trenberth and Caron, 2001; Lavin et al., 2003). However, this is not the only ability of ocean currents since they can also transport all kind of materials and organisms from their origin to practically any region. One of the most remarkable examples is the Gulf Stream, which influences the climate of northwestern Europe, making it much more temperate than any other region at the same latitude (Sutton and Hodson, 2005). In addition, The Gulf Stream also influences the flora and fauna of the places it passes through due to transport of plankton, fish larvae, and nutrients (Kettle and Haines, 2006; Bonhommeau et al., 2008; Bonhommeau et al., 2009a, b; Young et al., 2012). This is possible since the continuous movement of the water allows the temperature to stabilize and distributes nutrients (Lavin et al., 2003; Williams et al., 2011) and plankton (Steinberg et al., 2002) in the ocean and seas. This water movement also allows the development of organisms and the transfer of larvae from spawning areas to habitats where adult fishes are found (Marancik et al., 2011).

Lagrangian models along with ocean currents velocity fields (from databases like SODA or HYCOM) let us simulate the trajectories of dispersion of thousands of particles in the ocean and study their dispersal patterns.

Therefore, the lagrangian model used in the numerical simulations will be described in Chapter 2. In Chapter 3 and 4, the lagrangian model will be applied to analyze the dispersion of particles in the North Atlantic Ocean where the Gulf Stream is the main driving force, taking into account different initial conditions at each chapter. Since the Gulf Stream is not the only current capable of transporting particles, in Chapter 5, the lagrangian model will be applied to study larval connectivity in the Indian Ocean. Finally, in Chapter 6, the lagrangian model will be applied to find a plausible explanation to the SST pattern observed along the Texas-Louisiana Shelf.

1.2. Ocean Circulation

The ocean circulation can be defined like the global movement of water, which occurs in the ocean basins. These movement of water constitutes the ocean currents, which plays

an important role in the climate since store and distribute heat, microorganisms like nutrients and freshwater all over the world. Therefore, any change that modifies the ocean circulation will alter drastically the global climate. In this section it will be broadly explained the factors, which determine the ocean circulation and a classification will be presented.

1.2.1. Influential factors in ocean circulation.

The ocean currents are influenced by several factors like the interaction between Earth, the Sun and the Moon, the wind and also by physical properties.

1.2.1.1. The Earth-Sun-Moon interaction

The gravitational attraction of the Sun and the Moon over Earth's ocean causes waves which directions vary according to high and low tides. This movement is known as tidal current and it occurs along the coast (see Figure 1.1). Tidal currents can be responsible of the accumulation of sediments in areas like bays or estuaries. The main differences with ocean current is that tidal currents are predictable since the movement and position of the mentioned celestial bodies is well known. New and full phase of the Moon causes stronger tidal current velocities than the other phases. In addition, tidal currents are stronger when the Earth and the Moon are in their closest position.

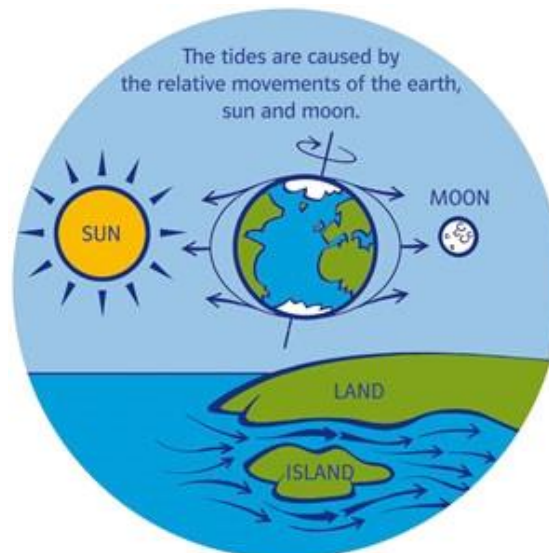


Figure 1.1. Sketch of tidal current. Source: "Generating Marine Electricity: Transitioning From Subsidies to Commercial Financing" submitted by Alexander Mcphail to The water blog: <http://blogs.worldbank.org/water/energy/category/tags/tidal>.

1.2.1.2. The wind

The wind is the main factor that influences the ocean circulation. When the wind blows over the sea surface, it transfers part of its momentum to the ocean establishing the currents. Therefore, it exists a direct relationship between the speed of the wind and the

strength of the surface currents through the wind stress, which is the frictional force between the wind and the sea-surface. This circulation is known as surface wind driven circulation.

These wind driven currents are affected by the rotation of the Earth through the Coriolis force and by the topography. Due to the Coriolis force, wind driven current are diverted to the right of the wind direction in the Northern Hemisphere. The opposite occurs in the Southern Hemisphere where currents are diverted to the left. This effect is not observed at the Equator because there the Coriolis force is equal to zero. The topography, the bathymetry and the location of the coasts, can interact with wind induced currents. An example of the effect of topography on wind driven currents is the coastal upwelling. This phenomenon consists in a vertical movement of deep water to replace the surface water transport moving away from coast. For example, this occurs at the Northern Hemisphere when northerly wind flows parallel to the coast and the ocean is on the right, causing offshore surface currents.

1.2.1.3. Physical properties

The ocean circulation is also driven by the variations in its physical properties like the temperature, the salinity and therefore, its density. Changes in these variables are linked to the solar radiation.

On the one hand, temperature alterations are due to the fluxes of heat between the atmosphere and the sea. The Earth does not absorb these fluxes of heat homogenously due its curvature. Thus, the poles receive less solar radiation than the equator. In addition, its obliquity causes that the heating varies with the seasons.

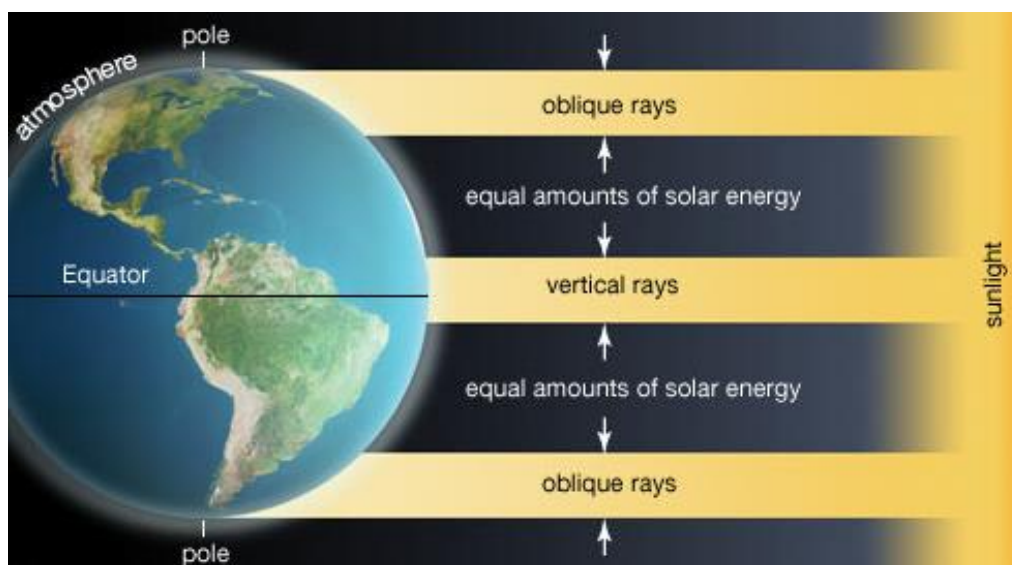


Figure 1.2. Solar radiation. The equator receives more radiation than the poles because the vertical incidence of the sun's rays. Copyrights: 2008 Encyclopaedia Britannica, Inc.

On the other hand, salinity is modified by the freshwater input into the ocean, which is caused by precipitation, evaporation and the melting of ice. Salinity varies with latitude since the highest values are found between 20° and 30° both south and north of the Equator where evaporation exceed the precipitation. At the remaining latitudes, salinity values are lower because the balance between precipitation and evaporation is opposite to the previous one. In addition, the low salinity around the poles is intensified by the melting of ice and by the freezing of seawater. Near coast, salinity varies due to the inputs of freshwater from surface runoffs and river discharges. Overall, salinity decreases in those areas affected by river plume especially, when the discharge is very high as happens with the Amazon or the Congo River.

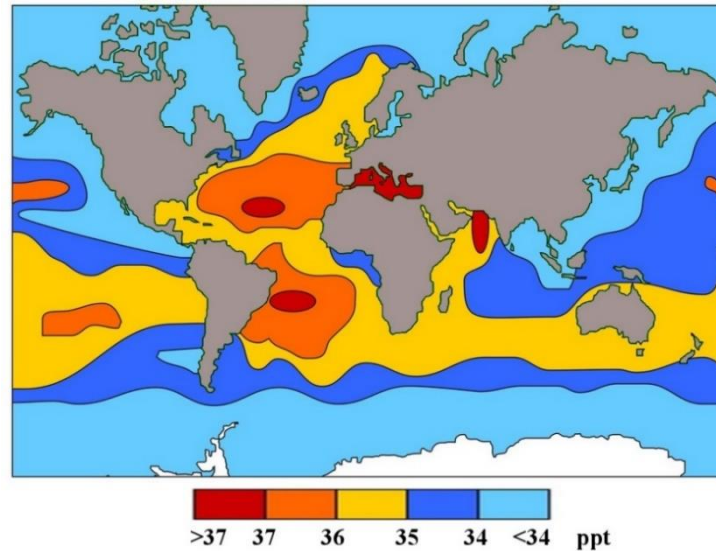


Figure 1.3. Global salinity map. This figure was adapted from the website: www.sciencelearn.org.nz.

Any modification in temperature and salinity disrupts the density of the water. If surface water is denser than subsurface water, sinks of denser surface water occurs. Thus, a vertical movement of water appears as consequences of modifications in the content of salt and/or heat. This circulation is known as thermohaline circulation.

1.2.2. Classification

1.2.2.1. Density driven deep ocean circulation

This circulation moves slowly but transports a massive current around the globe. It acts like a conveyor belt (see Figure 1.4) moving warm less dense surface water and forcing an upward movement of cold denser deep water.

This circulation starts at latitudes close to the North Pole to move southward to the Antarctica flowing between South America and Africa. At this point, the current gets cold again intensifying the conveyor belt. Then, it splits into two branches. One branch moves into the Indian Ocean and the other one moves into the Pacific Ocean. These branches of cold water warm up becoming into a surface water due to the reduction of their density. That is the reason why this circulation is known as density-driven. Finally, the surface

warm water flows south and westward to continue its circulation until it returns to the North Atlantic Ocean to complete the cycle and start over.



Figure 1.4. Sketch of the conveyor belt. Blue lines represent cold deep water while red line represents warm surface water. This figure was obtained from the NOAA’s National Ocean service website: https://oceanservice.noaa.gov/education/tutorial_currents/05conveyor2.html.

1.2.2.2. Wind driven surface ocean circulation

The surface ocean circulation is driven by the global wind pattern that is formed by the Trade winds, the Westerlies and the Easterlies. Figure 1.5 shows a sketch of the global wind pattern.

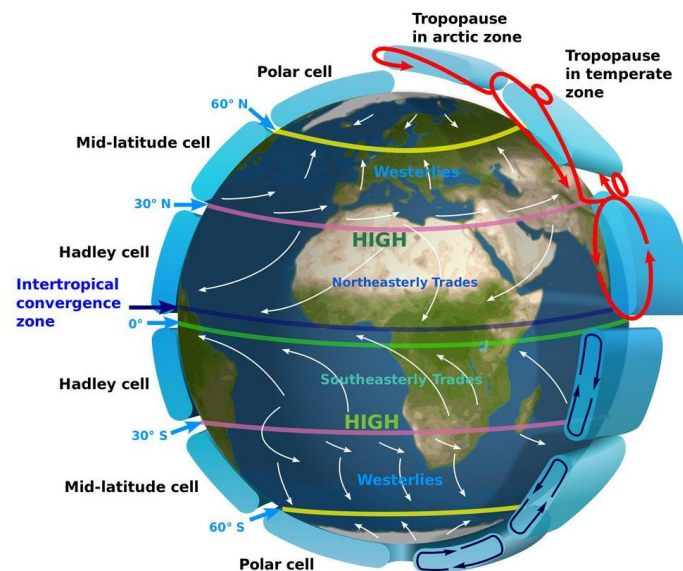


Figure 1.5. The global wind pattern. Source: This figure was obtained from the National Geographic’s website: <https://www.nationalgeographic.org/photo/prevaling-winds/>. Copyrights: “Prevailing winds” by Kaidor is licensed under CC BY-SA 3.0.

On the one hand, the Trade winds are those blowing from areas of high pressure to areas of low pressure towards the Equator. Winds from both hemispheres converge at the Equator where the temperature is higher. This convergence is known as the Intertropical

Convergence zone. Just like the surface currents, the Coriolis force modifies these Trade winds. Thus, Trade winds are known as Southeasterly trades and Northeasterly trades depending on the direction where the winds come from. On the other hand, westerlies occur at mid latitudes at both hemispheres while the air moves northward or southward respectively. The polar easterlies occur when the westerlies get closer to the poles.

Finally, the combination of Trade winds and westerlies originates a circular wind pattern, which flows clockwise in the Northern Hemisphere. The opposite occurs in the Southern Hemisphere. As a result, these clock and counterclock wind flows originate ocean currents at both hemispheres named gyres. In concrete, there are five major gyres in the ocean: the North and South Atlantic gyres, the North and South Pacific gyres and the Indian Ocean gyre. Figures 1.6 shows a map with the five gyres and its related currents.

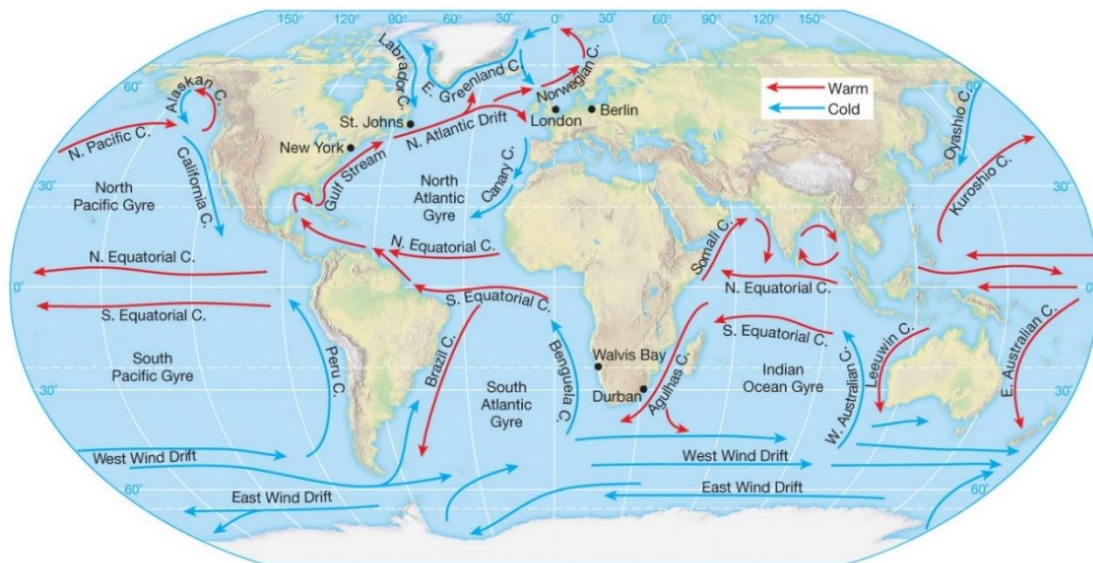


Figure 1.6. Map of the ocean gyres and its associated currents. The color indicates warm currents (red) and cold currents (blue). Copyrights: 2013 Pearson Education, Inc.

1.3. Lagrangian models

Lagrangian studies can be related to lagrangian drifters or lagrangian models. The first kind uses drifters (see Figure 1.7), which allow studying surface velocity of ocean currents, transport or variables like salinity or temperature. For example, some studies employ them to obtain patterns of ocean circulation in different regions as the Indian Ocean (Shenoi et al., 1999), the Bay of Biscay (Charria et al., 2013) or the Mozambique Channel (Hancke et al., 2014).

However, here we will focus on lagrangian models. These models allow obtaining pathways in the ocean by using a set of virtual particles. These particles trajectories are calculated using velocity fields generally from Ocean General Circulation Models (OGCMs). This kind of analysis date back to 1980s (Awaji et al., 1980; Imasato et al., 1980).

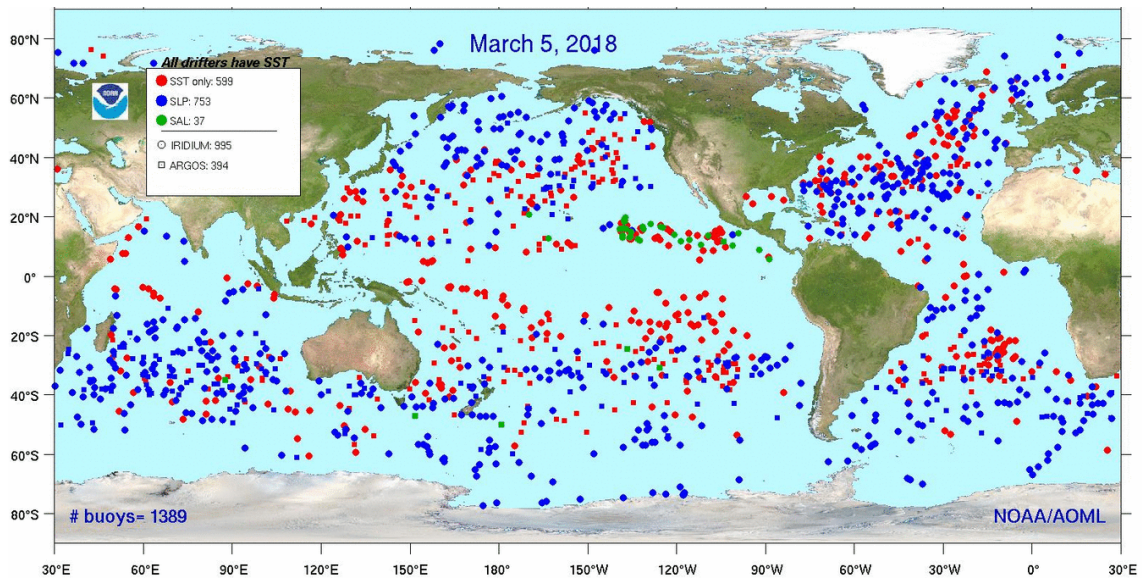


Figure 1.7. Map with the locations of worldwide drifters on March 5th, 2018. This picture was downloaded from The Global Drifter Program's website: http://www.aoml.noaa.gov/phod/dac/gdp_maps.php.

Pioneer studies with Lagrangian models were limited to numerical simulation at basin scale. For example, [Imasato and Qiu \(1987\)](#) analyzed water masses on the Kuroshio Current; [Böning and Cox \(1988\)](#) studied the transport of particles in a subtropical gyre; [Fujio and Imasato \(1991\)](#) focused on the analysis of deep circulation in the Pacific Ocean and [Kawase \(1993\)](#) on the abyssal circulation in the North Atlantic Ocean. Several years later, the first studies of particle dispersal including wind observation and global ocean circulation models were published. For example, [Döös \(1995\)](#) applied the model to study water masses in the Southern Ocean; [Drijf et al. \(1996\)](#) focused on the conveyor belt; and [Blanke and Raynaud \(1997\)](#) studied the annual-mean structure of the Pacific Equatorial Undercurrent (EUC).

In the last decades, the Lagrangian models were applied to a wide variety of topics. Several studies have considered these models to obtain ocean circulation patterns and transport routes using Lagrangian trajectories of particles in different regions as: the Atlantic Ocean ([Sala et al., 2013, 2016](#)), the Indian Ocean ([Bull and van Sebille, 2016](#)); to understand the global circulation and interoceanic connections ([Blanke et al., 2001](#); [van Sebille et al., 2012](#); [Paris et al., 2013](#)); to study circulation pattern in small areas as rias ([Montero et al. 1996, 1999](#)); or even to analyze river plumes ([Osadchiev and Zavialov, 2013](#); [Kubryakov et al., 2016](#); [Allahdadi et al., 2017](#));

Dispersal of particles has been also considered to analyze more specific topics as the dynamics of marine debris and the possible concentration areas. These recent studies used Lagrangian particle tracking models to simulate transport and accumulation of floating debris in the world ocean showing the formation of five accumulation zones mainly in the northern ([Lebreton et al., 2012](#)). These areas were also detected by direct measurements showing that Lagrangian models can constitute a useful tool to improve

waste management or to guide monitoring and clean-up strategies. Other studies analyzed floating litter particles in specific regions as: the Mediterranean Sea (Mansui et al., 2015; Politikos et al., 2017); the southern North Sea (Neumann et al., 2014); the Adriatic Sea (Carlson et al., 2017); the UK Shelf Seas (Elliot et al., 1992) or even at small scale as the Ria de Aveiro Lagoon (Portugal) (Dias et al., 2001), or A Coruña and Vigo Rias (NW Spain) (Gomez-Gesteira et al., 1999),

Lagrangian studies have also focused on larval dispersal across different areas. For example, Pous et al. (2010) investigated how the circulation in the South-Western Indian Ocean affects the spawning areas of tropical eels. Gargano et al. (2017) used lagrangian simulations to analyze dispersal between spawning and nursery areas of the mollusk *Mullus barbatus* in the Mediterranean Sea. Chiswell and Booth (2017) focused on the study of the long larval life of the lobster *Jasus edwardsii* around Australia. Hsu et al. (2017) studied the larval transport of Japanese eel in relation with the Pacific North Equatorial Current. Dispersal is an important factor in the distribution and population dynamics of different species because it is related to the connectivity between marine populations (Cowen and Sponaugle, 2009; McClain and Hardy, 2010).

Several studies have also focused on larval dispersal over the North Atlantic Ocean even targeting the same ecological phenomena like the estimation of the migration of eel larvae (Kettle and Haines, 2006; Bonhommeau et al. 2009a, b; Pacariz et al., 2014). Others have been carried out in specific areas of the North Atlantic. For example, Young et al. (2012) studied the distance of dispersion of seven deep-sea species from three release areas near the Straits of Florida using realistic biological data. They found that most larvae are retained in the same geographic areas as the adult habitat within the Gulf of Mexico/Caribbean Sea region. Nevertheless, larvae released in the northern Gulf of Mexico were capable of reaching the mid-Atlantic during a drifting period lasting from 7 to 14 months. More recently, Blanke et al. (2012) studied the effect of the spatial and temporal model resolution on the estimation of European eel larval migration duration and Etter and Bower (2015) used a Lagrangian model to present a first approximation of how larvae disperse near the sea floor across the continental slope in the western North Atlantic.

Other topics where Lagrangian models have been recently applied are the tracking of small tracers like microorganisms (Hellweger et al., 2014), nutrients (Chenillat et al., 2015) or oil spill (Elliot et al. 1992; Balseiro et al., 2003; Kim et al., 2014) among others. Finally, the reader is referred to van Sebille et al., (2018) for a more complete description of the study cases using Lagrangian models.

Chapter 2

Data and Methodology

The aim of this chapter is to describe the particle tracking model developed to analyze the dispersion of particles in ocean currents as well as the data necessary to apply the model to each case.

2.1. Data

2.1.1 Oceanographic databases and River discharge data

2.1.1.1. Simple Ocean Data Assimilation (SODA)

SODA is a reanalysis database with several versions (Carton et al., 2005; Carton and Giese, 2008). Version 2.2.4 and version 2.1.6 were used in this document to carry out different numerical simulations (Chapter 3 and 5 respectively). SODA uses an ocean model based on Parallel Ocean Program physics (Carton et al., 2000a, b). The database includes several variables but only meridional and zonal velocity components were used in the present study. Data were downloaded from the website: <http://sodasrer.tamu.edu/>.

SODA v.2.2.4 data covers the period 1871-2010 at monthly scale. However, in the present document the period was limited to 1899-2010. The resolution of the output variables is $0.5^{\circ} \times 0.5^{\circ} \times 40$ levels ranging from 5 to 5,375 m with a 10 m spacing near surface and 250 m near bottom.

SODA v.2.1.6 data covers the period 1958-2008 with a timescale of 5 days and with the same resolution as the previous version.

2.1.1.2. HYbrid Coordinate Ocean Model (HYCOM)

HYCOM + Navy Ocean Data Assimilation (NCODA) Global $1/12^{\circ}$ version GLBu0.08 contains several experiments that covers the period from 1992 to nowadays (Cummings, 2005; Cummings and Smedstad, 2013). HYCOM GLBu0.08 data were used to carry out different numerical simulations (Chapter 3, 4 and 6). The database includes several variables but only meridional and zonal velocity components, salinity and water temperature were used depending on the goal of each study case. Data were download from the website: <http://hycom.org/data/glb0pt08>. The resolution of the output variables from the global version of HYCOM is $1/12^{\circ} \times 1/12^{\circ} \times 40$ levels ranging from 0 to 5,000 m at daily scale.

2.1.1.3. Daily $\frac{1}{4}^\circ$ Optimum Interpolation SST (OISST $_{1/4}$)

SST data were obtained from $\frac{1}{4}^\circ$ daily Optimum Interpolation Sea Surface Temperature database version 2 (OISST $_{1/4}$) (Reynolds et al., 2007). Data were downloaded from the NASA Ocean Color website: <http://oceancolor.gsfc.nasa.gov>.

The database combines in situ data from ships and buoys and satellite data to construct a regular global grid by means of a special form of kriging called Optimal Interpolation. This procedure retains large-scale correlation structures and allows assimilating very sparse data coverage (Reynolds, 2009; Reynolds and Chelton, 2010).

Data from the Advanced Very High Resolution Radiometer (AVHRR) sensor was used because it provides an uninterrupted SST data since March 1981 (Casey et al., 2010) with a spatial resolution of $0.25^\circ \times 0.25^\circ$. Daily files for the Northwestern area of the Gulf of Mexico ($86-98^\circ\text{W}$, $26-31^\circ\text{N}$) were retrieved over the period 1982-2015 to be used in Chapter 6. Daily SST values were averaged at monthly scale. Monthly anomalies were obtained subtracting for each month, the mean monthly SST over the whole period (e.g. the mean of all Januaries from 1982-2015) from the monthly SST value (e.g. January 1982). Finally, linear SST trends were calculated using monthly anomalies.

2.1.1.4. Moderate Resolution Imaging Spectroradiometer (MODIS)

MODIS is a sensor located on board the Aqua and Terra satellites, providing information about several parameters related to ocean dynamic. MODIS data were downloaded from the NASA Ocean Color web site (<http://oceancolor.gsfc.nasa.gov>). Normalized water-leaving radiance (nLw) with a standard resolution of 1 km from 2003 to 2015 was selected to develop the study described in the Chapter 6 of this thesis. Although MODIS allows selecting several normalized water-leaving radiances to analyze plume dynamic, the band centered on 645 nm was used because its low penetration into the water, avoiding the overestimation of turbidity caused by upwelling blooms or bottom influence (Chen et al., 2007). In addition, a turbid threshold of $0.25 \text{ mW cm}^{-2} \mu\text{m}^{-1} \text{ sr}^{-1}$ was obtained as the most suitable to differentiate the area influenced by turbid plume from the surrounding ocean water following the methodology applied by Fernández-Nóvoa et al. (2015).

2.1.1.5. River discharge data

Daily runoff data for Mississippi and Atchafalaya Rivers were obtained from gauging stations operated by the US Army Corps of Engineers (<http://rivergages.mvr.usace.army.mil/WaterControl/new/layout.cfm>) to use in the Chapter 6 of this thesis. In particular, river discharge data were retrieved at Tarbert Landing station for Mississippi and at Simmesport for Atchafalaya River (Figure 6.1, green dots). Daily data over the period 1982-2015 were averaged at monthly scale.

2.1.2. Atmospheric database

2.1.2.1. Climate Forecast System Reanalysis (CFSR)

CFSR is a global, high resolution coupled atmosphere-ocean-land surface-sea ice system developed by NOAA's National Centers of Environmental Prediction (Saha et al., 2010). CFSR includes several variables. However, only wind data was downloaded from the website (<http://rda.ucar.edu/pub/cfsr.html>).

The spatial resolution of wind data is $0.3^{\circ} \times 0.3^{\circ}$ from January 1982 to April 2011 and $0.2^{\circ} \times 0.2^{\circ}$ from then on. Data from the latter period were interpolated on a $0.3^{\circ} \times 0.3^{\circ}$ grid to use a common resolution over the whole period. Wind data are provided at a reference height of 10 m with a time resolution of 6 h. Data was daily averaged for each pixel.

2.1.3. Climate indices

The correlation with the main teleconnection patterns which influence the North Atlantic Ocean was analyzed in *Chapter 3*. Thus, the North Atlantic Oscillation (NAO) index and the Atlantic Multidecadal Oscillation (AMO) index were downloaded from the website of the National Center for Atmospheric Research (NCAR) / University Corporation for Atmospheric Research (UCAR), Climate Data Guide (<https://climatedataguide.ucar.edu/climate-data>).

2.1.3.1. The North Atlantic Oscillation (NAO)

NAO is the most influencing teleconnection pattern over the North Atlantic. The NAO index was calculated as the difference of normalized sea level pressure (SLP) between two locations: one in Portugal and the other one in Iceland (Hurrell, 1995). NAO data cover the period 1899-2010 at monthly scale. NAO pattern has two phases (Figure 2.1A and 2.1B). The positive one is associated with a reinforcement of the gradient between the two locations mentioned above whilst the negative one is associated with a weakening of the gradient. The positive phase of NAO is associated with moderate and rainy winters over northern Europe, dry winter over southern Europe, stronger than average winds from the west over mid latitudes, cold winter over northern Canada and moderate and rainy winter over eastern USA. During the negative phase of NAO, these conditions reverse.

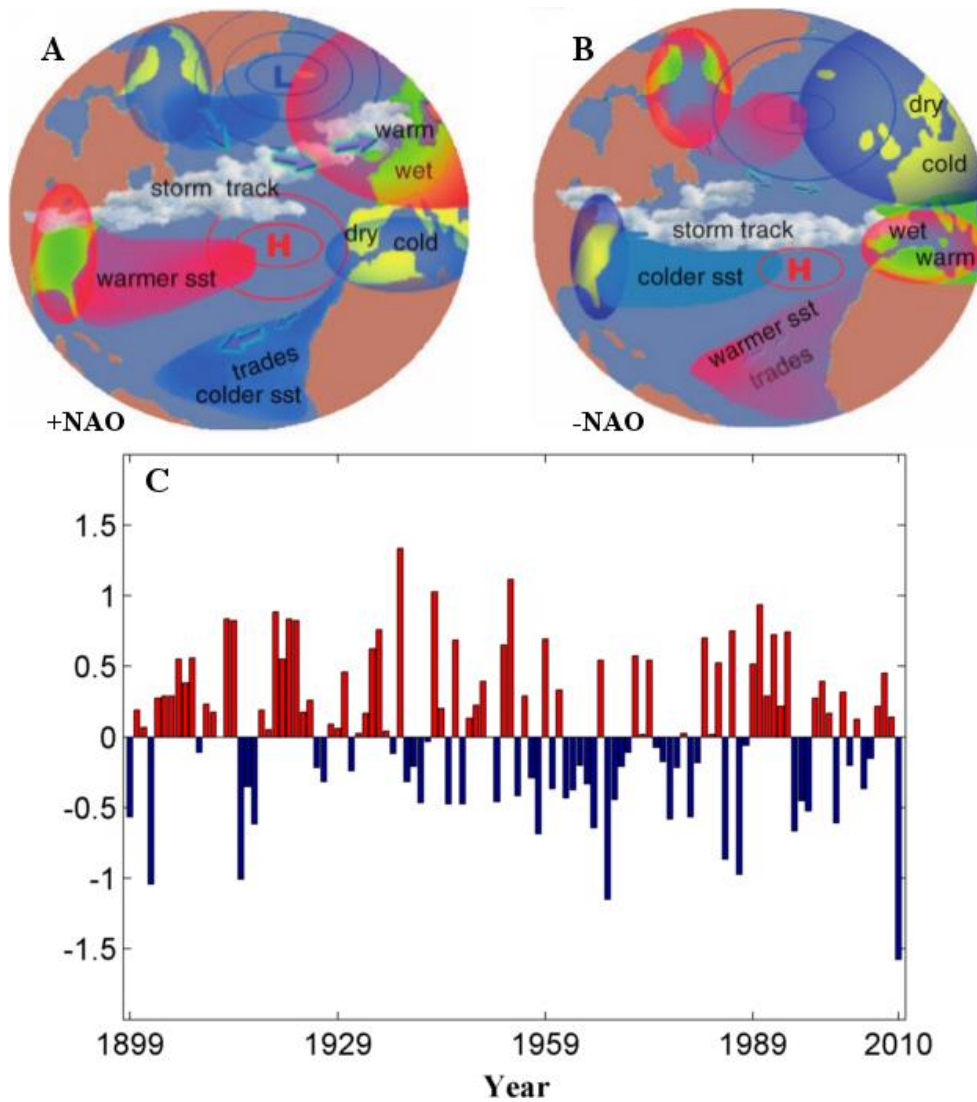


Figure 2.1. Sketch of the NAO phases and the annual index. (A) and (B) was obtained from [Bojariu and Gimeno, 2003](#). Source: Reprinted from Earth-Science Reviews, Vol. 63 Issues 1-2, Bojariu, R. and Gimeno, L. Predictability and numerical modelling of the North Atlantic Oscillation, 145-168, Copyright (2018). (C) The annual index of NAO is calculated using the monthly data for the period 1899-2010 downloaded from the website: (<https://climatedataguide.ucar.edu/climate-data>).

2.1.3.2. The Atlantic Multidecadal Oscillation (AMO)

The AMO index is calculated as the average anomaly of sea surface temperature (SST) over the North Atlantic Ocean ([Enfield et al., 2001](#)). AMO data covers the period 1899-2010 at monthly scale.

Several studies have shown the influence of AMO at global and regional scale ([Polyakov and Johnson, 2000](#); [Chylek et al., 2006](#); 2014, [Muller et al., 2013](#); [Kawada et al., 2013](#)). However, there are discrepancies when establishing the duration of AMO's cycle ([Timmermann et al., 1998](#); [Kerr, 2000](#); [Dima and Lohmann, 2007](#)).

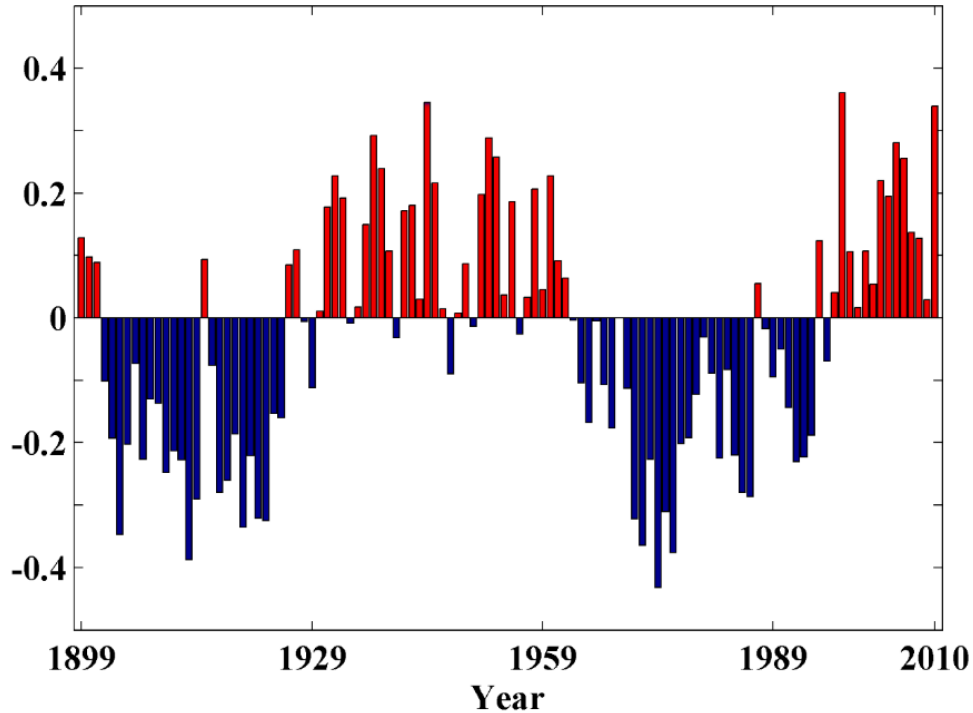


Figure 2.2. Annual index of AMO. The index is calculated using the monthly data for the period 1899-2010 downloaded from the website: (<https://climatedataguide.ucar.edu/climate-data>).

2.2. Eddy kinetic energy (EKE)

Previous studies centered in the Atlantic Ocean (Menard, 1983; Heywood et al., 1994; White and Heywood, 1995; Hakkinen and Rhines, 2009) reported that EKE can be used to identify major currents paths and their changes. Thus, EKE was evaluated in *Chapter 3* and *4*. Surface EKE was computed as the sum of the variance of meridional and zonal velocity components.

$$EKE = (u')^2 + (v')^2$$

$$u' = u - \bar{u}$$

$$v' = v - \bar{v}$$

Finally, trends are calculated at each pixel as the slope of the linear regression of the variable (including EKE) versus time. The Spearman rank correlation coefficient is used to analyze the confidence limit of trends due to its robustness to deviations from linearity and its resistance to the influence of outliers.

2.3. Particle tracking model

2.3.1. Initial release configurations

The particle tracking model is designed to analyze the dispersion of particles in ocean currents starting from different initial release configurations which depend on the cases

under study. In fact, the initial release of particles can be classified based on the spatial or the time configuration.

Regarding the spatial configuration, the initial release of particles can be as follows:

- Release at a point: At this case, particles are released at a fixed point centered at the grid pixel. The size of the grid depends on the resolution of the database used at each study case.
- Release at a polygonal area: In this case, particles are released inside a polygonal area, not necessarily regular, whose shape and size depend on the study case.

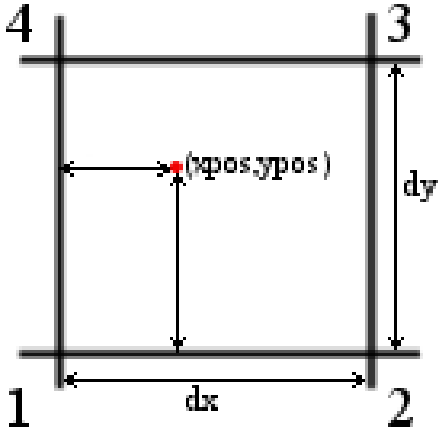
Regarding the temporal configuration, the release of particles can be of two different ways:

- Instantaneous release: At this case, all particles are released at the same instant.
- Periodic release: In this case, particles are released periodically. The number of releases and the interval between releases ($t_{release}$) depend on the case. In addition, the lagrangian model can implement, during periodic release simulations, another temporal variable named flying time (t_{flying}) which determine the period of time in which the particle remains active and can be disperse. For example, let us consider a 3-months simulation where particles are released daily during the first two months with a flying time of 30 days. In this case, particles released on day one remain active until day 30 when they are stopped. In the same way, particles released on day two remain active until day 31 when they are stopped. Finally, particles released on day 61 are stopped on day 90.

2.3.2. Interpolation process

Each velocity component, obtained from the database, is characterized by three indices (i,j,k) that determine the grid point. However, when a particle is located at a certain point (both in time and in space), neither the time nor the position coincide with the actual time and node at which the velocity fields from the database were recorded. Therefore, some interpolation process must be carried out both in time and in space.

Regarding the interpolation in space, the first step is identified the vertical grid point as the nearest node in the vertical. Then, the value of the horizontal components of velocity is calculated by bilinear interpolation considering the nearest four nodes in XY plane:



$$dxn = \frac{xpos - lon(node)}{dx}$$

$$dyn = \frac{ypos - lat(node)}{dy}$$

$$0 < dxn, dyn < 1$$

$$dx * dy = \text{pixel size}$$

The values of V_x, V_y velocity at each node are used to calculate the value of the horizontal components of velocity at $(xpos, ypos)$ as follows:

$$V_x^1 = V_x(indx, indy)$$

$$V_x^2 = V_x(indx + 1, indy)$$

$$V_x^3 = V_x(indx + 1, indy + 1)$$

$$V_x^4 = V_x(indx, indy + 1)$$

$$V_y^1 = V_y(indx, indy)$$

$$V_y^2 = V_y(indx + 1, indy)$$

$$V_y^3 = V_y(indx + 1, indy + 1)$$

$$V_y^4 = V_y(indx, indy + 1)$$

Thus, the velocity at the desired point is:

$$V_x = (1 - dxn)(1 - dyn)V_x^1 + dxn(1 - dyn)V_x^2 + dxn \, dyn V_x^3 + (1 - dxn)dynV_x^4$$

$$V_y = (1 - dxn)(1 - dyn)V_y^1 + dxn(1 - dyn)V_y^2 + dxn \, dyn V_y^3 + (1 - dxn)dynV_y^4$$

Regarding the interpolation in time, the velocity is calculated following the next procedure. When the simulation is at a given instant t and velocities were recorded at instant t_a and t_b ($t_b < t < t_a$), then velocity at t is calculated as a weighted mean of those instants, being the weights inversely proportional to the distance between the present time (t) and the instants when velocities were recorded:

$$V(t) = \frac{t_a - t}{\Delta t_{rec}} V_b + \frac{t - t_b}{\Delta t_{rec}} V_a$$

where the subscript b refers to the last record before instant t , a to the next record after instant t and $\Delta t_{rec} = t_a - t_b$ is the time interval between successive records. It should be noted that when $t = t_a(t_b)$ then $V(t)$ is equal to $V_{a(b)}$ and in the middle point $t = \frac{t_a + t_b}{2}$ the interpolated velocity $V(t)$, is equal to the mean value: $V(t) = \frac{V_a + V_b}{2}$.

Once the velocity components are interpolated following this protocol for each particle, which is located at an arbitrary position in time and space (x, y, t) , the position of the particle evolves following the expressions:

$$x(t + \Delta t) = x(t) + V_x \Delta t \quad (2.2)$$

$$y(t + \Delta t) = y(t) + V_y \Delta t \quad (2.3)$$

Here V_x and V_y refer to the velocity in the X and Y direction and Δt is a variable time step different at every instant during computation.

On the one hand, Δt can be chosen by the user (manual value) or calculated automatically taking into account both components of velocity at every instant and meeting the Courant-Friedrichs-Lewy (CFL) criterion (Courant et al., 1928, 1967) previously used in other lagrangian model Pacariz et al., (2014). The criterion is based on the fact that the time step must be smaller than the time spent by a particle to go over the grid point. The next equation is used to calculate the value of Δt automatically:

$$\Delta t = \frac{d_x}{V_{max}} * C$$

where d_x is the size of the pixel, V_{max} is the maximum of the velocity and $C < 1$ is a constant to meet the CFL criterion.

On the other hand, V_x and V_y have two terms: V^A and V^R . The term V^A (the advective velocity) is the mean term directly estimated from the velocity field provided by the database (used in each study case), and interpolated as described above. The term V^R is the turbulent or fluctuating term, in such a way than previous equations (2.2 and 2.3) become:

$$x(t + \Delta t) = x(t) + V_x^A \Delta t + V_x^R \Delta t \quad (2.4)$$

$$y(t + \Delta t) = y(t) + V_y^A \Delta t + V_y^R \Delta t \quad (2.5)$$

In this study, the fluctuating term is assumed to depend indirectly on the advective velocity as $v^R = \xi v^A$ (Gomez-Gesteira et al., 1999; Diaz et al., 2008). Thus, the previous equations (2.4 and 2.5) become:

$$x(t + \Delta t) = x(t) + (1 + \xi) V_x^A \Delta t \quad (2.6)$$

$$y(t + \Delta t) = y(t) + (1 + \xi) V_y^A \Delta t \quad (2.7)$$

where ξ is a white noise factor which limits depend on the random walk movement considered in each study case. Two cases of random walk were considered:

1. Fully random movement. Here ξ is a white noise with zero mean and bounded in the interval $\left[\frac{-\xi_{max}}{2}, \frac{\xi_{max}}{2} \right]$. Noise should be different and uncorrelated for each particle, time instant and direction (X and Y).

2. Downstream swimming. Here ξ is a white noise bounded in the interval $[0, \xi_{max}]$ and uncorrelated for each particle and instant but not for every direction. Basically, if a particle suffers an advective velocity $V^A = V_x^A i + V_y^A j$, the velocity experienced by that particle is $V = (1 + \xi)(V_x^A i + V_y^A j)$, with $\xi > 0$. Thus, the particle always swims downstream with a velocity in the same direction as the advective velocity but with a modulus slightly higher.

It should be noted that in general the random term must be considerably smaller than the advective one. As a rule of thumb, the amplitude of noise should not surpass 25% of the advective component $\xi_{max} \leq 0.25$.

Chapter 3

Has the probability of larvae crossing the North Atlantic changed over the twentieth century?

3.1. Motivation

The primary focus of this chapter is trans-Atlantic migration, across the North Atlantic, with the goal of the characterization of trends associated with long-term changes in ocean currents in particular from the beginning of the twentieth century (1899-2010) which is the longest available data series. Thus, the particle tracking model described in *Chapter 2* is applied to simulate the dispersion of passive tracers that mimic the main features of drifting species like the planktonic larval duration (PLD) which determines the length of larval life and spawning season (Rodríguez-Díaz et al., submitted manuscript, 2018). The EKE of the area under study is also evaluated since it is an aspect to take into account on the dispersion of particles in ocean currents. In addition, previous studies (Menard, 1983; Heywood et al., 1994; White and Heywood, 1995; Hakkinen and Rhines, 2009) reported that EKE can be used to identify major currents paths and their changes.

3.1.1. The North Atlantic Ocean

The area selected for this study ranges from 0.25°N to 80°N and from 0.25°W to 100.75°W , covering the entire North Atlantic Ocean (see Figure 3.1A). In this area, all the particles are tracked from the Straits of Florida (white square, Figure 3.1B).

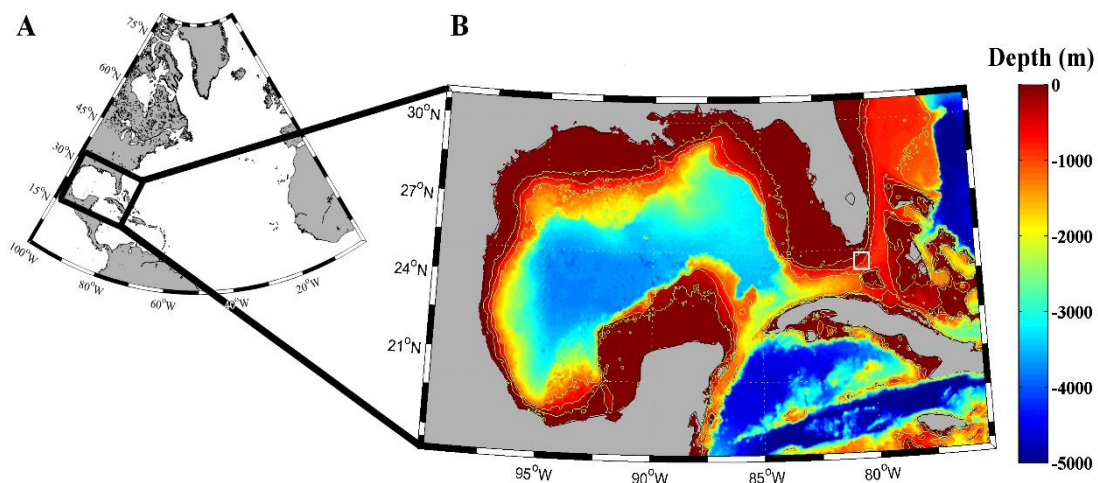


Figure 3.1. Area under study. (A) Location of the study area. (B) The color map shows the bathymetry of the Gulf of Mexico and the Straits of Florida. White square represents the release area and green lines correspond to the 100, 500 and 1,000 m isobaths.

The main ocean currents affecting the study are those belonging to the subtropical gyre of the North Atlantic Ocean (Figure 3.2). This oceanic gyre is composed of the North Equatorial Current (that emerges from north of the Cape Verde Islands to move west into the Caribbean Sea), the Antilles Current (that joins the Florida Current feed on the Loop Current formed for the water inside the Gulf of Mexico). The Gulf Stream emerges from the Straits of Florida and flows northward to Cape Hatteras, where it continues away from the continent. At approximately 50°W, the Gulf Stream divides into two main branches. The largest is known as the North Atlantic Current, which reaches the west coast of Europe and later turns north. The second branch turns southeastward to form the Azores, Portugal and the Canary Current to finally return and circulate into the subtropical gyre (Cornillon, 1992; Tomczak and Godfrey, 2003; Bowditch, 2017). The volume of water transported by the Gulf Stream is considerable with an average of 31 Sv in the Straits of Florida area and reaching peaks of 150 Sv around 65 °W (1 Sv $\approx 10^6$ m³ s⁻¹) (Brown et al., 2001; Tomczak and Godfrey, 2003). The fastest speeds (1.4 – 2 m s⁻¹) are located at the surface decreasing to around 0.2 m s⁻¹ near 1000 m (Richardson, 2001; Lillibridge and Mariano, 2012). The Gulf Stream, which is one of the strongest western boundary currents, plays an important role in the distribution of larvae from the Straits of Florida, allowing dispersion of several species across the North Atlantic Ocean from the west coast to the east coast.

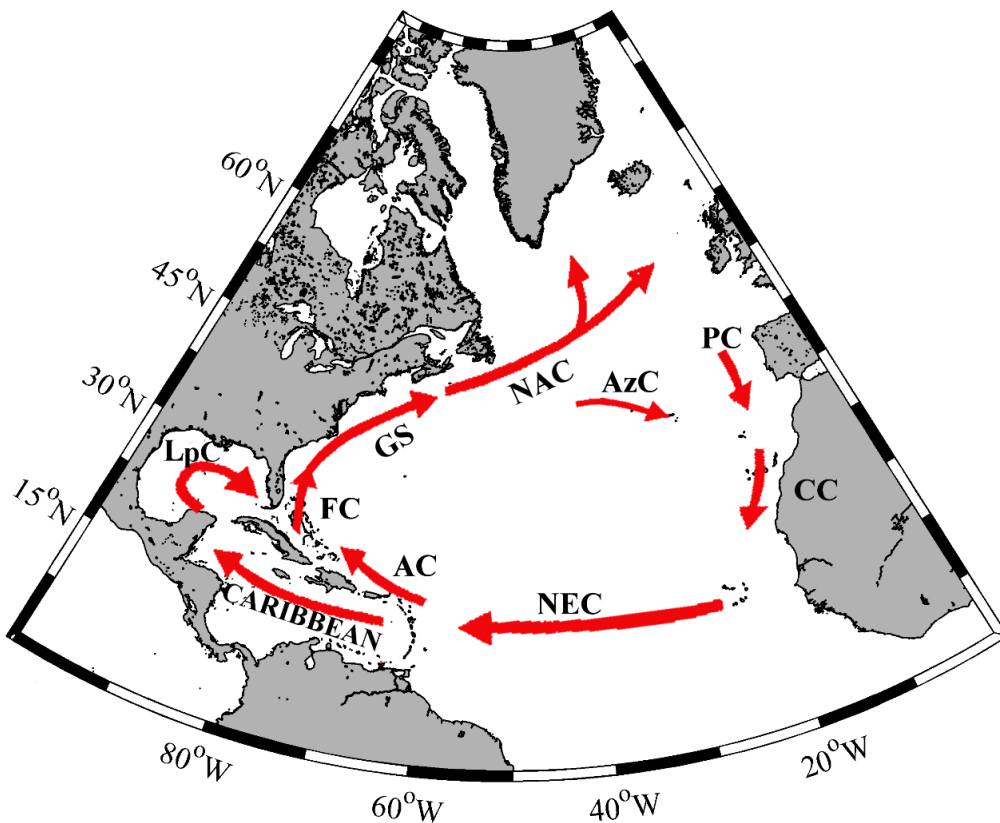


Figure 3.2. Subtropical gyre of the North Atlantic Ocean. Abbreviations refer to North Equatorial Current (NEC), Antilles Current (AC), Florida Current (FC), Loop Current (LpC), Gulf Stream (GS), North Atlantic Current (NAC), Azores Current (AzC), Portugal Current (PC) and Canary Current (CC).

3.2. Material and methods

3.2.1 Data

In *Chapter 2*, it was explained in detail the data used in the present study. In this section, only a summary is presented in table 3.1.

DATA	OBSERVATION	SOURCE
U, V velocity	Period 1899-2010. Data from 4 levels: 5, 35, 70 and 100 m	SODA version 2.2.4
U, V velocity	Period 1996-2009. Data at surface layer	HYCOM GLBu0.08 expt_19.1
AMO index	Calculated as the average anomaly of SST over the North Atlantic Ocean.	NCAR/UCAR
NAO index	Calculated as the difference of normalized SLP between one location in Portugal and another in Iceland.	NCAR/UCAR
EKE	Calculated as the sum of the variance of U and V over the period 1899-2010.	It was used the velocity data from SODA version 2.2.4

Table 3.1. Summary of data used in the study. Additional information is included in the observation column and the data source.

Velocity data from SODA have been previously used in several studies published during the last years over the Atlantic region, proving to be a really useful tool. In a recent work, [Tett et al., \(2014\)](#) compared in situ observations with six different ocean reanalysis to reproduce the circulation in the North Atlantic (Atlantic Meridional Overturning Circulation (AMOC)) over the period 1960-2007. They found that SODA was the best reanalysis to assess the North Atlantic circulation since it was able to reproduce the observed circulation paths and the magnitude of transport. [Gordon and Giulivi \(2014\)](#) used the latitudinal velocity component from SODA to study the water vapor flux

between the North Atlantic subtropical sea and the atmosphere. [Hakkinen et al., \(2011\)](#) used SODA to investigate the circulation in the subtropical and subpolar region of the Atlantic. [Schott et al., \(2009\)](#) applied SODA to study the Labrador Sea convection and the deep water in the subpolar region of the North.

The use of velocity components from SODA v.2.2.4 in the present study provide an important advantage due to the long period of available data, which covers more than a century, which allows investigating long-term trends. Although it is not the objective of the present study, general patterns and its change over such long time can be used, for example, to analyze implications of climate change over the past century. On the other hand, the low spatial and temporal resolution of SODA data can be a source of uncertainty. In fact, previous studies have suggested that the resolution of oceanographic data can influence the results in a Lagrangian simulation by affecting the modelled dispersal paths. Flow fields from a finer horizontal resolution model can have stronger mean currents and more small-scale features, which can lead to more complicated trajectories ([Blanke et al., 2012](#); [Putman and He, 2013](#); [Qin et al. 2014](#)).

To analyze this possible uncertainty, results from SODA and a high-resolution database (HYCOM) are compared over an overlapping time period (1996–2009) through three test:

- i. The overall dispersion pattern is calculated from the final position of particles after 18 months from the release date. Patterns are calculated for every month, depth and compared between both models.
- ii. Comparing the percentage of particles that crossed the 25°W meridian after 18 months from the release date. Results from both models are fitted to a straight line $y_i = ax_i$, where y_i is the percentage of particles that crossed the 25°W meridian calculated with SODA for year i and x_i is the same but calculated with HYCOM. This method allows identifying if SODA underestimates the migration obtained from a high resolution model like HYCOM. A value of the slope a close to 1 would indicate that the dispersal provided by both models is similar.

3.2.2. Lagrangian model

The particle tracking model described in *Chapter 2* is applied to the dispersion of larvae in the North Atlantic Ocean to track passive particles from water surrounding the American continent to those around Europe since the beginning of the twentieth century (1899-2010). Particles are released twice a year (May and October) for each year of the studied period at four different depths (5, 35, 70, 100 m) covering from near surface to the upper part of the mean permanent thermocline. Table 3.2 summarizes the initial conditions considered in our simulations.

Previous studies (Young et al., 2012) compared dispersal distance for larvae released above and below the thermocline over the same area of study, concluding that larvae drifting in the upper water column disperse significantly greater distances. In our case, particles (larvae) behave like passive tracers (i.e. they move with the currents). In addition, they do not undergo chemical or biological processes such as mortality. Mortality is a biological parameter specific to each species, and it was excluded because the study is not focused on any specific species. A previous study (Bonhommeau et al., 2009a) implemented the diel vertical migration (DVM) where particles were located at different depths during daylight and night-time also around the same area under study. Their results showed that this strategy was inefficient with an overall increasing in migration time. Thus, no vertical movements were considered in the present study.

Release dates (May and October) were chosen to coincide with the main spawning period of several species in the area of study like for example the gastropod *Bathinertia naticoidea* and the worm *Lamelibrachia luymeri* whose spawning season is in May or the bivalve *Bathymodiolus childressi* and the asteroid *Sclerasteria tanneri* whose spawning season is in October (Young et al., 2012).

PLD is a key parameter in the analysis of larval dispersal, but it can be difficult to estimate. Several studies of different species in the Gulf of Mexico and the Straits of Florida reported larval stages lasting for more than 1 year (Yeung et al., 2000; Arellano and Young, 2009; Morris et al., 2010). Previous research carried out in the Sargasso Sea (Bonhommeau et al., 2009a), which is in the vicinity of our release point, consider a period of 1.5 years in their numerical experiments. This value is adopted in the present study since our goal is to reproduce trans-Atlantic migrations from the western to the eastern coast for species with a long PLD, typically higher than 1 year.

CONDITION	VALUE	OBSERVATIONS
Release area	80.836°W 24.574°N	Straits of Florida
Depths (m)	5 35 70 100	From near surface to mean permanent thermocline (Young et al., 2012)
Release date	May October	Main spawning period for several species (Young et al., 2012)
Duration of each simulation	1.5 year	Bonhommeau et al., 2009a
Release type	Instantaneous	

Number of releases	1	At each depth and release date which means a total of 8 releases
Number of particles	5,000	Initially released at each depth and release date
t_{rec}	5 days	
Δt	1 day	Manual value
dx^0	0	All particles are released at the same point
Randomness	full	
Constant of randomness	0.25	
Vertical migration	No	Bonhommeau et al., (2009 a, b)
Mortality	No	Cowen et al., (2000) Hare et al., (2002)

Table 3.2. Initial conditions. Summary of the conditions used to run the simulations.

3.2.3. Selecting the release point

To analyze trans-Atlantic migrations across the North Atlantic, the ideal initial location to release particles in the Lagrangian model is firstly determined. Thus, several simulations are carried out considering ten points inside the Gulf of Mexico (Figure 3.3). This initial investigation allows analyzing the total particles that are able to leave this semi-enclosed area depending on the particular location of the point. Particles are released at four depths (5, 35, 70 and 100 m) twice a year (May and October) over the period 1899-2010. The number of particles released at the beginning of each numerical experiment is 5000 and the duration of each simulation is 1.5 years.

The percentage of particles that are able to leave the Gulf of Mexico is calculated considering those particles crossing the 80.5°W meridian (black line Figure 3.3A). Particles released in the innermost points of the area (west of 90°W) and in the point located further north, reach a success of leaving the Gulf of Mexico lower than 50% for all simulations. On the other hand, the percentage of successful particles crossing the 80.5°W meridian, increases as the location of the release point is closer to the Strait of Florida.

Taking into account these results, the initial release point to analyze trans-Atlantic migration is centered at 80.836°W, 24.574°N in a 56x56 km area (Strait of Florida) for the rest of the study (white square, Figure 3.1B).

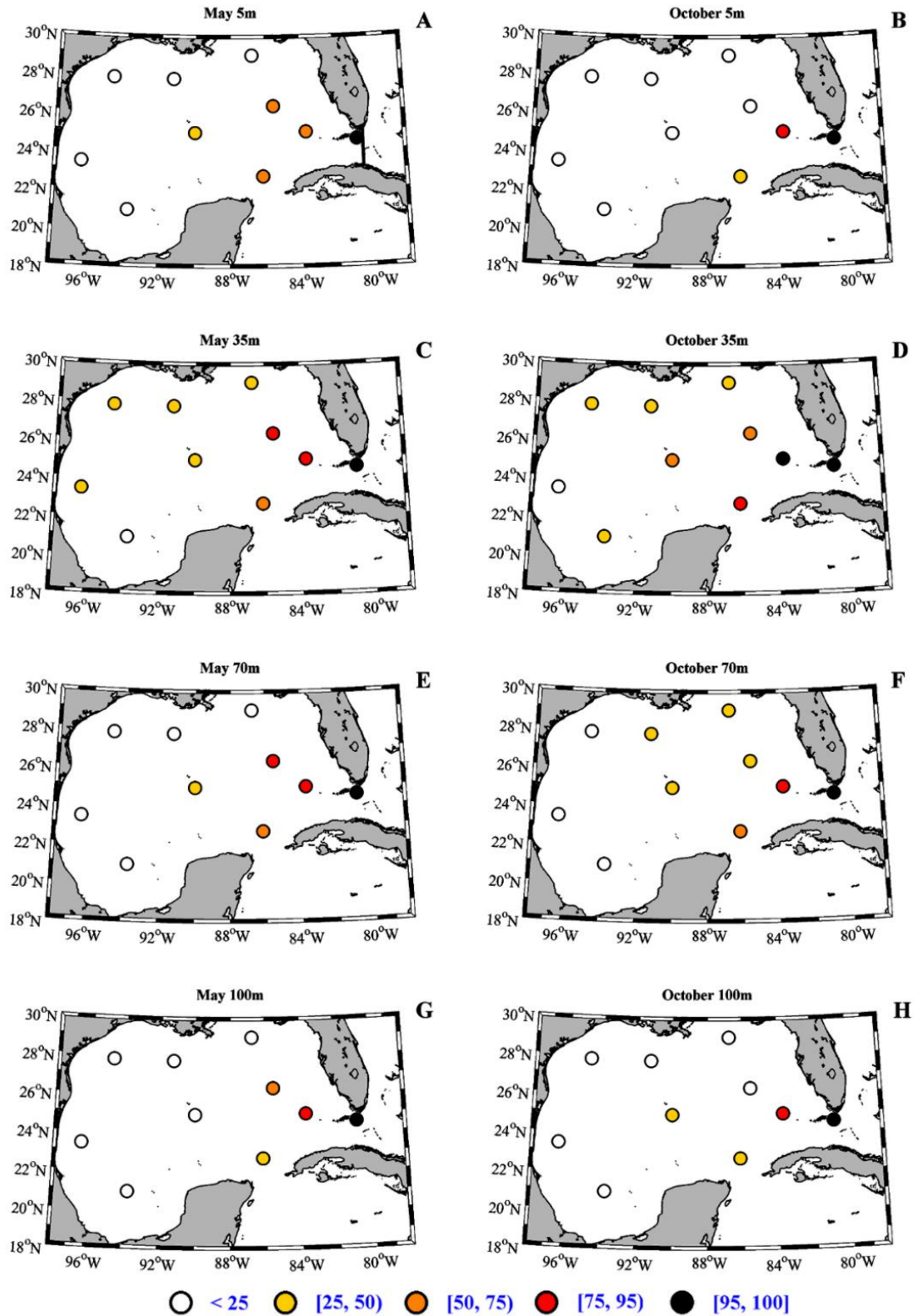


Figure 3.3. Analysis to determine the ideal release point. Percentage of particles that succeeded in crossing the 80.5°W meridian starting for different release points located inside the Gulf of Mexico. Black line in (A) represent the 80.5°W meridian.

3.2.4. Dependence on the number of particles

The probability of larvae crossing the North Atlantic can be described in terms of the dispersal of a set of particles. First, the number of particles needed to accurately represent the dispersal is determined. Thus, particles released in October 2000 at a fixed depth of 100 m were analyzed considering different numbers of tracers (200, 500, 1,000, 2,000, 3,000, 5,000, 7,000, 9,000, and 10,000).

Figure 3.4A corresponds to the simulation with the highest number of particles ($np=10,000$), which is used as the benchmark. The histogram shows the different numbers of particles found at each distance from the release point after a simulation of 1.5 years. Two maxima are found at around 3,000 km and 5,000 km from the release point. Both peaks are detected at the same distance regardless of the number of particles (from 200 to 10,000).

The maximum difference in the percentage of particles found at any distance on the histograms (relative to $np=10,000$) is shown in Figure 3.4B. The maximum value (on the order of 2.6%) is found for $np=200$, and this decreases when the number of particles increases. The maximum difference attains a minimum value on the order of 0.75% when np is about 5,000. Note that several realizations of the same experiment (with the same number of particles) do not necessarily provide exactly the same result due to the presence of the random term in the Lagrangian model.

Similar behavior can be observed when the mean difference among histograms (relative to $np=10,000$) is considered (Figure 3.4C). The maximum mean difference (close to 0.9%) is found for the smallest number of particles ($np=200$). Once again, satisfactory values are found for $np>5,000$.

Following [Kettle and Haines \(2006\)](#), particles are considered to succeed in crossing the Atlantic when they pass the 25°W meridian. In this study, the percentage of particles that crossed the 25°W meridian from west to east and never went back is analyzed for different values of np (Figure 3.4D) for a particular year ($yy=2002$). The same approximate percentage of particles is observed to cross the meridian for any $np>1,000$. Similar results are obtained for particles released in May and for other depths.

Taking into account these results, the value $np=5,000$ is considered for further analysis because it provides a good balance between accuracy and computational cost.

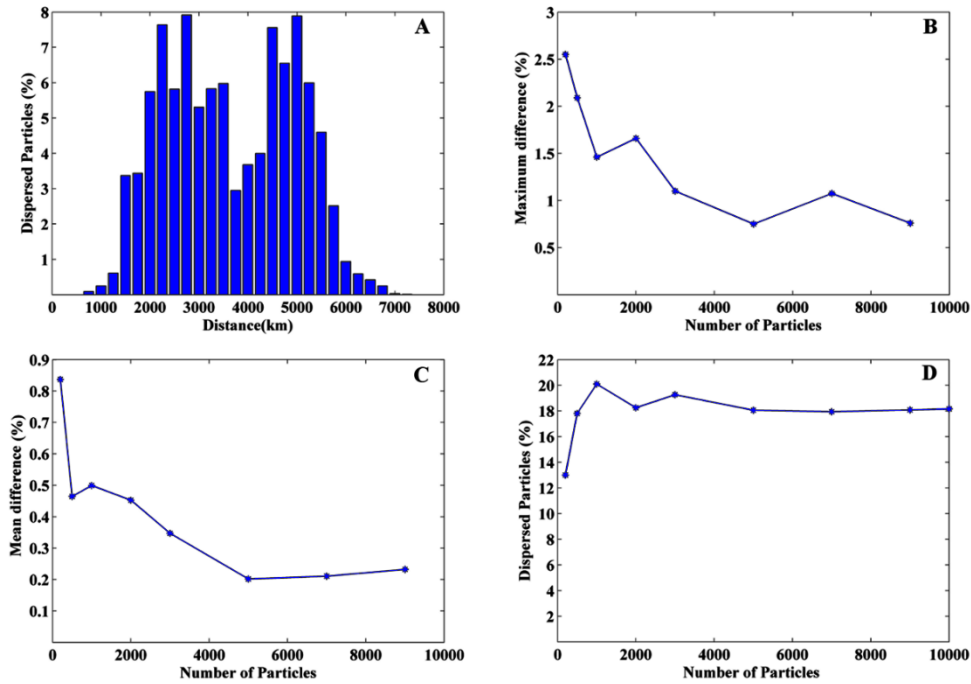


Figure 3.4. Analysis to determine the number of particles needed in the simulations. (A) Histogram of the dispersion for 10,000 particles. (B) Maximum difference (%) among histograms in the percentage of particles at any distance, relative to the case with 10,000 particles. (C) Mean difference (%) among histograms for different numbers of particles, relative to the case with 10,000 particles. (D) Percentage of dispersed particles that succeeded in crossing the 25°W meridian for runs with different numbers of particles. All particles were released at 80.836°W 24.754°N in October 2000 at a fixed depth of 100 m, and the final location corresponds to March 2002.

3.3. Results and discussion

3.3.1. Comparison with a high resolution model

Two test are used to compare results from SODA and HYCOM in order to analyze the influence of the low spatial and temporal resolution of SODA in the dispersal path of the released particles. Data are compared over an overlapping time period of 14 years (1996-2009).

Firstly, the final position of the particles after 18 months of dispersion is calculated for both databases at all depths and both spawning seasons from 1996-2009 (Figs. 3.5-3.8). This allows computing changes in the position of particles with dispersal time between SODA and HYCOM. For all figures, A and B refer to particles released in May using SODA (A) and HYCOM (B), and C and D refer to particles released in October using SODA (C) and HYCOM (D).

A considerable similarity is observed among the results from both databases. The particles follow a very similar dispersion pattern independently of the database. Regarding particles released at 5 m depth (Figure 3.5), the highest concentration of

particles is found along a continuous band across the North Atlantic Ocean that stretched from 30° to 35°N. However, for the rest of the depths (Figs. 3.6-3.8) there are two branches. The lower one is similar to the band found at 5 m, whereas the upper branch travels northward reaching latitudes close to 60°N. Although little differences are observed between both databases, results are very similar indicating that the dispersion areas obtained for SODA and HYCOM are similar.

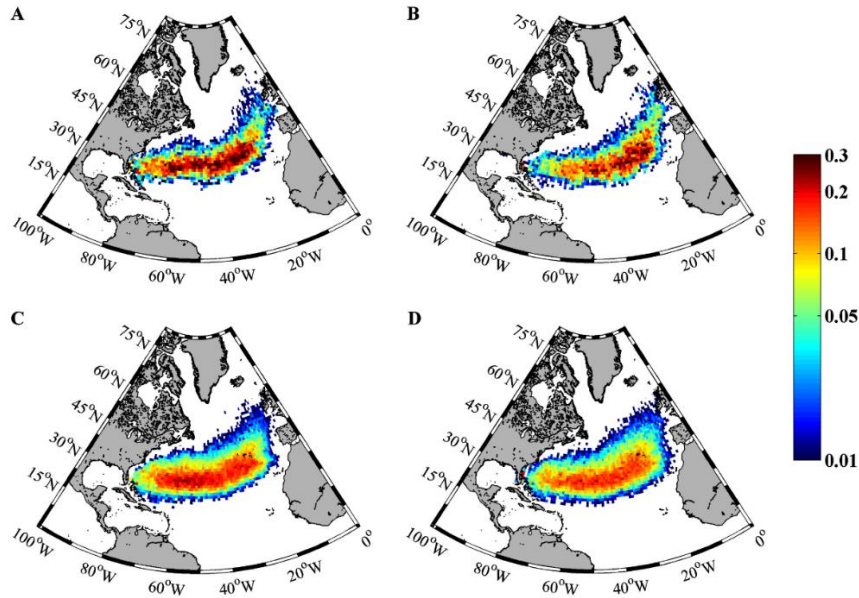


Figure 3.5. Final position of dispersed particles over the period 1996-2009. Percentage of particles found at the North Atlantic Ocean after a drift of 1.5 years for particles initially released at 5 m in (A) May using SODA. (B) May using HYCOM. (C) October using SODA. (D) October using HYCOM.

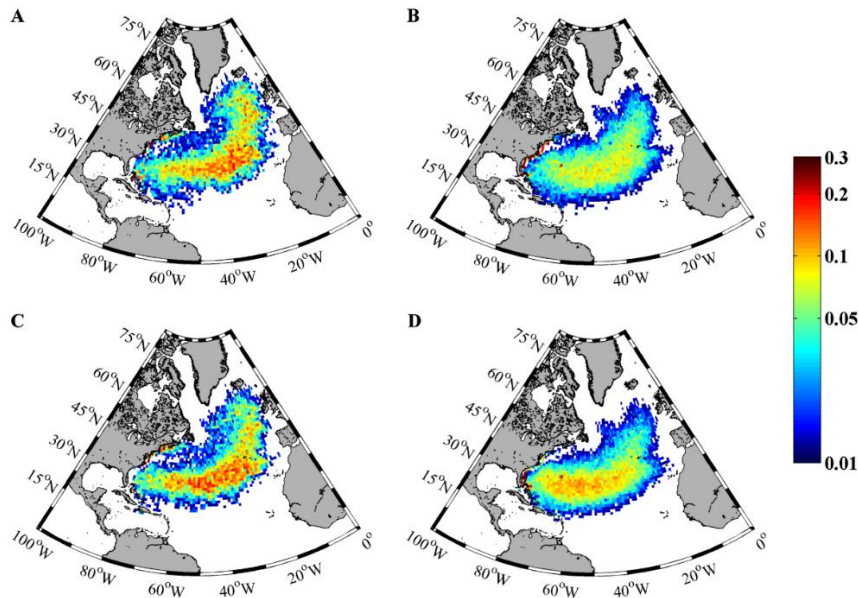


Figure 3.6. Final position of dispersed particles over the period 1996-2009. Percentage of particles found at the North Atlantic Ocean after a drift of 1.5 years for particles initially released at 35 m in (A) May using SODA. (B) May using HYCOM. (C) October using SODA. (D) October using HYCOM.

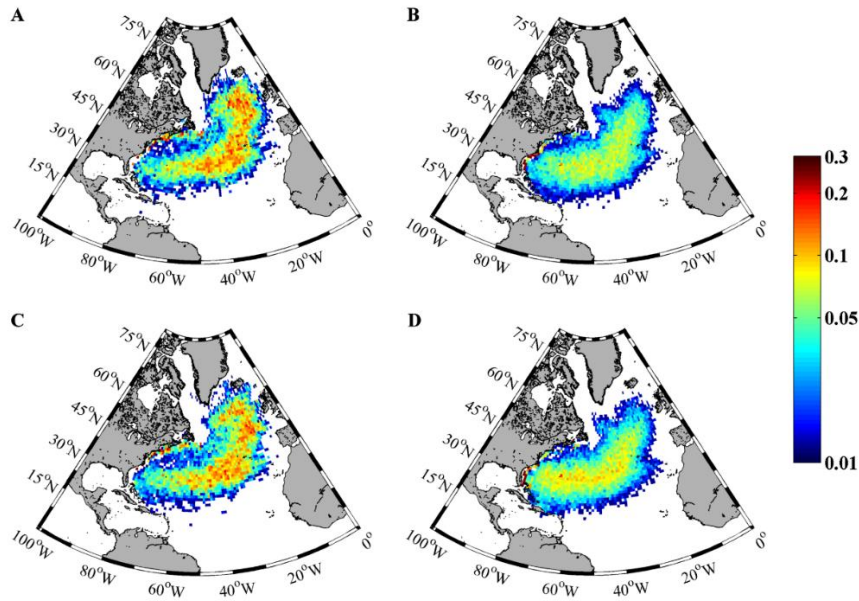


Figure 3.7. Final position of dispersed particles over the period 1996-2009. Percentage of particles found at the North Atlantic Ocean after a drift of 1.5 years for particles initially released at 70 m in (A) May using SODA. (B) May using HYCOM. (C) October using SODA. (D) October using HYCOM.

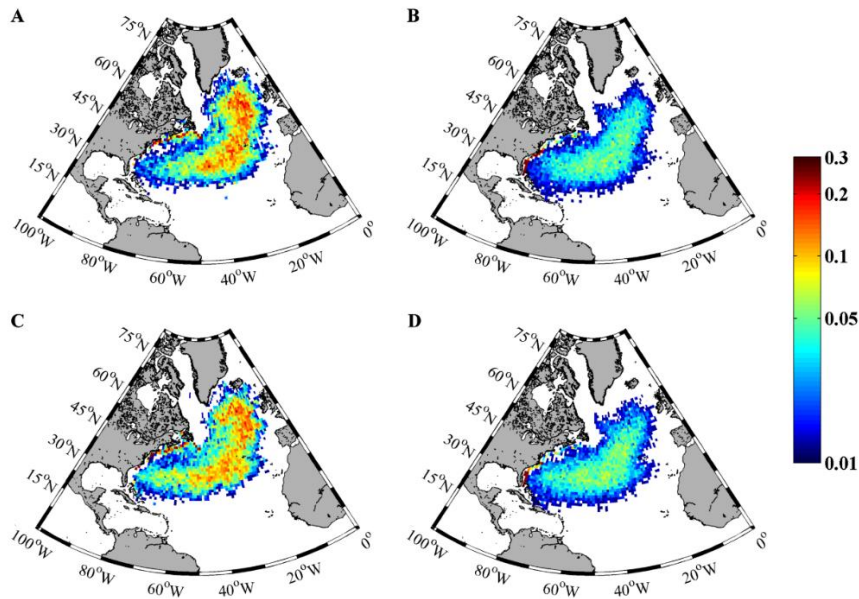


Figure 3.8. Final position of dispersed particles over the period 1996-2009. Percentage of particles found at the North Atlantic Ocean after a drift of 1.5 years for particles initially released at 100 m in (A) May using SODA. (B) May using HYCOM. (C) October using SODA. (D) October using HYCOM.

Secondly, the percentage of particles that succeeded in crossing the 25°W meridian using SODA and HYCOM databases is analyzed for particles released at 5 m (Figure 3.9). Figure 3.9A shows results for particles released in May and Figure 3.9B shows results for particles released in October. These percentages of success are adjusted to the equation $y_i = ax_i$ following the process described in the subsection “3.2.1 Data”. Thus, the

relation between percentages is calculated for both spawning seasons with values of $a=1.075$ for particles released in May and $a=1.004$ for particles released in October. These results indicate that besides year to year differences, overall both models disperse in a similar way.

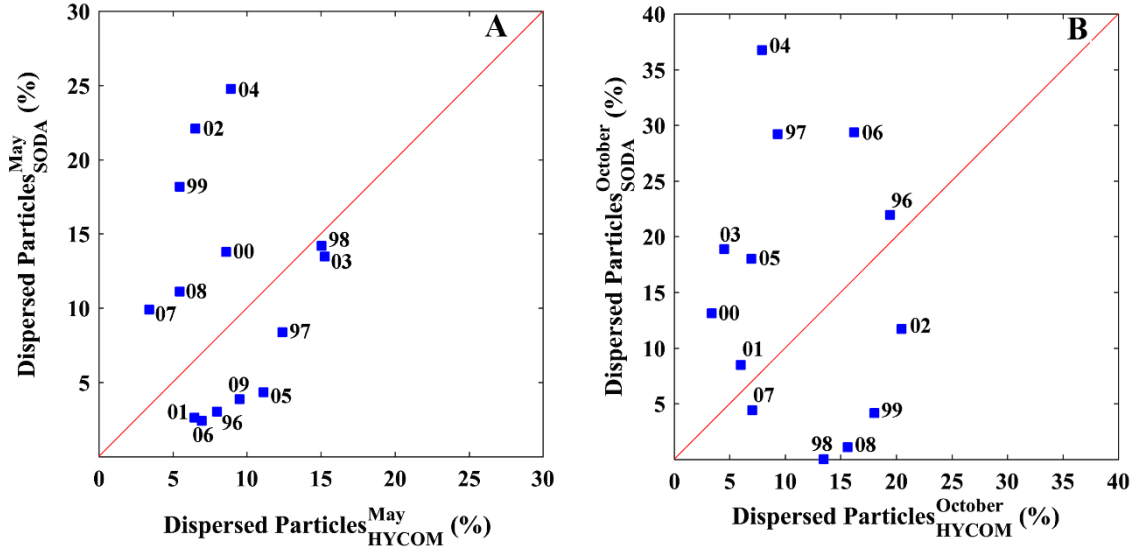


Figure 3.9. Comparison between the percentages of particles released at 5 m that succeeded in crossing the 25°W meridian using SODA and HYCOM over the period 1996-2009. (A) Particles initially released in May. (B) Particles initially released in October. The numbers represent the year.

To better analyze these results from a statistical point of view, trends in the number of particles that succeeded in crossing the 25°W meridian for both spawning seasons at surface layers are also evaluated over the 14 years for the two databases. Figure 3.10 shows these time series and fitted slope whose magnitude provides the trend.

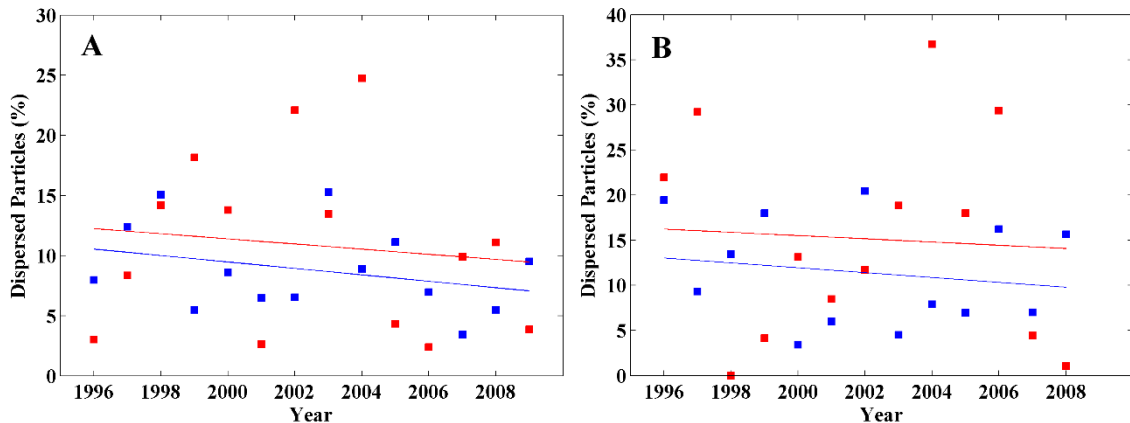


Figure 3.10. Percentage of particles that crossed the North Atlantic Ocean over the period 1996-2009. Time evolution of the percentage of particles released at 5 m depth in (A) May and (B) October that succeeded in crossing the 25°W meridian. Data were obtained with SODA (red) and HYCOM (blue).

A decreasing trend is obtained in all cases. Particles released in May show a similar trend for both databases with a value of -2.14% per decade for SODA and -2.68% per decade

for HYCOM. Trends are slightly different between databases in October, with a value of -1.79% per decade for SODA and -2.70% per decade for HYCOM.

From these results, it is possible to observe that in spite of the low spatial and temporal resolution of the SODA database, the movement of particles across the Atlantic is in accordance with the results obtained from HYCOM. In addition, the length of modelled data provided by SODA allows us to assess changes in the migration of particles crossing the North Atlantic over the last century, which is the main advantage of the database.

3.3.2. Distribution of particles

Lagrangian tracers are released at four different depths in the Strait of Florida, where the Gulf Stream is the main driving force distributing species. Particles are released twice a year (May and October) recording their position every 5 days and the duration of each numerical experiment is 1.5 years.

Figure 3.11 summarizes the final position (in percentage of dispersed particles) attained by particles released in May at the four depths. Similarly, Figure 3.12 presents the final position attained by particles released in October. Simulations for both spawning seasons show a similar pattern.

The areas with the highest number of particles are shown to depend on the depth and the season. Thus, for a depth of 5 m (Figure 3.11A and 3.12A), the highest percentage of particles is found along a continuous band that stretched from 30° to 35°N and crosses the North Atlantic Ocean. For the rest of the depths (Figure 3.11B–D and 3.12B–D), a continuous band around 33°N that splits into two branches at approximately 45°W is detected. The lower branch is similar to the band found at 5 m, whereas the upper one travels northward. This branch even reaches latitudes close to 60°N , especially for deep layers (Figure 3.11D and 3.12D).

Overall, Figure 3.11 and 3.12 indicate that the distribution of particles over the North Atlantic Ocean after a drift of 1.5 years clearly depicts the main macroscopic features of the Gulf Stream. This behavior is observed at all depths, except for near surface layers, where only the southern branch is important. It should be noted that near surface behavior is more dependent on wind forcing which could explain the differences in the dispersion pattern in comparison with deeper water.

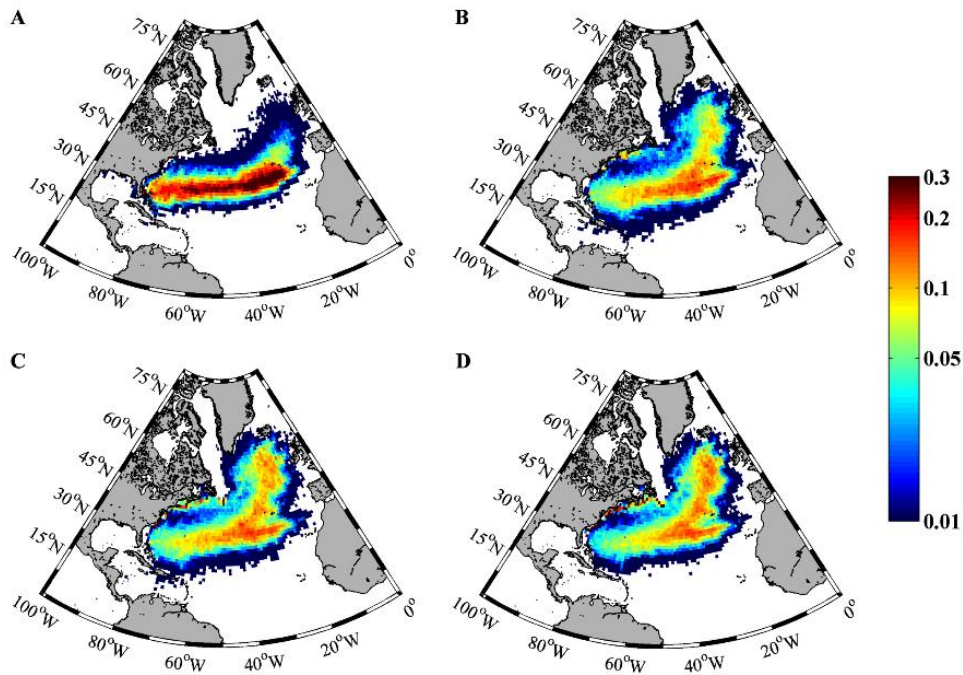


Figure 3.11. Final position of dispersed particles released in May over the period 1899-2010. Percentage of particles found at the North Atlantic Ocean after a drift of 1.5 years. Particles were initially released in May at a fixed depth of (A) 5 m. (B) 35 m. (C) 70 m. (D) 100 m.

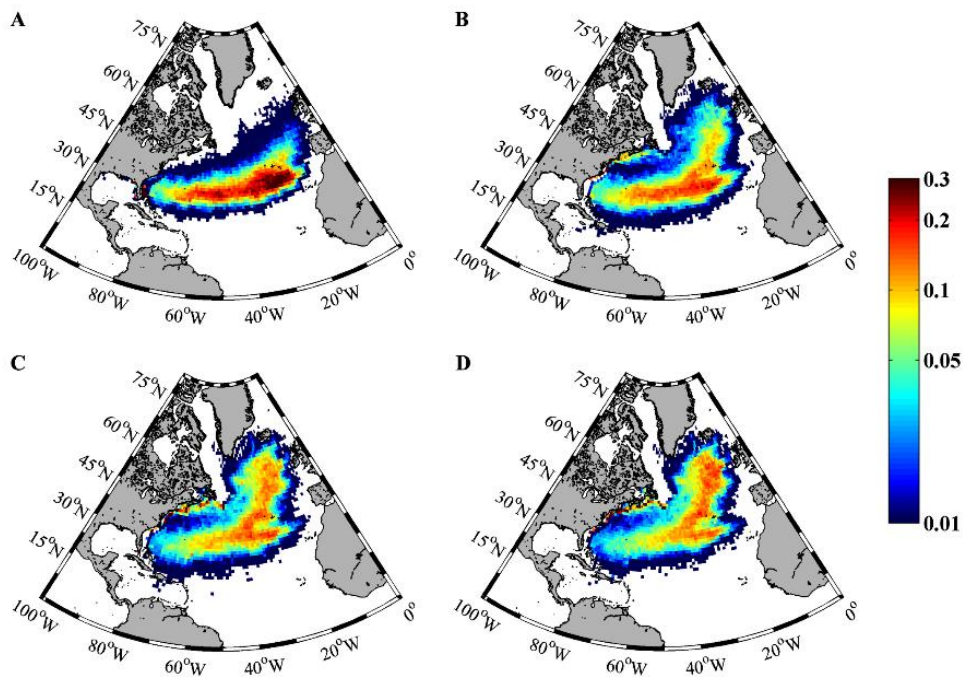


Figure 3.12. Final position of dispersed particles released in October over the period 1899-2010. Percentage of particles found at the North Atlantic Ocean after a drift of 1.5 years. Particles were initially released in October at a fixed depth of (A) 5 m. (B) 35 m. (C) 70 m. (D) 100 m.

3.3.3. Particles crossing the Atlantic

Figures 3.11 and 3.12 also show that some fraction of the released particles succeeded in crossing the Atlantic. Table 3.3 summarizes the locations where the highest percentage of particles is found. A maximum peak in longitude is observed between 29.0° and 31.5°W for all cases, which corresponds to a distance of ~4500 km along a straight line from the release area. To analyze the distribution in latitude, particles that succeeded in crossing 25°W are considered. Thus, two main concentration peaks are observed in latitude. The first one is detected for all simulations between 32.5° and 33.5°N, which is in good agreement with previous studies (Kettle and Haines, 2006; Bonhommeau et al. 2009a, b). The second one, around 54.5°N, is observed for particles released in May at 35, 70, and 100 m and for particles released in October at 70 and 100 m at approximately 50°N which is also in agreement with results from Bonhommeau et al., (2009a, b). The highest number of particles that crossed 25°W corresponding to the surface simulation is identified around 40°–41.5°N for both spawning seasons.

Released Date	Depth (m)	Longitude (°W)	Latitude (°N)	
			Peak 1	Peak 2
May	5	30.5	33.5	41.5
	35	29.0	33	54.5
	70	30.0	33.5	54.5
	100	30.5	33	54.5
October	5	29.5	33	40
	35	30.0	33	47
	70	29.5	32.5	54.5
	100	31.5	33	54.5

Table 3.3. Distribution of the maximum number of particles by longitude and latitude. The longitude column indicates the longitude position where the maximum number of particles was found considering all latitudes. The latitude column is divided into two peaks corresponding to the latitude position where the highest percentage of particles that succeeded in crossing the 25°W meridian was found.

The mean monthly percentage of particles that crossed the 25°W meridian is analyzed for the whole period (1899-2010). Figure 3.13 and 3.14 show the results for particles released in May and October respectively. The percentage of particles crossing the 25°W meridian increases continuously with the dispersal time without attaining a plateau.

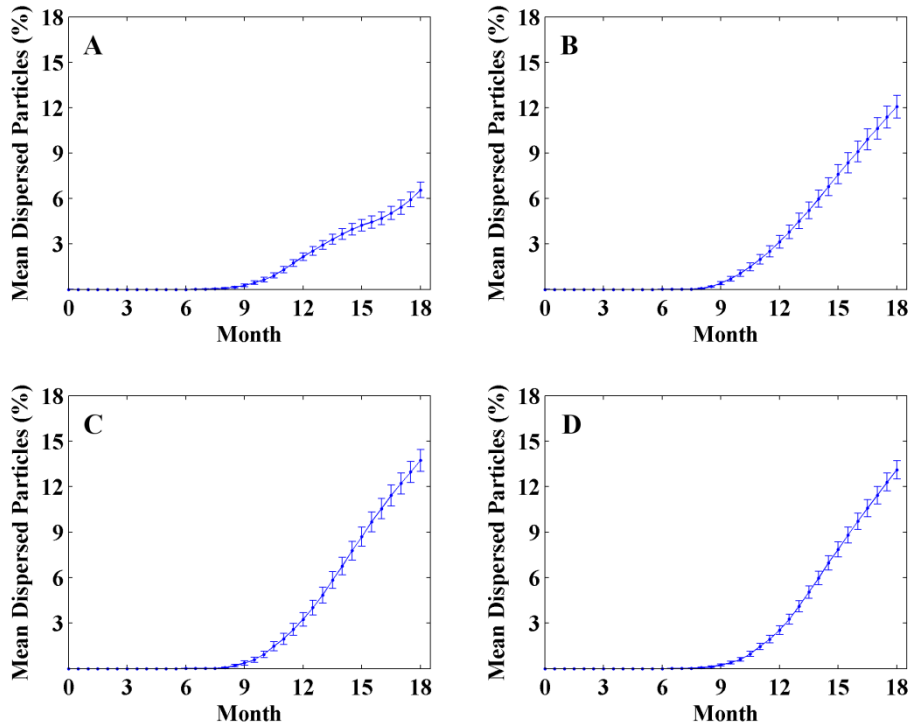


Figure 3.13. Monthly evolution of dispersed particles over the entire period of study. Percentage of particles that succeeded in crossing the 25°W meridian over the entire period of study for particles initially released in May at a fixed depth (A) 5 m. (B) 35 m. (C) 70 m. (D) 100 m. Errors bars represent the standard deviation of the mean.

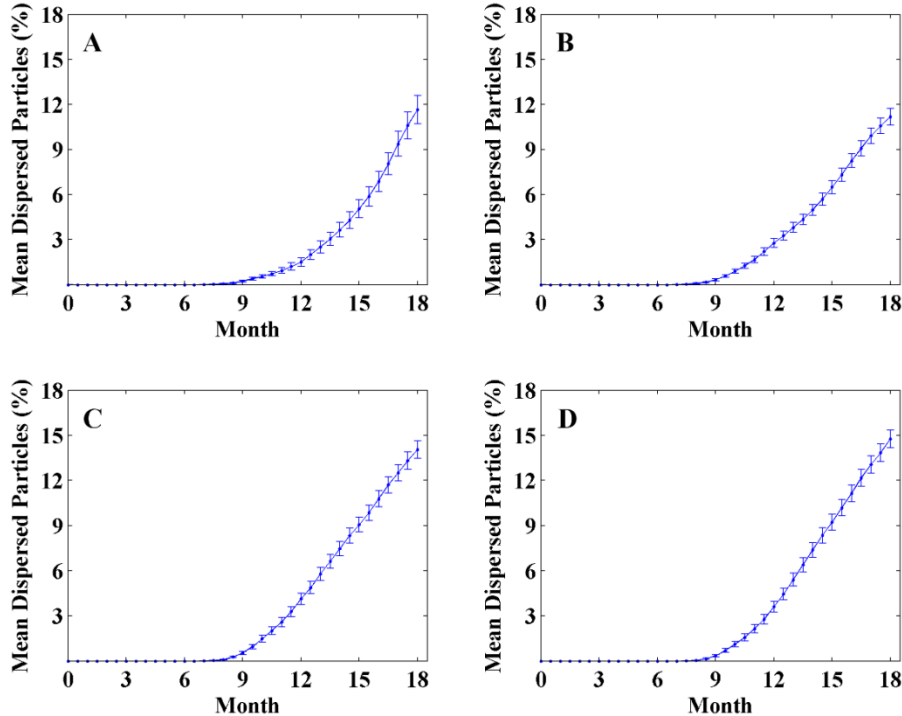


Figure 3.14. Monthly evolution of dispersed particles over the entire period of study. Percentage of particles that succeeded in crossing the 25°W meridian over the entire period of study for particles initially released in October at a fixed depth (A) 5 m. (B) 35 m. (C) 70 m. (D) 100 m. Errors bars represent the standard deviation of the mean.

3.3.4. Variability and trends

The variability in particles that succeeded in crossing the 25°W meridian is also studied through statistical analysis for both spawning seasons and the four depths. Figure 3.15 shows the percentage of particles crossing this meridian over the whole period under study. An increasing trend is obtained in all cases despite the high interannual variability. Statistical analysis of the dispersal particles performed for all simulated cases is shown in Table 3.4. Most of the simulations show a mean percentage of success that ranges from 11% to 15% over the whole period, except for particles released in May near surface, where the percentage is considerably lower (~7%). The probability of succeeding in crossing the Atlantic is shown to increase over the last century, being the increase significant for all the simulated cases, except for particles released in May at 5 m depth.

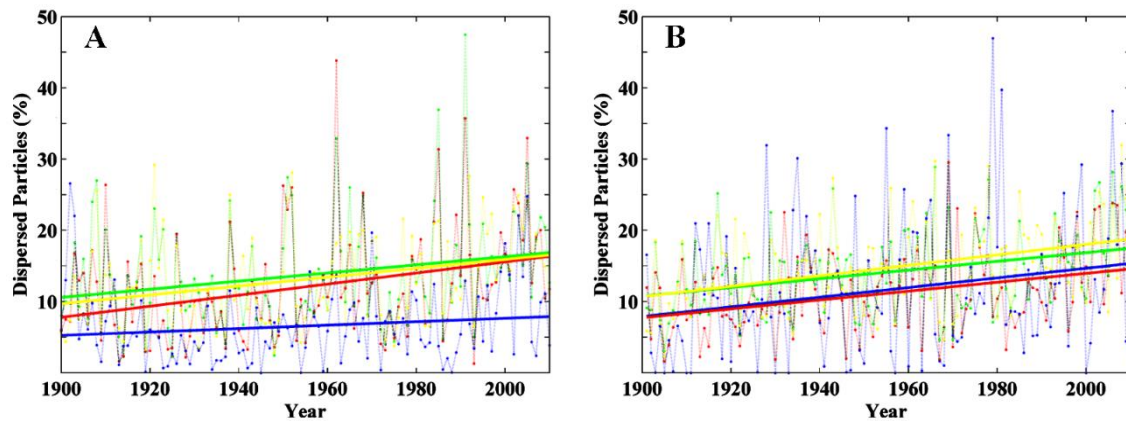


Figure 3.15. Percentage of particles that crossed the North Atlantic Ocean over the entire period of study. Time evolution of the percentage of particles released in (A) May and (B) October that succeeded in crossing the 25°W meridian at fixed depths: 5 m (blue), 35 m (red), 70 m (green) and 100 m (yellow).

Release Date	Depth (m)	Mean (%)	Trend (% dec ⁻¹)	SL (%)
May	5	7	0.24	—
	35	12	0.78	> 99
	70	14	0.57	> 99
	100	13	0.62	> 99
October	5	12	0.68	> 95
	35	11	0.62	> 99
	70	14	0.61	> 99
	100	15	0.73	> 99

Table 3.4. Statistical analysis of the number of particles crossing the 25°W meridian for all simulated cases. Mean indicates the average percentage of particles that have succeeded in crossing the 25°W for each simulation. Trend indicates the increase in the percentage of particles that succeeded in crossing the 25°W. Values are expressed in percentage per decade. The significance level was calculated using the Spearman correlation.

In particular, the trend is significant for all simulations starting in October, with values ranging from 0.61% to 0.73% per decade. The simulations starting in May also show a

significant increasing trend ranging from 0.57% to 0.78% per decade, except for near surface layers. Once again, particles located near surface show higher variability, which is also reflected in a lower mean number of particles that succeeded in crossing the Atlantic. Previous studies (Kelly, 1991; Zlotnicki, 1991; Hogg and Johns, 1995) analyzed the variability of the Gulf Stream at the surface layer. They found seasonal changes in the intensity of the current and a marked annual cycle in water transport, which is observed to be minimum in spring and maximum in autumn. This pattern may explain the difference observed at surface layer for particles released in May and October.

3.3.5. Minimum travel period

The time elapsed for the first particles that succeeded in crossing the 25°W meridian is calculated for every year from 1899 to 2010 and recorded as T_{min} . Two variables are obtained from these series of data, namely, the infimum (T_{inf}), which corresponds to the smallest T_{min} ; and T_{mean} calculated like the average of all T_{min} . Both variables are calculated for every season and depth (Table 3.5). T_{inf} is observed to range from 6 to 7 months. Previous studies have analyzed the minimum migration time using Lagrangian simulation of particles released in the Sargasso Sea to study the fastest migration across the Atlantic experienced by eel larvae. Results reported different estimations for the duration of eel migration, which ranged from 6 months to 2 years (Wang and Tzeng, 2000; Kettle and Haines, 2006; Kuroki et al., 2008; Bonhommeau et al., 2009a, b; Blanke et al., 2012; Pacariz et al., 2014). It is important to note that these studies considered a specific specie and a different release point than in the present study. In addition, T_{mean} values are observed to range from 9.2 to 10.2 months, with significant decreasing trends ranging from -0.15 to -0.40 months per decade, indicating that the minimum time needed to cross the ocean basin was longer at the beginning of the twentieth century than at present.

Release Date	Depth (m)	T_{inf} (month)	T_{mean} (month)	Trend (months dec ⁻¹)	SL (%)
May	5	6.5	9.8 ± 1.8	-0.25	> 99
	35	6	9.5 ± 1.5	-0.26	> 99
	70	6	9.4 ± 1.3	-0.15	> 99
	100	6.5	9.8 ± 1.3	-0.21	> 99
October	5	6	10.2 ± 2.3	-0.40	> 99
	35	6	9.3 ± 1.4	-0.24	> 99
	70	6.5	9.2 ± 1.3	-0.22	> 99
	100	7	9.4 ± 1.3	-0.21	> 99

Table 3.5. Statistical analysis of the minimum travel period for all simulated cases. T_{inf} indicates the minimum migration time needed for the first particles that crossed the 25°W meridian. T_{mean} indicates the minimum migration time, in average, to cross the 25°W meridian being the error the standard deviation. Trend indicates changes in the time needed to cross the 25°W meridian. Values are expressed in months per decade. The significance level was calculated using the Spearman correlation.

3.3.6. Eddy Kinetic Energy

To analyze changes in EKE since the beginning of the twentieth century, trends in EKE are calculated using SODA velocity fields at surface layer over the North Atlantic (Figure 3.16A). EKE has decreased on the northern side of the Gulf Stream and along a band around 32°N between 50°W and 75°W. In contrast, EKE has increased along the Gulf Stream path. Black dots in Figure 3.16A show the coordinates where the highest EKE is found at each longitude across all latitudes. Trends obtained for these points are shown in Figure 3.16B. Black circles mark those points that achieved or exceeded the 95% confidence limit. Most of the points with maximum EKE coincide with the points with a higher trend, showing the path of the current.

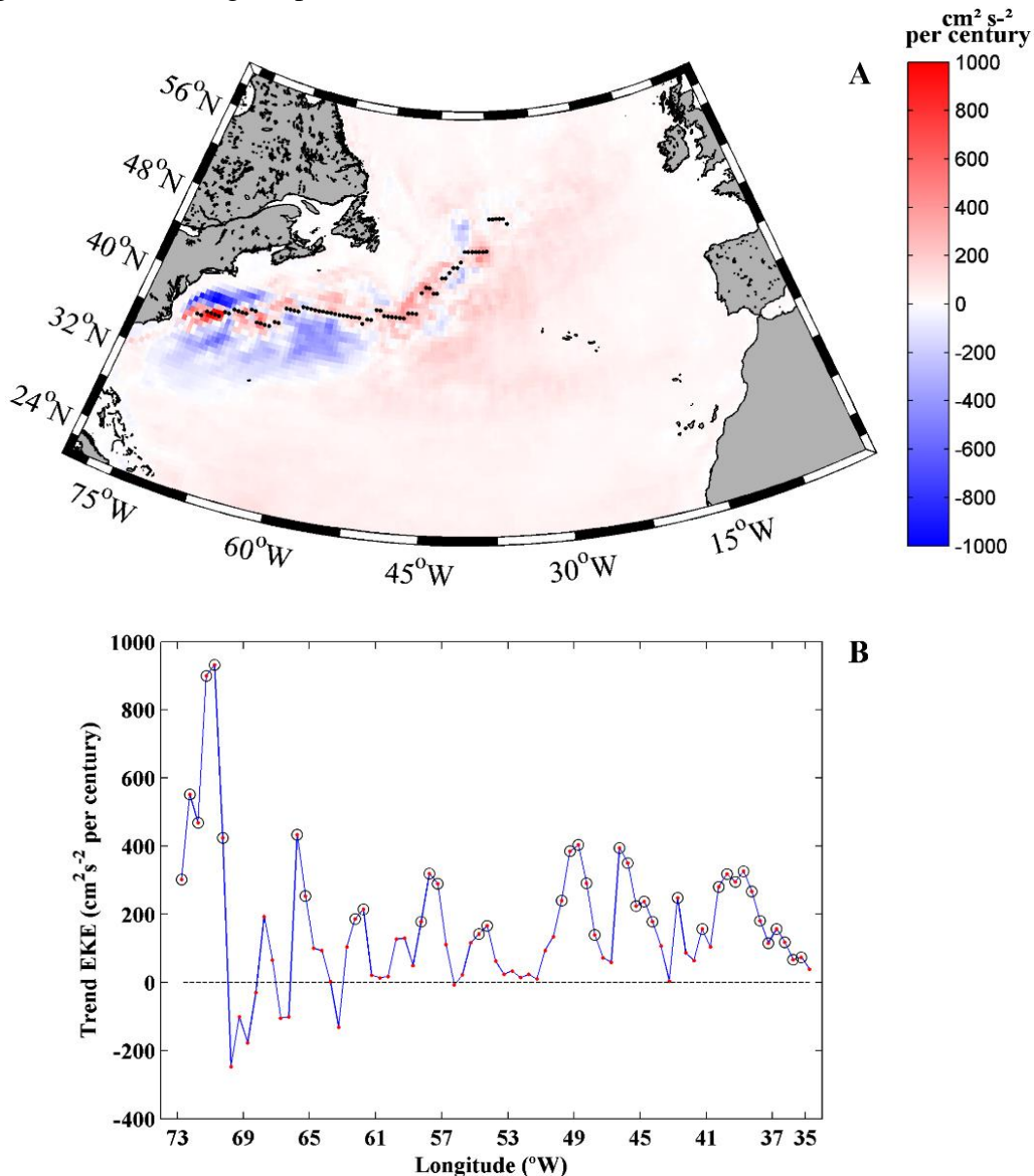


Figure 3.16. Changes in EKE since the beginning of 20th century. (A) Trend in EKE for the North Atlantic Ocean calculated using SODA velocity fields at surface layer. Black dots represent the location where the highest EKE was found. (B) Trends at the points marked with black dots in (A). Black circles indicate the confidence limit $\geq 95\%$.

3.3.7. Influence of atmospheric forcing

The extensive period of available data from SODA allows analyzing possible dependence on teleconnection patterns. Dispersal over such a long time could be affected by phenomena with inter-decadal or multi-decadal time scales as the main teleconnection patterns, which influence the North Atlantic Ocean (AMO and NAO).

Nevertheless, no significant results are obtained from the correlation analysis between the percentage of particles that succeeded in crossing the 25°W meridian and these teleconnection patterns (Table 3.6). Low values of the correlation coefficient (lower than 0.2) are obtained for all the simulations. Lagged correlations (up to 5 years) with the NAO index were also calculated without significant correlation. The chaotic nature for the atmosphere and ocean system could lead to quite noisy connections between ocean circulations and macroscopic patterns.

A					B				
AMO	MAY		OCTOBER		NAO	MAY		OCTOBER	
	R	SL (%)	R	SL (%)		R	SL (%)	R	SL (%)
5 m	—	—	0.10	66.33	5 m	—	—	—	—
35 m	0.14	84.51	0.21	97.16	35 m	—	—	—	—
70 m	—	—	0.10	68.03	70 m	—	—	-0.10	66.83
100 m	—	—	-0.11	76.96	100 m	-0.15	87.17	—	—
Mean	—	—	0.11	72.90	Mean	-0.10	71.74	—	—

Table 3.6. Statistical analysis of the teleconnection patterns performed for all simulated cases. Mean indicates the average of the percentage of particles that have succeeded in crossing the 25°W meridian of the four depths. Only values of $R \geq 0.10$ are shown in the table for the correlation between the percentage of particles that have succeeded in crossing the 25°W meridian for each simulation and the teleconnection patterns. A) The AMO index. B) The NAO index. The significance level (SL) is calculated using the Spearman correlation.

3.4. Conclusions

Changes in the probability of larvae crossing the North Atlantic Ocean have been studied over the period 1899–2010. This analysis has been carried out using a Lagrangian model to track particles from the Straits of Florida, an area where the Gulf Stream is the main driving force, across the North Atlantic. The main findings of the present work can be summarized as follows:

- a) First of all, the comparison between SODA and HYCOM, over the overlapping period 1996-2009, shows that the results from both databases are comparable. The dispersed particles follow almost the same dispersion pattern (Figure 3.5-3.8). A

decreasing trend, for the percentage of particles that succeeded in crossing the North Atlantic for all the simulated cases, is obtained (Figure 3.10). In addition, the adjustment to the equation $y = ax_i$ shows that the dispersion rate is very similar for both databases supporting the use of the database SODA for the current study.

- b) The analysis of the dispersion pattern of particles that succeeded in crossing the Atlantic since the beginning of the twentieth century show results in good agreement with previous research. Indeed, the two main concentration peaks in latitude (Table 3.2) were previously detected by [Kettle and Haines \(2006\)](#) and [Bonhommeau et al. \(2009a, b\)](#). In addition, the general percentage obtained for deep layers (Table 3.4) is in good agreement with [Bonhommeau et al., \(2009a\)](#).
- c) The increase in the success of crossing the Atlantic over the last century (Figure 3.15) is in agreement with changes in EKE, which has intensified along the Gulf Stream path (Figure 3.16).
- d) The minimum time needed for passive particles to cross the Atlantic (T_{min}) till the 25°W meridian is on the order of 6-7 months which is comparable to the values obtained from the analysis of the microstructure of eel otoliths. In addition, the significant negative trends mean particles move faster than at the beginning of the twentieth century.
- e) In terms of species dispersal, the results indicate that species with PLD (>6-7 months) have increased their chances to cross the Atlantic since the beginning of the twentieth century.
- f) The results presented here do not show any correlation with the teleconnections patterns AMO or NAO.

Chapter 4

The migration time of European eel

4.1. Motivation

The European eel (*Anguilla anguilla*, Linnaeus, 1758) is a migratory species that starts its journey at the Sargasso Sea towards the European shelf (Kleckner and McCleave, 1988; Schmidt, 1923; Tesch, 1977) and undergoes one of the longest marine larval migrations (> 6000 km). The worldwide decline in eel population (Dekker et al., 2003), observed over the last decades makes mandatory to understand the duration of migration across the Atlantic. The Gulf Stream, described in *Chapter 3*, is the main current involved in the dispersion of eel larvae after hatching.

Considerable effort has been devoted to determine the migration duration of European eel larvae using different methods with estimations ranging from months to years (see Table 4.1).

AUTHORS	METHOD	DURATION
Boëtius and Harding (1985)	Growth curves	1.5yr
van Utrecht and Holleboom (1985)	Macrostructure of eel otoliths	2-6yrs
Lecomte-Finiger (1992) Arai et al., (2000)	Microstructure of eel otoliths	7-9 months
Kuroki et al., (2008)	Microstructure of eel otoliths	11 months
Kettle and Haines (2006)	Lagrangian model	2yr
Bonhommeau et al., (2009a)	Lagrangian model	10 months and 3 days
Blanke et al., (2012)	Lagrangian model	285 days

Table 4.1. Migration duration of European eel larvae. Summary of previous estimations of the migration duration of European eel based on different methods.

The aim of this chapter is to determine whether or not the duration of migration obtained from the analysis of the microstructure of eel otoliths can be reconciled with the minimum migration time provided by numerical models (Rodríguez-Díaz and Gómez-Gesteira, 2017). The sensitivity of Lagrangian models to different conditions (spatial and time

resolution, release depth and initial distribution) and to migration strategies are analyzed. Different migration strategies have been considered:

- i. Passive migration: particles horizontally advect by currents at a fixed depth.
- ii. Passive migration in the horizontal with diel vertical migration, where particles are located at 50 m during nighttime and 300 m during daylight.
- iii. Migration with added random walk that can be fully random or locally oriented following currents.

4.2. Material and methods

4.2.1 Data

In *Chapter 2* it was explained in detail the data used in the present study. In this section, only a summary is presented in table 4.2.

DATA	OBSERVATION	SOURCE
U, V velocity	Period 1996-2012. Data from several levels: surface, 50 m, 100 m, 150 m 200 m and 300 m.	HYCOM GLBu0.08 expt_19.1
EKE	Calculated as the sum of the variance of U and V over the period 2006-2008 with a time resolution of 3 h.	It was used the velocity data from HYCOM GLBu0.08 expt_19.1

Table 4.2. Summary of data used in the study. Additional information is included in the observation column and the data source.

4.2.2. Lagrangian model

Simulations are run over the entire North Atlantic Ocean (see Figure 4.1) using the particle tracking model described in *Chapter 2*. Table 4.3 summarizes the initial conditions used in the simulations. In the base case, an initial interparticle spacing of $0.06^\circ \times 0.06^\circ$ is considered. Approximately 50,000 particles are initially released in an area (23–30°N; 48–72°W) located in the Sargasso Sea (black rectangle, Figure 4.1). The release area is chosen to fit the spawning area of the European eel larvae (Schmidt, 1925;

1932; Scoth and Tesch, 1982; van Ginneken and Maes, 2005). Three subareas (1-red, 2-green and 3-blue, see Figure 4.1) are defined to analyze the influence of the initial position on further dispersion. The release date (April) is chosen to fit the spawning period of the European eel larvae, which mainly occurs from March to June with a peak in April (Schmidt, 1922, 1923, 1925). Following previous research (Bonhommeau et al., 2009a), each numerical experiment is run for a period of 18 months recording the position of particles every day. As it is mentioned above different migration strategies are considered:

- i. Particles are uniformly distributed at five depths covering the mixed layer (surface, 50 m, 100 m, 150 m and 200 m) with an advection-driven movement in the horizontal direction and without vertical movement
- ii. The movement is advection-driven in the horizontal direction and a diel vertical migration (DVM) is implemented considering a daylight depth of 300 m and a nighttime depth of 50 m. This active behavior has been observed for wild European eel larvae (Castonguay and McCleave, 1987; Jespersen, 1942; Schmidt, 1925; Tesch, 1980)
- iii. Passive migration with added random walk, assuming a constant depth, particles are allowed to move following the current plus an additional random walk.

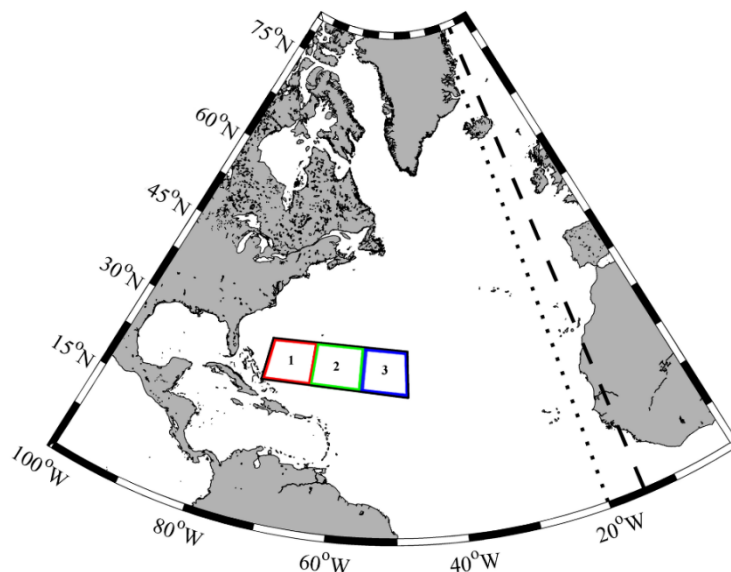


Figure 4.1. Area under scope. Map of the North Atlantic Ocean and the release area (black rectangle) in the Sargasso Sea divided in 3 subareas (1-red, 2-green and 3-blue). Dotted and dashed line represent the 20°W and 15°W meridians respectively.

Previous research has fixed different limits to succeed in crossing the Atlantic. Kettle and Haines (2006) considered the finishing line at 25°W, Bonhommeau et al., (2009a) at 20°W and Blanke et al., (2012) at 15°W. Here we have considered both 20°W and 15°W for comparison purposes.

Following previous research (Cowen et al., 2000; Bonhommeau et al., 2009a; Rudorff et al., 2009), chemical or biological processes such as mortality are not implemented in the model since the goal of the study is to analyze the minimum duration of migration, not the real amount of European eel larvae that has succeeded in crossing the North Atlantic Ocean.

The time step (Δt) was calculated to meet the CFL criterion (Courant et al., 1928, 1967, Pacariz et al., 2014), based on the fact that the time step must be smaller than the time spent by a particle to go over a grid point ($1/12^\circ$).

CONDITION	VALUE	OBSRVATIONS
Release area	48°W - 72°W 23°N - 30°N	Sargasso Sea Spawning area
Depths (m) of each migration strategy	Surface	Particles were uniformly distributed at the five depths without vertical movement
	50 m	
	100 m	
	150 m	DVM
	200 m	
	Daylight depth: 300 m Nighttime depth: 50 m	
	Surface	Passive migration with added random walk
Release date	April	Spawning peak
Duration of each simulation	1.5 year	Bonhommeau et al., (2009a)
Release type	Instantaneous	
Number of releases	1	At each depth of each migration strategy
Number of particles	50,000	Initially released
t_{rec}	Daily	
Δt	1 h	Automatically calculated
dx^0	$0.06^\circ \times 0.06^\circ$	Initial interparticle spacing and in the base case

dx^0	[0.01°, 0.25 °]	Interval considered to evaluate the effect of the initial distribution
Randomness	Full	In the case of the migration strategy: i)
	Full	In the case of the migration strategy: ii)
	Downstream swimming	In the case of the migration strategy: iii)
Constant of randomness	[0, 0.25]	In the case of the migration strategy: i)
	0	In the case of the migration strategy: ii)
Constant of randomness	[0, 0.25]	In the case of the migration strategy: iii) to evaluate the depending on randomness
Vertical migration	Yes	DVM implemented on the migration strategy: ii)
Mortality	No	Cowen et al., (2000) Bonhommeau et al., (2009a) Rudorff et al., (2009)

Table 4.3. Initial conditions. Summary of the conditions used to run the simulations.

4.3. Results and discussion

As we mentioned above, different migration strategies are considered to calculate the minimum migration time to elucidate whether or not the duration based on otolith growth ([Lecomte-Finiger, 1992](#); [Arai et al., 2000](#); [Kuroki et al., 2008](#)) is consistent with the duration estimated from Lagrangian models. First of all, we will focus on the characterization of the migration to prove that the calculations performed with the model are in good agreement with research conducted by other authors.

4.3.1. Characterization of larval migration

First of all, the effect of time resolution is analyzed in terms of its impact on EKE. Surface EKE is computed as the sum of the variance of meridional and zonal velocity components over the period 2006–2008 (Figure 4.2) considering the time resolution provided by the model (3 h). The image is in perfect agreement with surface EKE derived from satellite altimetry over the same period (see Figure 5 in [Blanke et al. \(2012\)](#)). Surface EKE

calculated at coarser time resolutions (6 h, 12 h and 24 h) provides the same macroscopic pattern. To analyze differences among resolutions, the mean EKE is calculated both for the whole North Atlantic and for the most energetic part of the Gulf Stream (from 33°N to 41°N and from 75°W to 55°W). Changes in the mean values due to time resolution are observed to be smaller than 0.5% in both areas. The importance of time resolution has been highlighted in previous research (Blanke et al., 2012), where they found that losses in EKE were higher than 5% when using time resolutions coarser than 1 day (ranging from 6.5% for a resolution of 3 days to >28% for a resolution of 12 days). Here, all resolutions finer than 1 day provide the same pattern without any appreciable loss of energy. Thus, although the use of the finest resolution is always desirable, a balance between computational resources and accuracy must be found and a time resolution of 12 h has been adopted for the rest of the study. Actually, a resolution of 24 h would be enough in most of the computations, but one of the migration strategies considers a diel vertical migration with different depth at day and night, so a semidiurnal time resolution seems the most suitable option.

The latitudinal distribution of successful particles (crossing the 20°W meridian) is analyzed over the whole period of study. Figure 4.3 shows the histogram calculated for a depth of 50 m assuming a passive (advective) movement in the horizontal direction and no movement in the vertical. Successful particles tend to accumulate around two main peaks centered at 30–35°N and 45–50°N respectively. This latitudinal distribution is due to the effect of the North Atlantic Ocean current system over the Lagrangian trajectories of particles. As we mentioned above, the Gulf Stream splits into two branches around 50°W and particles follow either the North Atlantic Current towards latitudes between 45°N–60°N or the Azores Current towards latitudes between 30°N–45°N. These high concentration peaks are in good agreement with the ones obtained in previous studies (Kettle and Haines, 2006; Bonhommeau et al., 2009a, b; Pacariz et al., 2014). Similar results are found for the rest of the depths, although the northern branch tends to become more important with depth in good agreement with Blanke et al., (2012).

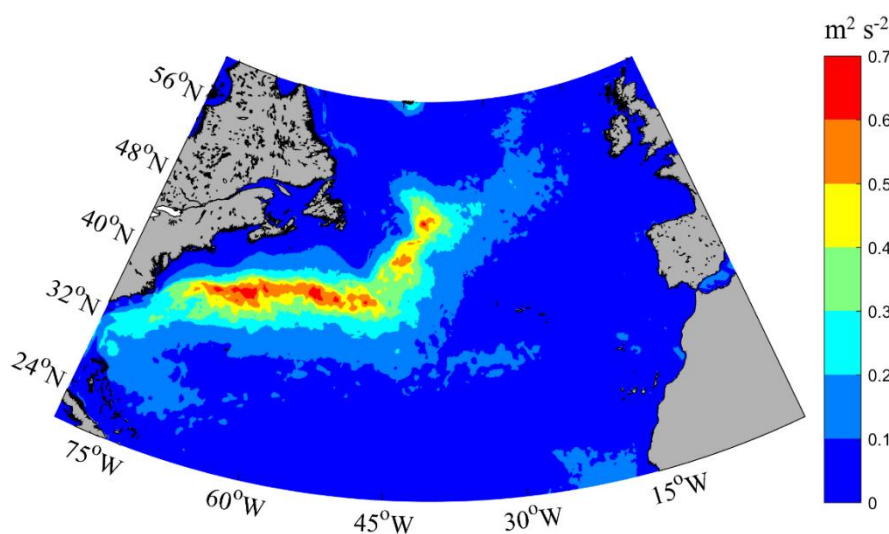


Figure 4.2. Eddy Kinetic Energy. Mean surface EKE obtained from HYCOM data with a time resolution of 3 h over the period 2006–2008.

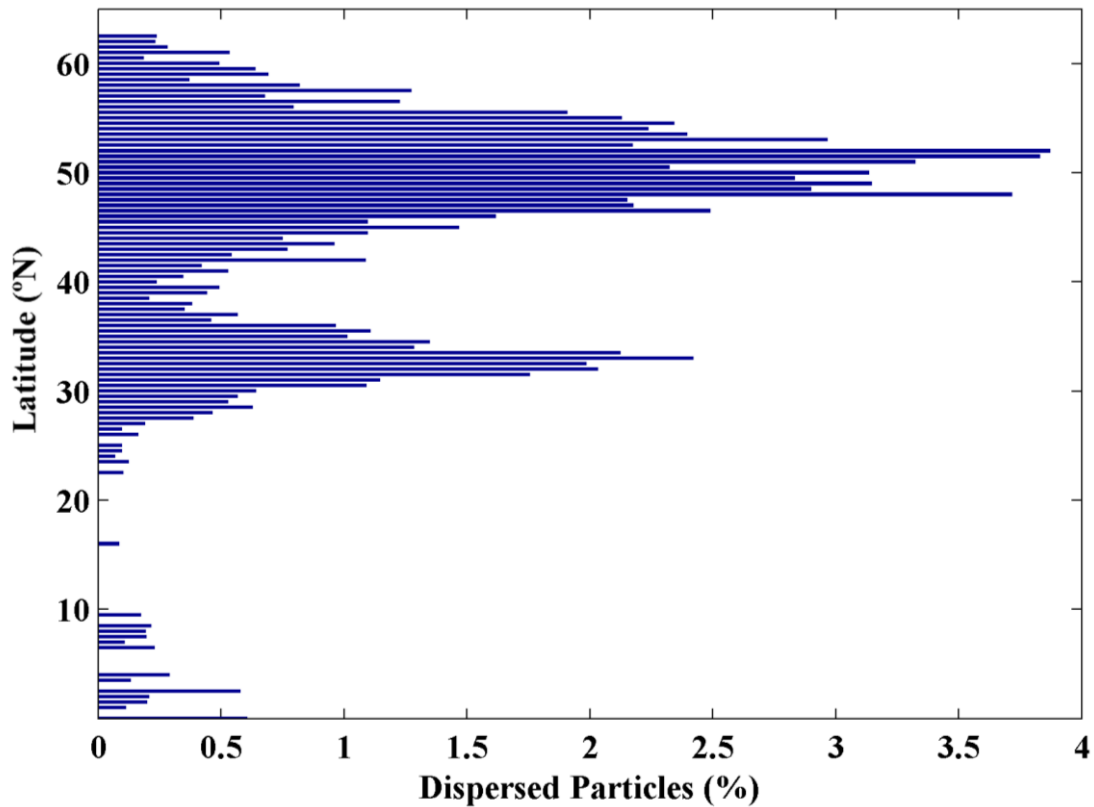


Figure 4.3. Histogram of the percentage (per latitude) of dispersed particles that have succeeded in crossing the 20°W meridian. Particles were released at the Sargasso Sea at a layer 50 m deep.

The origin of the particles that succeeded in crossing the 20°W meridian is traced back. Three subareas are considered inside the release zone at the Sargasso Sea (see Figure 4.1). Table 4.4 summarizes the obtained results.

A significant percentage of successful particles is obtained for any of the three areas. Particles released at the westernmost subarea (red) shows a higher probability of success, in good agreement with Pacariz et al., (2014). Subareas 2 (green) and 3 (blue) show similar probability of success being the easternmost subarea (blue) slightly more probable than the central one (green). In general, particles released at the westernmost subarea are dispersed northward due to the North Atlantic Current and particles released at the easternmost subarea are dispersed southward following the Azores Current.

Thus, particles released at the westernmost subarea preferentially arrive at North European coasts (from Galician to Great Britain including the Bay of Biscay; see the upper high concentration peak in Figure 4.3) and particles released at the easternmost subarea tend to reach the North African coasts (lower high concentration peak in Figure 4.3).

Depth (m)	Subarea 1 (%)	Subarea 2 (%)	Subarea 3 (%)
0	49.3	27.0	23.6
50	46.6	21.8	31.6
100	60.4	16.8	22.8
150	62.4	18.0	19.6
200	69.7	13.8	16.5
DVM	62.7	18.1	19.1

Table 4.4. Analysis of the origin of successful particles. Values indicate the origin (in percentage) of successful particles. The analysis covers the period 1996–2012. Particles were released at the Sargasso Sea in April of each year and followed for 18 months. The finish line was placed at 20°W.

4.3.2. Dependence on depth

The minimum migration time is analyzed for different depths assuming no vertical movement and passive movement in the horizontal direction. Once again, the finishing line to succeed in migration is considered at 20°W. Figure 4.4A shows the mean minimum time (T_{mean}) and its standard deviation calculated for each depth over the whole period (1996–2012). In average, the fastest migration is found at the surface layer with $T_{mean} = 260 \pm 33$ days. T_{mean} is observed to increase with depth, attaining values of 351 ± 37 days at 200 m deep.

The fastest migration for a particular year, 201 days, is also obtained at surface layer, being considerably faster than the values calculated by [Bonhommeau et al., \(2009a\)](#) who found a minimum migration time of 308 days. Results should be qualitatively independent of the particular location of the limit for successful crossing. Thus, the crossing longitude is considered at the 15°W meridian to compare our results with those by [Blanke et al., \(2012\)](#), who found the fastest Atlantic crossing to date. In average, the fastest migration in our calculations is also found at the surface layer with values on the order of ten months ($T_{mean} = 307 \pm 31$ days), being the fastest migration for a particular year of 243 days (around 8 months), which is lower than the 285 days obtained by [Blanke et al., \(2012\)](#).

The DVM strategy shows to be inefficient with $T_{mean} = 352 \pm 28$ days to attain the finishing line at 20°W, which is similar to the values shown in Figure 4.4A for a depth of 200 m. The value is even higher, $T_{mean} = 465 \pm 40$ days, when considering the finishing line at 15°W. As pointed out by [Blanke et al., \(2012\)](#) eddies can speed up the eastward spread of particles that jump from one structure to another. This mechanism is partially hindered by diel migrations since the structures at different depths cannot be coherent. Figure 4.4B shows the comparison between the annual values of T_{min} calculated assuming migration at the surface layer and with the DVM strategy for the period under study

(1996–2012). Points are always placed above the diagonal proving the lack of efficiency of the vertical movement. Other authors like [Bonhommeau et al., \(2009a\)](#) also found that the migration time increases by including active behavior.

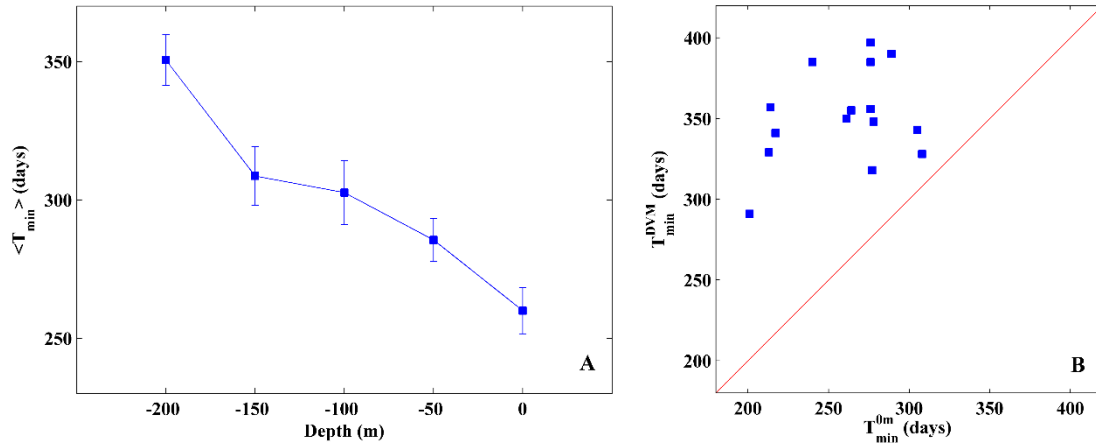


Figure 4.4. Minimum duration of migration depending on the depth. (A) Average of the minimum migration time needed to cross the Atlantic at different depths. Error bars represent the standard deviation of the mean. (B) Comparison between the minimum migration time obtained for a strategy with surface advective movement in the horizontal and no movement in the vertical (X-axis) vs the DVM strategy (Y-axis). The finish line is placed at 20°W.

4.3.3. Effect of the initial distribution

As we mentioned above, the fastest migration is obtained at the surface layer for a particular year, 1998, assuming passive movement in the horizontal direction and no vertical migration. Results shows to be qualitatively independent of the particular location of the finishing line, so the 15°W meridian has been adopted for the rest of the study.

The effect of the initial distribution is evaluated by changing the interparticle spacing (Δx_0 , Δy_0) in the release area (Sargasso Sea). Particles are initially distributed on a cartesian grid, in such a way that $\Delta x_0 = \Delta y_0$. Thus, only one coordinate (Δx_0) will be considered from now on. Δx_0 had been considered to be 0.06° in the base case, here Δx_0 is assumed to vary within the interval [0.01°, 0.25°]. Figure 4.5 shows that the migration time has a clear dependency on the initial interparticle spacing. In general, T_{min} increases with the interparticle spacing at a significant rate of 29 days per each 0.1° of increase in Δx_0 . As a rule of thumb, the finer the initial distribution the faster the migration. However, the increase is not completely monotonic, suggesting that T_{min} is actually dependent on the initial position of the particles. Small changes in the initial position led to changes in the trajectory followed by the particles. [Blanke et al., \(2012\)](#) analyzed the effect of different resolutions of the velocity field on the migration time of European eel, concluding that only databases with fine resolution (eddy-resolving models) could be able to reproduce eddy and mesoscale phenomena present in the ocean. For that reason, [Blanke et al., \(2012\)](#) considered that horizontal scale on the order of $1/12^\circ \times 1/12^\circ \times 1$ day was fine enough for Lagrangian computation. Even they affirm that switching from $1/4^\circ$ to $1/12^\circ$ does not modify much the age estimates. Thus, any resolution finer than $1/4^\circ$ can

provide reliable results. In the present study, we have considered a model (HYCOM) resolution of $1/12^\circ \times 1/12^\circ \times 1/2$ day, which are well suited to evaluate dispersion trajectories and migration times, even when diel vertical migration is implemented. In addition, we have proved that, even when the velocity field is fine enough, the initial distribution of particles can also play an important role, especially when the fastest migrations are analyzed. Finally, from a practical point of view, the distribution used for the base case ($\Delta x_0 = 0.06^\circ$) seems to be fine enough and it has been adopted for the rest of the study.

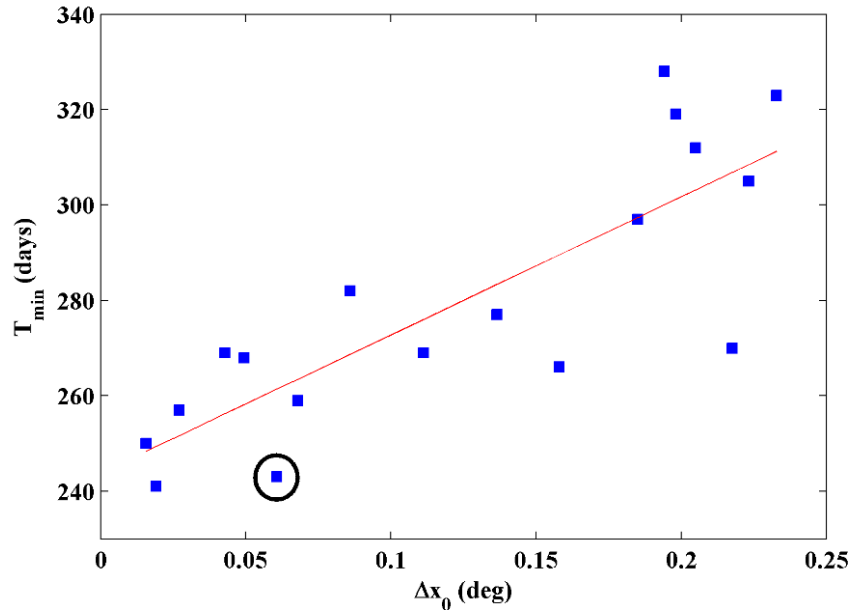


Figure 4.5. Minimum duration of migration depending on the initial distribution. Dependence of the minimum migration time needed to cross the Atlantic on the initial interparticle spacing. The black circle represents the initial interparticle spacing used for the base case. Particles are released in April 1998 and the finishing line is placed at 15°W .

4.3.4. Random walk effect

Finally, the effect of the constant of randomness is also evaluated. Once again, the year of the fastest migration is considered to analyze whether or not the active movement of larvae can decrease the migration time. Following the results shown in previous subsection, the initial distribution of the base case ($\Delta x_0 = 0.06^\circ$) is considered and different random processes are analyzed. Note that the existence of random terms can result in a different evolution starting from the same initial configuration. So, each case is run fifty times to increase the robustness of the obtained results.

Assuming the fully random case described above, the minimum migration time needed to cross the 15°W meridian (Figure 4.6A) is in average 262 ± 3 days, which is 20 days longer than the base case (243 days). Nevertheless, not all the realizations are necessarily slower. In fact, a few realizations provide a faster migration than obtained with the base case. This improvement is of 20 days in the most favorable case. In addition, results do not vary with the degree of randomness since even the smallest noise can lead to a similar

loss of efficiency in crossing the Atlantic. To sum up, this active behavior seems to be an inefficient strategy.

Results are different when assuming the downstream swimming strategy (Figure 4.6B). In average, the strategy is also less effective than the passive behavior, $T_{mean} = 256 \pm 4$ days which is around 13 days longer than the base case (243 days), although it is more efficient than the fully random movement described above. Even if downstream swimming is inefficient in average, a non-negligible number of realizations show to be faster than the base case. Thus, the fastest crossing is achieved in just 204 days (approximately 7 months). This strategy, which seems more natural since larvae take advantage of the existing velocity field to swim, can provide crossing durations comparable to the shortest ones obtained from the measurement of the otoliths of captured individuals. Even if the random movement is extremely simplified since it considers the same volitive movement of larvae (the same randomness constant) no matter their age, it suggests that the downstream swimming strategy can result in faster crossing. Although is a well-known fact that eel leptocephali do not possess developed muscles for continuous swimming (Leonard and Summers, 1976; McCleave et al., 1998) and that the energy expenditure needed to maintain such activity can be extremely high, this current oriented swimming can lead to a less energetic and more affordable strategy.

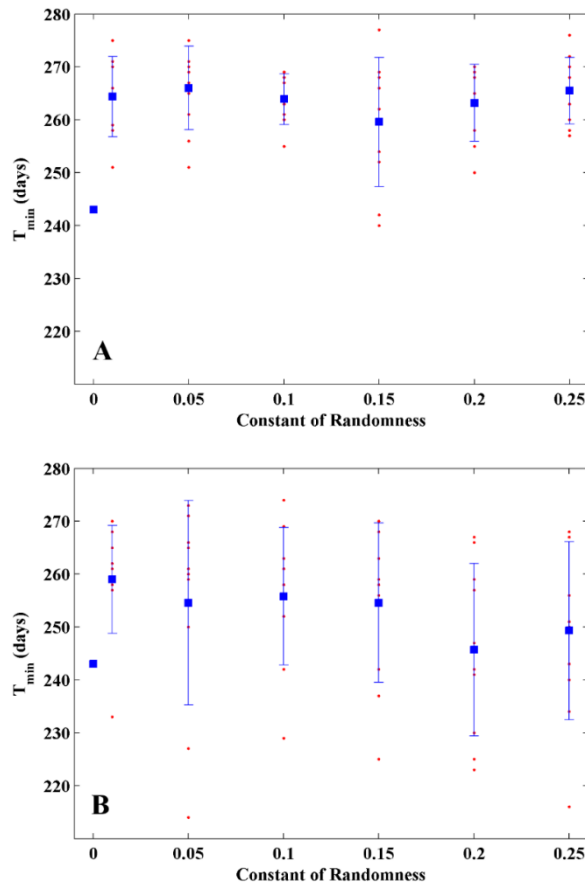


Figure 4.6. Minimum duration of migration depending on randomness. Dependence of the minimum migration time needed to cross the Atlantic on randomness. (A) Fully random process. (B) Downstream swimming strategy. Particles were released in April 1998 and the finishing line was placed at 15°W .

4.4. Conclusions

The minimum migration time to cross the North Atlantic Ocean for particles released at the Sargasso Sea has been analyzed. The main results can be summarized as follows:

- a) The minimum time needed for passive larvae to cross the Atlantic (T_{min}) till the 15°W meridian is on the order of 8 months (243 days).
- b) Minimum migration time has shown to be sensitive to depth, migration strategies (some of them involving the volitive movement of larvae) and initial distribution of particles.
- c) Larvae travel faster near surface. Actually, T_{min} is observed to increase with depth.
- d) The initial distribution of particles also influences T_{min} . In general, the lower the initial interparticle spacing the lower the time needed to cross the Atlantic. In addition, migration is also dependent on the particular initial location of tracers.
- e) Multilayer migration, using different depths at day and night, show to be slower than migration at a single layer.
- f) Active migration strategies based on the random walk of larvae superimposed to the movement induced by currents show to be, in average, slower than purely advective migration. Nevertheless, for particular realizations the so called downstream swimming strategy shows to be very fast, giving rise to T_{min} values on the order of just 7 months, which are comparable to the shortest ones obtained from the analysis of the microstructure of eel otoliths.

Chapter 5

On the connectivity of *Panulirus penicillatus* populations in the Indian Ocean

5.1. Motivation

Some lobsters of the Palinuridae family have their habitat into the Indian Ocean system. They are characterized by long larval stages which can last for 1 year or longer (Booth, 1986; Pitcher, 1993; Booth and Phillips, 1994; Kittaka et al., 2005; Phillips et al., 2006). The dispersion of these lobsters, like the spiny lobster *Panulirus penicillatus* (widely distributed into the Indian Ocean), depends not only on the velocity of the oceanic currents but also on biological parameters like the spawning season and the PLD. Previous genetic study carried out by Abdullah et al., (2014) on the geographic structure and genetic diversity of the spiny lobster *Panulirus penicillatus* in the Indian Ocean has highlighted the interconnection among populations located at different areas, pointing out that gene flow can be probably due to the effect of prevailing ocean currents during the larval stage. They found a geographic structure of two main groups: the first one located at the Red Sea and the second one at other locations of the Indian Ocean covering Java, Aceh, Maldives and Madagascar. All the populations at these distant locations are related among them suggesting the existence of an important gene flow.

However, the suggestion of an interconnection pattern among populations generated by ocean currents is not so straightforward due to the migration pattern of the spiny lobster *Panulirus penicillatus*. Indeed, spiny lobsters prefer deeper depths during daylight and the opposite during nighttime (Pitcher, 1933; Feng et al., 2011; Griffin et al., 2001; Minami et al., 2001; Bradford et al., 2005). Thus, this diurnal migration pattern affects the migrations trajectories of *Panulirus penicillatus* larvae.

The aim of this chapter is to analyze the possible connectivity among populations of larvae in the Indian Ocean over the period 1958-2008 using the particle tracking model described in Chapter 2 and the velocity fields from SODA database (Rodríguez-Díaz et al., submitted manuscript)

5.1.1. The Indian Ocean

The area selected for this study covers the entire Indian Ocean. Following Abdullah et al., (2014), particles are released at five different positions marked with red squares ($5^\circ \times 5^\circ$) in Figure 5.1. Despite squares cover land and ocean, particles are only released at ocean locations.

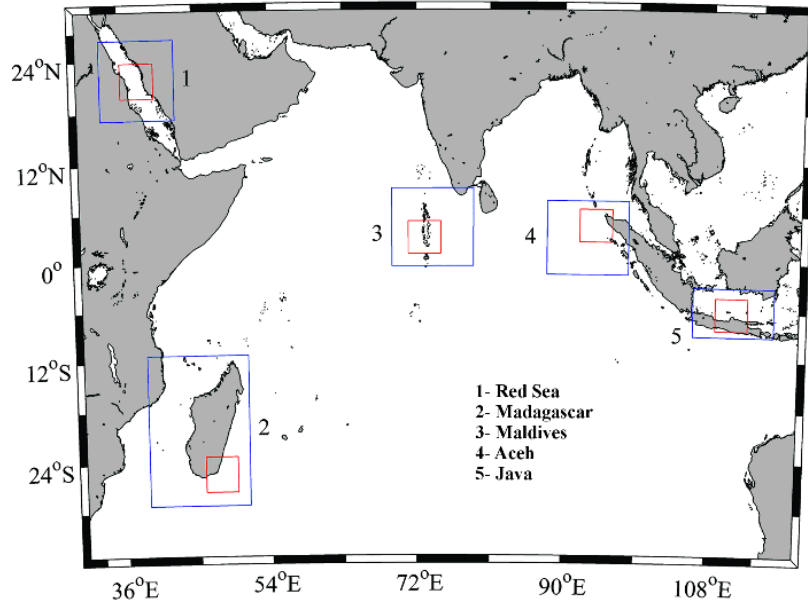


Figure 5.1. Region under scope. The map of the Indian Ocean and the release areas (red) and target areas (blue) are shown.

The Indian Ocean Surface Currents system (Figure 5.2) is characterized by numerous currents namely: the Leeuwin Current (LC), South Java Current (SJC), East Indian Current (EIC), East Arabian Current (EAC), South Equatorial Current (SEC), Northeast and Southeast Madagascar Current (NEMC and SEMC), Somalia Current (SC), East African Coast Current (EACC), South Equatorial Countercurrent (SECC) and Southwest (during summer monsoon) and Northeast (during winter monsoon) Monsoon Current (SMC and NMC) (Shenoi et al., 1999; Brown et al., 2001; Schott and McCreary, 2001). One of the main features of the area is the current system seasonality characterized by the reversal of the Somali Current flowing southwestward during winter months and northeastward the rest of the year.

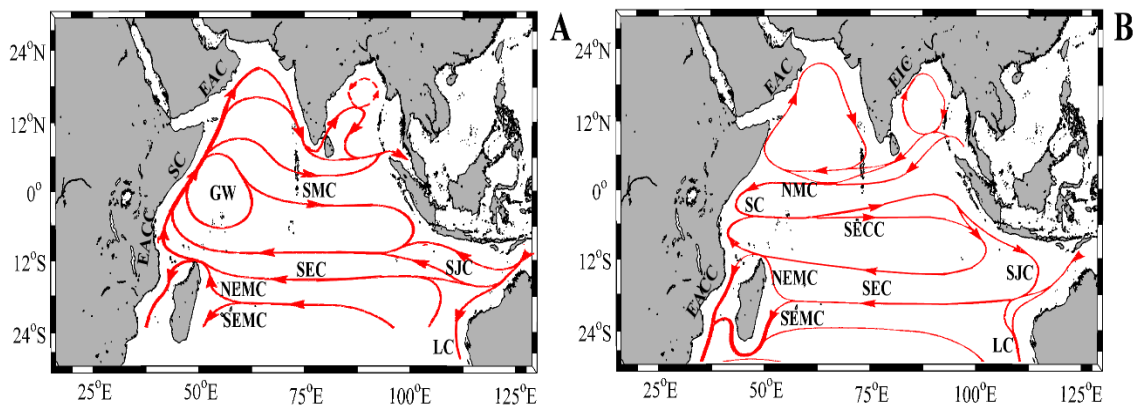


Figure 5.2. Surface system current of the Indian Ocean. (A) Summer monsoon. (B) Winter monsoon. Abbreviations refer to the Leeuwin Current (LC), South Java Current (SJC), South Equatorial Current (SEC), Northeast and Southeast Madagascar Current (NEMC and SEMC), Somalia Current (SC), East African Coast Current (EACC), South Equatorial Countercurrent (SECC), Southwest and Northeast Monsoon Current (SMC and NMC), The Great Whirl (GW), East Indian Current (EIC) and East Arabian Current (EAC). This figure was adapted from Tomczak and Godfrey (2003).

5.2. Material and methods

5.2.1 Data

In *Chapter 2* it was explained in detail the data used in the present study. In this section, only a summary is presented in table 5.1.

DATA	OBSERVATION	SOURCE
U, V velocity	Period 1958-2008. Data from 2 levels: 5 m and 100 m	SODA version 2.1.6

Table 5.1. Summary of data used in the study. Additional information is included in the observation column and the data source.

5.2.2 Lagrangian model

Simulations are run using the particle tracking model, described in *Chapter 2*, to track passive particles and study their dispersion in the Indian Ocean. Table 5.2 summarizes the initial conditions of the simulations. The release areas are centered on the five positions (Red Sea, Madagascar, Maldives, Aceh and Java) described by [Abdullah et al., \(2014\)](#) and represent the location of particles at the beginning of the simulation. The target areas (blue) were defined to analyze the percentage of particles released at position α that succeeded in reaching a certain location β . A particle success in reaching a target area if it is inside that area at any time during the simulation. It should be noted that the particles do not necessarily stay at that target area at the end of the simulation since the simple passage through that area can ensure gene flow. A sensitivity analysis is carried out in order to determine the extent of the target areas. Areas around $10^\circ \times 10^\circ$ are optimal to identify target sites. No significant differences in the percentage of succeeding particles are observed considering target areas a bit smaller or bigger.

Release dates (May-September for North Hemisphere and November-March for South Hemisphere) are chosen according to the spawning period of the spiny lobster *Panulirus penicillatus* which mainly occurs during summer months at each hemisphere ([MacDonald, 1979, 1988](#); [Junio, 1987](#); [Plaut, 1993](#); [Chang et al., 2007](#); [Sabatini et al., 2008](#); [Pakoa et al., 2012](#); [Milton et al., 2014](#)). Previous studies focused on the spiny lobster *Panulirus penicillatus*, established a larval duration around 9 months ([Johnson, 1968](#); [Matsuda et al., 2006](#)), which is also assumed in this study.

Panulirus penicillatus, as it is common in spiny lobsters' larvae, is characterized by a migration pattern ([Pitcher, 1933](#), [Silvestre and Pauly, 1997](#); [Griffin et al., 2001](#), [Minami et al., 2001](#); [Coutures, 2003](#); [Bradford et al., 2005](#); [Chang et al., 2007](#); [Feng et al., 2011](#)).

Thus, particles are initially released during nighttime at a fixed depth of 5 m (Dennis et al., 2001). In addition, a daylight depth of 100 m (Feng et al., 2011) is established following Milton et al., (2014). Changes in maximum depth attained during different larval stages (Buttler et al., 2011) were not considered following Milton et al., (2014).

Particles do not undergo chemical or biological processes such as mortality (Rudorff et al., 2009) that can influence larval concentration. However, the main goal of the present study is to analyze the possible connections between populations of the *Panulirus penicillatus* in the Indian Ocean, not the real amount of larvae that arrive at a certain target area. Consequently, mortality is not considered (Cowen et al., 2000; Bonhommeau et al., 2009a; Rudorff et al., 2009).

The time step (Δt) is calculated to meet the CFL criterion (Courant et al., 1928, 1967; Pacariz et al., 2014), based on the fact that the time spent by a particle to go over 0.5° (grid size) must be bigger than the time step. Time steps are on the order of 4 hours depending on the particular features of every calculation.

In summary, Lagrangian simulations are carried out every year over the period 1958-2008 assuming 5 different initial locations and 5 release months (November-March for the Southern Hemisphere and March-September for the Northern Hemisphere). Runs last 9 months matching the PLD of the species under study. This involves 250,000 passive particles per year (more than 10 million during the whole period).

CONDITION	VALUE	OBSRVATIONS
Release area	Red Sea Madagascar Maldives Aceh Java	Abdullah et al., (2014)
Depth (m)	Daylight depth: 100 m Nighttime depth: 5 m	DVM
Release date	May-September November-March	Spawning season
Duration of each simulation	9 months	Johnson, (1968) Matsuda et al., (2006)
Release type	Instantaneous	
Number of releases	1	At each release area and season which means a total of 25 releases

Number of particles	5,000	Initially released at each release area and depth
t_{rec}	15 days	
Δt	4 h	Automatically calculated
dx⁰	1° x 1°	Initial interparticle spacing
Randomness	full	
Constant of randomness	0.25	
Vertical migration	Yes	DVM
Mortality	No	Cowen et al., (2000) Bonhommeau et al. (2009a) Rudorff et al., (2009)

Table 5.2. Initial conditions. Summary of the conditions used to run the simulations.

5.3 Results and discussion

5.3.1. Indian Ocean surface current system

The main currents that characterize the circulation in the Indian Ocean are described in multiple text books and research papers (see, for example, [Schott and McCreary, 2001](#)). Nevertheless, the provided picture is rather schematic and mainly reflects the behavior during the winter and summer monsoon. To obtain an in-deep knowledge on currents at near surface and at 100 m we have averaged the velocity field provided by SODA over the period of study.

This average is carried out at seasonal scale due to the remarkable intra-annual variability in the zone (Figure 5.3). Arrows mark the mean intensity and direction of the currents. Colors only indicate the zonal component of velocity to highlight the different currents crossing the Indian Ocean, which are the main driver of larvae drift among zones.

Overall, at the surface layer, the situation during winter monsoon (Figure 5.3A) is characterized by an eastward current (red) crossing the Indian Ocean near the Equator and two westward currents (blue) under and above the Equator. During the inter-monsoon period (AMJ in Figure 5.3C and OND in Figure 5.3G), there is a westward current between 5 and 15°S and an eastward current between 5°S and 5°N. The most complex

situation is observed during summer monsoon (Figure 5.3E), characterized by two westward currents (between 5 and 15°S and slightly north of Equator, respectively) and an eastward current displaced farther north. The Great Whirl, one of the most conspicuous features in the area (Beal and Donahue, 2013; Santos et al., 2015), is clearly patent near the coast of Somalia. In spite of the importance of this structure at regional level, it has little influence on the migration of larvae across the Indian Ocean.

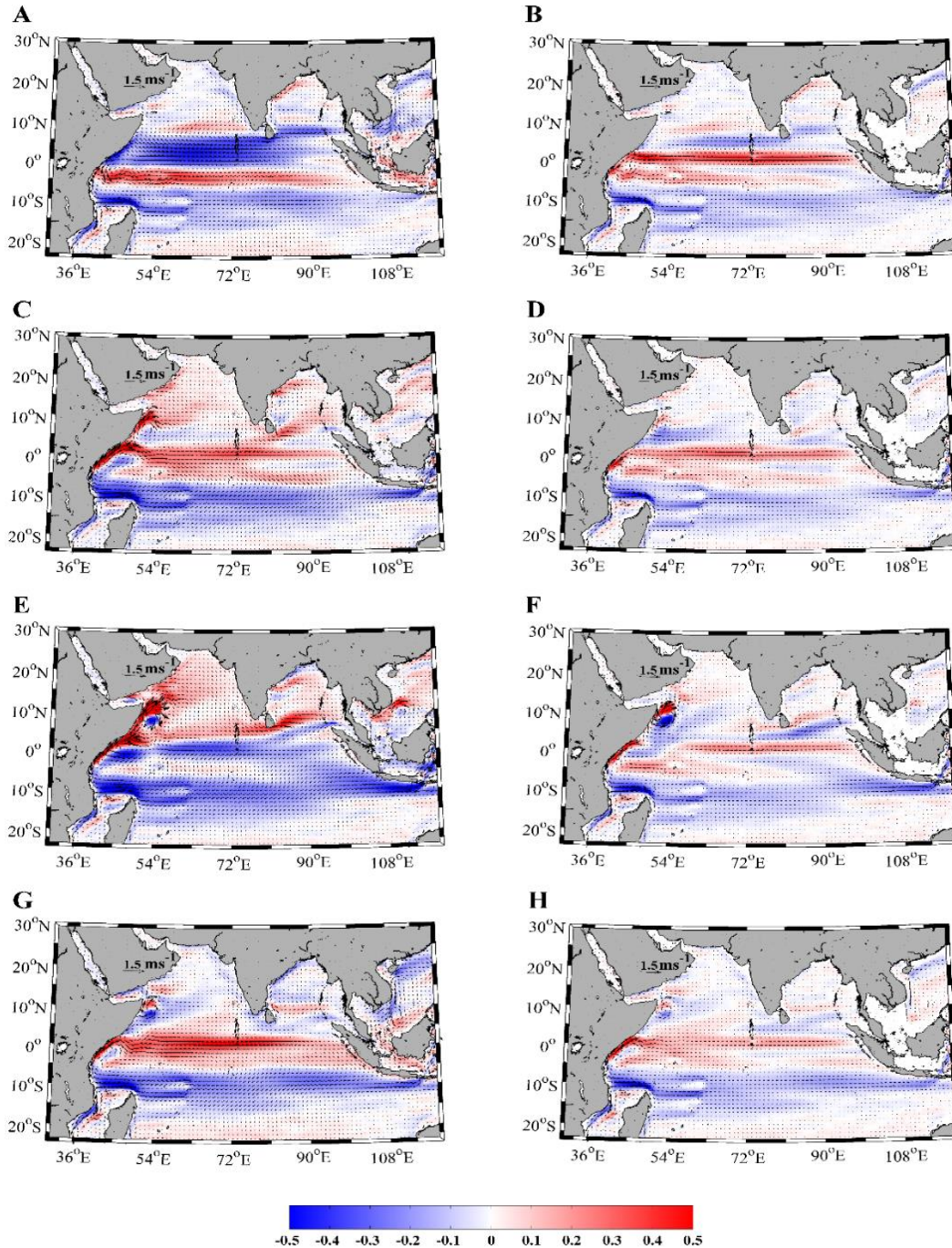


Figure 5.3. Seasonal average velocity of Indian Ocean surface and 100 m currents. The velocity field of Indian Ocean currents is averaged by seasons over the period of study 1958-2008 at the surface layer (A, C, E, and G) and at 100 m (B, D, F and H). Colors only apply to the zonal component of velocity. (A and B) Winter (January to March). (C and D) Spring (April to June). (E and F) Summer (July to September). (G and H) Autumn (October to December).

Overall, currents are weaker at 100 m (Figure 5.3B, D, F, H) and do not present remarkable seasonal variations as observed at the surface layer. The situation during winter monsoon (Figure 5.3B) and inter-monsoon periods (Figure 5.3D, H) is mostly characterized by an eastward current crossing the Indian Ocean near the Equator and two westward currents south and north of the Equator. During summer monsoon (Figure 5.3F) the situation is characterized by an eastward current (near and slightly south of the Equator) and two westward currents (between 0 and 10°N and between 5 and 20°S respectively). Regarding the Great Whirl, it is still patent but markedly smaller compared to the surface layer.

5.3.2. Red Sea

It is possible to observe how the Red Sea, the north-easternmost location, is completely isolated from the rest of the areas. Indeed 93.0% of the particles released from Red Sea remain in this area during the whole calculation (Table 5.3). The Mandeb Strait, which connects the Red Sea with the Gulf of Aden, acts like a barrier for the oceanic currents blocking the dispersal of particles. The remaining particles (~10%) leave the area but do not attain any of the target areas. The percentage of particles that remains close to the release area is markedly lower for the rest of the zones, namely, 21.1% for Madagascar, 19.0% for Maldives, 29.3% for Aceh and 35.2% for Java (see Table 5.3).

		RELEASE				
		RED SEA	MALDIVES	ACEH	MADAGASCAR	JAVA
T A R G E T	JAVA	--	--	5.7 ± 0.6	--	35.2 ± 0.8
	MADAGASCAR	--	--	-	21.1 ± 0.6	--
	ACEH	--	28.2 ± 1.7	29.3 ± 1.0	--	--
	MALDIVES	--	19.0 ± 0.8	13.1 ± 0.8	--	--
	RED SEA	93.0 ± 0.4	--	--	--	--

Table 5.3 Mean and standard deviation performed for all simulated cases. Mean indicates the percentage of particles that have remained in the release areas and/or have succeeded in reach the target areas over the period of study (1958-2008). Only mean values > 5% are shown.

5.3.3. Madagascar

Particles released from Madagascar do not reach other target areas. The SEMC and the Agulhas Current (AC) are the main currents around the release area of Madagascar. The SEMC flows south along the east coast of Madagascar to connect with the AC at Cape Saint Marie then it continues flowing south along the east coast of Africa. Therefore, the scattering of the passive tracers released from Madagascar follows an opposite direction respect to the position of the target areas. The distribution of particles (in percentage) released from Madagascar in December is shown in Figure 5.4. Particles are tracked

fortnightly since the instant of release. The pattern is similar for particles released over the period November-March.

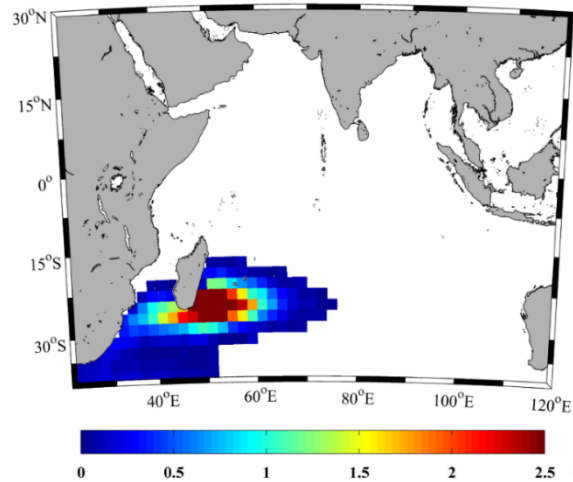


Figure 5.4. Distribution of particles released from Madagascar. The percentage of particles dispersed is shown for those particles released from Madagascar in December over the period of study (1958-2008).

5.3.4. Java

Particles released from Java do not attain other target areas. Most of them move to the northwestern coast of Australia and to the Pacific Ocean through the Java Sea. The distribution of particles (in percentage) released from Java in December is shown in Figure 5.5. The pattern is similar for particles released over the period November-March. Java shows a relatively high percentage of particles (35.2% in Table 5.3) remaining in the release region. Previous research (Milton et al., 2014) also found a considerable percentage of *Panulirus penicillatus* lobsters spawned in south coast of Java that contributed to their recruitment. They also show the importance of local and regional sources. Note that the spawning season of lobsters in Java coincides with the monsoon. In such a way that the response of the current to monsoon winds (Sofian, 2007; Mayer et al., 2010; Schiller et al., 2010; Ogata and Masumoto, 2011), can explain this result (Milton et al., 2014).

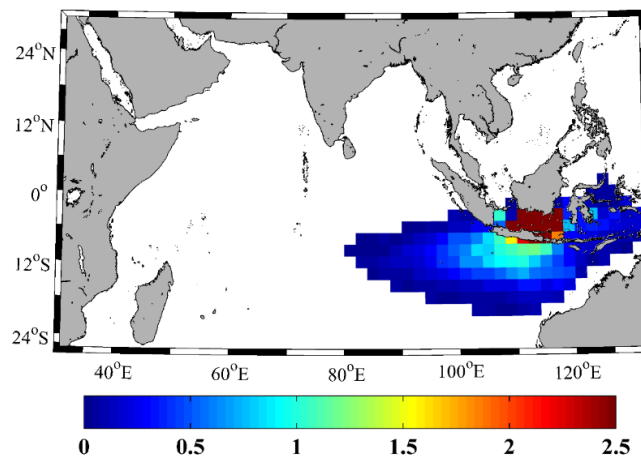


Figure 5.5. Distribution of particles released from Java. The percentage of particles dispersed is shown for those particles released from Java in December over the period of study (1958-2008).

5.3.5. Maldives

Maldives shows a direct exchange with Aceh (Table 5.3). Thus, 28.2% of the particles released from Maldives attains Aceh. The distribution of particles released from Maldives is shown (in percentage) in Figure 5.6. Figure 5.6A corresponds to the distribution of the particles released in June over the period 1958-2008. Particles can be observed at practically every location in the Indian Ocean between 18°S and 18°N. Thus, larvae from Maldives can potentially arrive at Aceh and Java through a straightforward migration. Previous studies (Abdullah et al., 2014) also found a genetic connection between larvae from Maldives and Madagascar. However, the results of the present study do not show a direct connection between both areas. This is possibly due to the migration pattern of *Panulirus penicillatus* larvae since velocities at 100 m are considerably smaller than near surface. Actually, considering a different migration strategy (larvae drifting at surface layer without vertical migration), the direct connection between Maldives and Madagascar is re-established (not shown). Connection between both areas is possible assuming a migration by stages from Maldives to islands like Seychelles (where *Panulirus penicillatus* is one of the main spiny lobster in the area (Govinden and Hollanda, 2013)) and from these islands to Madagascar, which would explain results from Abdullah et al., (2014).

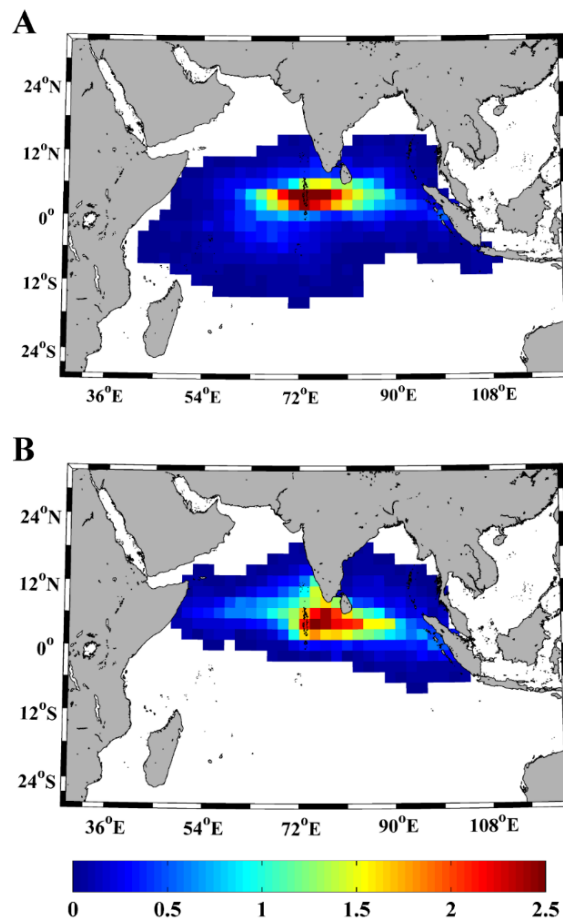


Figure 5.6. Distribution of particles released from Maldives. The percentage of particles dispersed is shown for those particles released from Maldives over the period of study (1958-2008). (A) June. (B) September.

In the pattern corresponding to the particles released in June (Figure 5.6A), most of the initial displacement (first 3 months) take place under the influence of summer Monsoon (Figure 5.3E, F). The area of Maldives, where particles are released, splits into two zones: the northern one characterized by a strong eastward current mainly at the surface layer (Figure 5.3E) and the southern one characterized by a westward current which becomes weaker at 100 m and even reverses at the equatorial band. Thus, larvae are dispersed in both directions during their first stages. During the second trimester after release, the prevalent oceanographic conditions are depicted in Figure 5.3G, H. There, most of particles located at equatorial latitudes, drift eastward (both at surface layer and at 100 m) increasing the migration toward Aceh. The pattern corresponding to the particles released in September (Figure 5.6B) presents some different features. Particles released from Maldives do not longer attain Madagascar and Java due to changes in the circulation patterns. Now, larvae drift during their early stages (3 months) under the oceanographic conditions depicted in Figure 5.3G, H, where most of the circulation at Maldives area is under the influence of eastward currents, increasing the percentage of particles attaining Aceh. During the following stage (second trimester after release, Figure 5.3A, B), the winter monsoon conditions are prevalent, which results in a westward displacement of particles North of Equator both at surface and at 100 m. However, the circulation at 100 m is characterized by a strong eastward current at the Equator. As a result, particles cover most of the North Indian Ocean and even the Bay of Bengal. As for the rest of months (not shown) May and July are similar to June, and August shows an intermediate situation between June and September.

5.3.6. Aceh

Aceh also shows an important exchange with neighbor areas (see Table 5.3). Thus, particles released from Aceh are observed to reach both Maldives (13.1%) and Java (5.7%). In particular, larvae released in June (Figure 5.7A) move in all directions following the pattern characteristic of summer Monsoon (Figure 5.3E, F). Some particles follow the westward branch that starts from the northern part of Sumatra and crosses the North Indian Ocean (both at the surface and at 100 m). In addition, there is a southward current along the western coast of Sumatra, which becomes stronger at 100 m connected to the eastward equatorial current, forcing particles to follow the shoreline. Particles released in September follow a different pattern (Figure 5.7B). On the one hand, the westward spread of particles, mainly west of Maldives, is higher and, on the other hand, the percentage of particles reaching Java is smaller at the expense of the percentage of particles covering the Bay of Bengal. These facts are due to the eastward current North of Equator over the period October to December (see Figure 5.3G, H) which becomes weaker and even opposite at some longitudes at 100 m. In addition, during winter monsoon (see Figure 5.3A, B) a westward current prevails north of Equator crossing the North Indian Ocean and penetrating inside the Bay of Bengal. As for the rest of months (not shown) May is similar to June, August is similar to September and July shows an intermediate situation.

Once the connectivity among regions is proved, the following step is to elucidate whether or not the connectivity among areas has changed over the period under study. Results are summarized in Table 5.4. The number of particles released from Maldives that reached Aceh has shown an increasing trend of 6.5% per decade. The particles moving from Aceh to Java has shown an increasing trend of 1.4% per decade. All trends are significant at a significance level >95%.

	Trend (% per decade)	Significant level (%)
MALDIVES		
ACEH	6.5	> 99
ACEH		
JAVA	1.4	> 99

Table 5.4. Statistical analysis performed for particles released from Maldives and Aceh. Trend indicates the increase (in percentage per decade) in the number of particles that have succeeded in reaching the target areas. The significance level was calculated using the Spearman correlation.

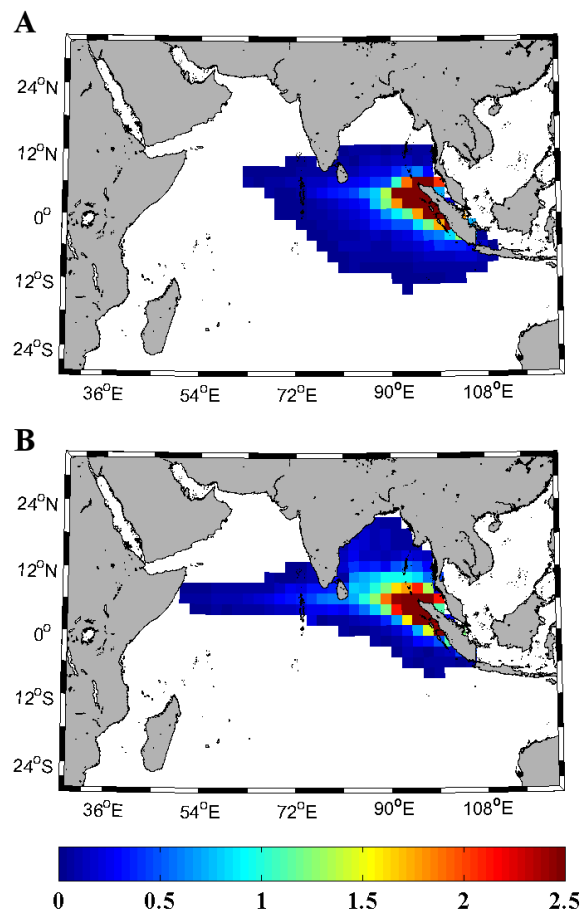


Figure 5.7 Distribution of particles released from Aceh. The percentage of particles dispersed is shown for the particles released from Aceh over the period of study (1958-2008). (A) June. (B) September.

5.4 Conclusions

First of all, Figure 5.8 shows the sketch of migration paths obtained in the present study.

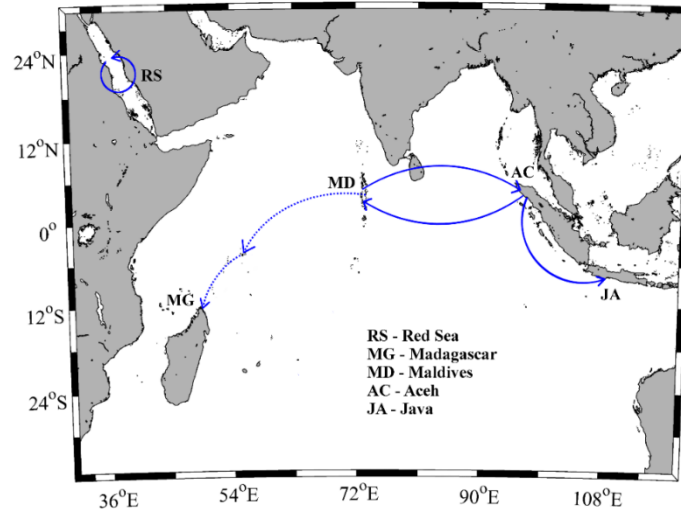


Figure 5.8. Sketch of migration paths. Solid color lines represent the connection between areas due to a direct migration. The dashed line represents the possible connection between Maldives and Madagascar due to a migration by stages. The circular arrow over the Red Sea represents the isolation of this area.

In addition, the main findings of the present work can be summarized as follows:

- a) Passive tracers have been used to mimic the drift of larvae during their larval stages that can last up to 9 months.
- b) Five different releasing points (Red Sea, Madagascar, Maldives, Aceh and Java) have been considered following (Abdullah et al., 2014) who analyzed the genetic connectivity among different lobster populations in the Indian Ocean.
- c) The drift of these passive tracers shows that the Red Sea area is completely isolated from the rest whilst the other areas can potentially exchange genetic information.
- d) Particles released in Maldives can reach Aceh and Java through a straightforward migration and probably Madagascar through a migration by stages. Those particles released in Aceh can reach Maldives and Java. Madagascar and Java can receive particles from other locations but particles released from these locations cannot reach the rest. The observed connections are in good agreement with the prevalent surface currents. See Figure 5.8 where the sketch of migration paths is shown.
- e) Trends show that connectivity from Maldives to Aceh has increased over the period 1958-2008.

Chapter 6

On the use of Lagrangian to identify drivers in SST warming

6.1. Motivation

Sea Surface Temperature (SST) has shown a strong warming since the 1980s (IPCC, 2013) due to the increase in the heat content of the Earth, which has been mainly absorbed by oceans (Church et al., 2011; Levitus et al., 2012). Although SST warming has been the dominant trend in all basins, variations are highly dependent on time and spatial scales. Thus, the sign of the trend can change depending on the decades considered (deCastro et al., 2009; Gouretski et al., 2012) and on the season of the year examined (Costoya et al., 2015). Regarding spatial scales, warming rates change from basin to basin (Levitus et al., 2012) being variations more marked at regional scales.

Trends in coastal areas have also shown high spatial heterogeneity over the last three decades (Lima and Wethey, 2012). Coastal areas can be subjected to different driver favoring different warming pattern when compared with oceanic areas. The main factors contributing to the different behavior are: freshwater inputs (e.g: Howden and Murtugudde, 2001; Vizu and Cook, 2010; Park et al., 2011; Matera et al., 2012; White and Toumi, 2014; Costoya et al., 2016), upwelling (e.g: Relvas et al., 2009; Santos et al., 2012a, b, c, 2015; Varela et al., 2015) or the presence of transitional water bodies (e.g: Kozlov et al., 2014). These forcing in combination with global warming can modulate or even reverse SST trend depending on the coastal area and the season considered.

The aim of this study is to investigate the SST in the Northwestern part of the Gulf of Mexico from 80s to nowadays as well as the influence of the plume formed by the Mississippi-Atchafalaya (MA) River system on it (Fernández-Nóvoa et al., submitted manuscript, 2018). In addition, factors able to determine the plume dynamic and, therefore, to modify coastal SST, will be assessed to determine their influence. One of the methods applied will be the particle tracking model described in *Chapter 2* which will be used to analyze the currents in the area under scope. This approach proves the interest of the lagrangian models, which can be used not only to describe the transport of larvae, pollutants and debris but also constitute an alternative and complementary tool for climate studies.

6.1.1 The Mississippi-Atchafalaya River System

The area selected for this study is shown in Figure 6.1. In this area, Mississippi and Atchafalaya rivers flow into the Gulf of Mexico. Mississippi is one of the most important rivers worldwide and the largest one in North America (6,300 km), with an average discharge of about $20,000 \text{ m}^3\text{s}^{-1}$, draining approximately 41% of the continental United States (Walker et al., 2005; Zhang et al., 2012). The Mississippi splits into two distributaries upstream of the Tarbert Landing station. The Old River outflow channel, carrying one-third of the upper Mississippi River flow, merges with the Red River, near Simmesport, to form the Atchafalaya River. The MA is the seventh largest river system by water discharge ($>5 \times 10^{11} \text{ m}^3 \text{ y}^{-1}$) in the world (Milliman and Meade, 1983; Allison et al., 2012; Marta-Almeida et al., 2013). This river system provides, at Louisiana-Texas shelf, around 90% of the river discharges into the Gulf of Mexico (Androulidakis et al., 2015). The Texas-Louisiana shelf is located in the Northwestern area of the Gulf of Mexico (Figure 6.1). The width of the shelf is around 200 km in the area close to Atchafalaya bay and less than 50 km near the Mississippi River mouth (Zhang et al., 2012).

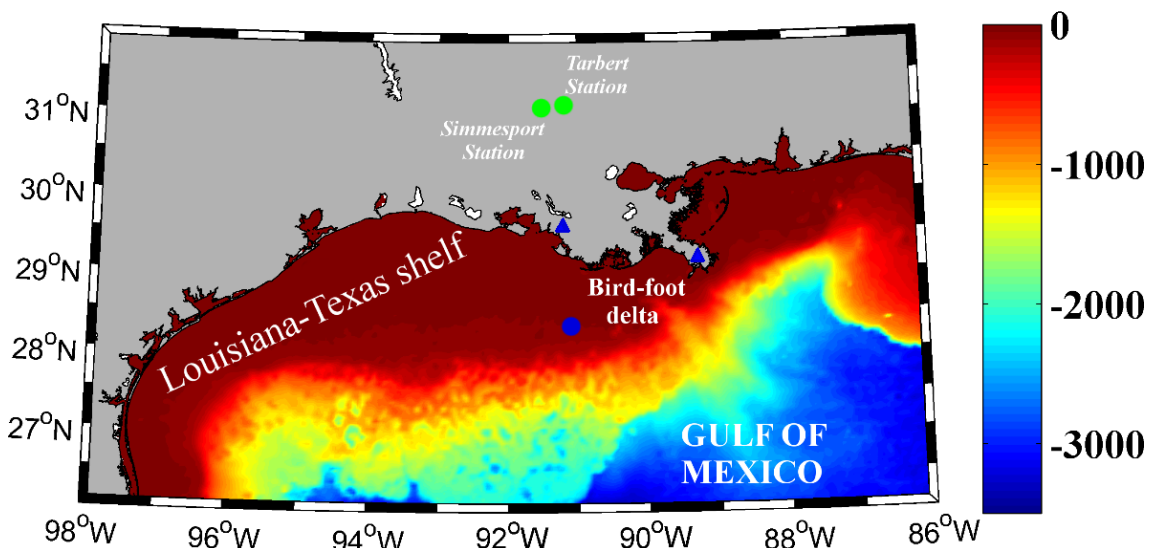


Figure 6.1. Bathymetry of the region under scope. Green dots mark the location where river discharge was sampled. Blue triangles mark the location of the main mouth of Atchafalaya and Mississippi Rivers. Blue dot marks the location where wind data were acquired.

MA River system provides an important input of freshwater, sediment, nutrients, and pollutants, causing a major impact on the parameters controlling the continental shelf oceanography in the northern Gulf of Mexico. On the one hand, the supply of nutrients enhances the phytoplankton and zooplankton productivity. This fact makes the Louisiana-Texas shelf a very productive fishery area, with around 30% of total U.S. catchment, being also the spawning area of several essential species (Walker, 1996). On the other hand, this high productivity presents some negative consequences such as a large zone of hypoxia generated during summer months leading to eutrophication (Walker, 1996). For

these reasons, it is of great importance tracking the MA plume development and its impact on the most relevant oceanic parameters.

The impact of MA River plume on different oceanic parameters was analyzed for several authors due to the great importance of the area. These studies were developed through numerical modelling (Xu et al., 2011; Hetland and DiMarco, 2012; Zhang et al., 2012; Marta-Almeida et al., 2013; Rong et al., 2014; Androulidakis et al., 2015), satellite imagery (Miller and McKee, 2004; Salisbury et al., 2004; Walker et al., 2005; Hu et al., 2005; Shi and Wang, 2009), in situ data (Corbett et al., 2004; Allison et al., 2012; Joung and Schiller, 2014) or with the combination of several of these methodologies (Kolker et al., 2014). The majority of these studies are focused on the displacement of the plume along the Louisiana-Texas shelf under different conditions and on the analysis of the plume influence on some parameters related to primary productivity.

In general, the MA plume tends to be displaced to the west due to the buoyant forcing and the predominant east component of the winds, especially during non-summer months. This westward transport is reduced during summer due to the predominant, although weak, upwelling favorable winds (Walker et al., 2005; Marta-Almeida et al., 2013). The Loop Current and eddies (Figure 6.2) can also affect the river plume in the vicinity of the Mississippi delta especially under conditions favoring the offshore movement of the plume.

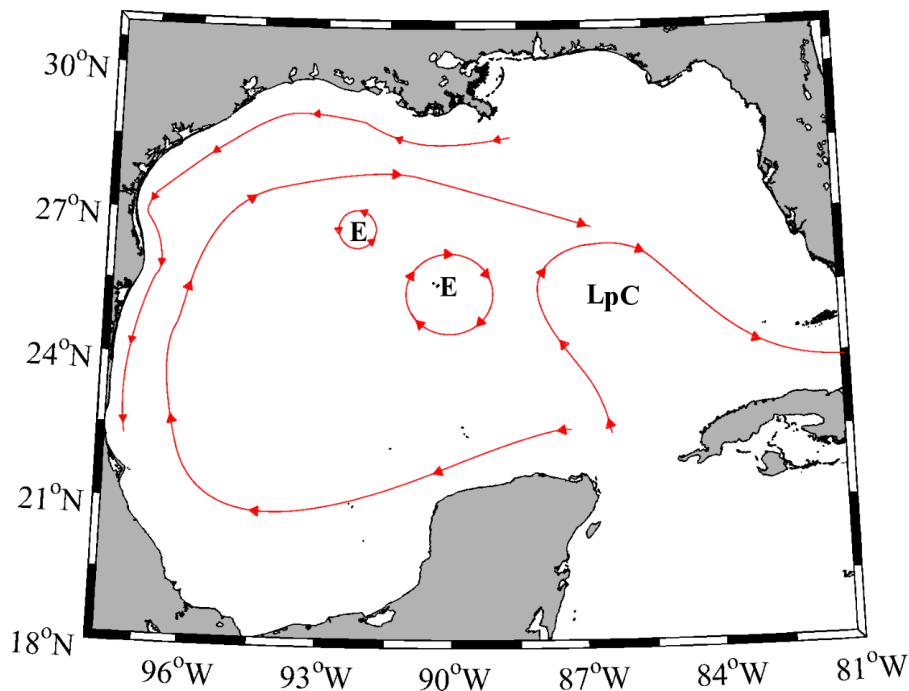


Figure 6.2. Sketch of the surface currents in the Gulf of Mexico. Abbreviations refer to Loop Current (LpC) and eddies (E). The figure was adapted from NOAA: (https://flowergarden.noaa.gov/image_library/regionmaps.html).

6.2. Material and methods

6.2.1. Data

The databases used in the present study were explained in detail in *Chapter 2: Section 2.2 “Data”*. In this section, only a summary is presented in table 6.1.

DATA	OBSERVATION	SOURCE
SST	Satellite SST data from the AVHRR sensor: daily files for the period 1982-2015.	Daily OISST _{1/4} (Version 2)
Radiance	Data from the band centered on 645 nm for the period 2003-2015. Turbid threshold of $0.25 \text{ mW cm}^{-2} \mu\text{m}^{-1} \text{ sr}^{-1}$	MODIS
River discharge	Daily data for Mississippi and Atchafalaya Rivers for the period 1982-2015.	Mississippi River: Taber Landing station. Atchafalaya River: Simmesport
Wind	Data at a reference height of 10m since January 1982.	CFSR
Salinity	Period 1993-2015.	
Water temperature	Salinity and temperature data till a depth of 10m.	HYCOM GLBu0.08
U, V velocity	Velocity data at surface layer.	

Table 6.1. Summary of data used in the study. Additional information is included in the observation column and data source.

6.2.2. Lagrangian model

The particle tracking model, described in *Chapter 2: Section 2.1 “Particle tracking model”*, based on velocities derived from HYCOM database is applied to analyze the dispersion of passive particles in the MA River plume area. In this particular implementation, particles are released at two areas chosen to fit the mouths of Atchafalaya

and Mississippi rivers with an initial interparticle spacing of $0.01^\circ \times 0.01^\circ$. Particles are released at surface layer every day and tracked during 60 days recording their position every day. Table 6.2 summarizes the initial conditions considered for our simulations.

CONDITION	VALUE	OBSERVATIONS
Release area	Polygonal area	Mouth of Atchafalaya river
	Polygonal area	Mouth of Mississippi river
Depths (m)	0	Surface
Release date	November to February	Period of interest
Duration of each simulation	6 months	---
Release type	Periodic	Release type
Number of releases	120	
Number of particles	2,649	Initially released at the mouth of Atchafalaya river
	4,996	Initially released at the mouth of Mississippi river
t_{release}	Daily	During the period of interest: release date
t_{rec}	Daily	
t_{flying}	60 days	Enough time to dispersion
Δt	1.3 h	Automatically calculated
dx^0	$0.01^\circ \times 0.01^\circ$	Initial interparticle spacing
Randomness	Full	
Constant of randomness	0.01	

Table 6.2. Initial conditions. Summary of the conditions used to run the simulations.

6.3. Results and discussion

Monthly SST trends in the Northwestern part of the Gulf of Mexico are calculated for the period 1982-2015 using OISST_{1/4} database (Figure 6.3). Overall, warming is the prevalent trend for all months with maximum values of 0.5° C per decade. However, there is a cooling strip along the Louisiana-Texas shelf from November to February that contrasts with the warming observed at ocean locations. The difference in the warming rate between coastal and oceanic locations is even more patent in December and January.

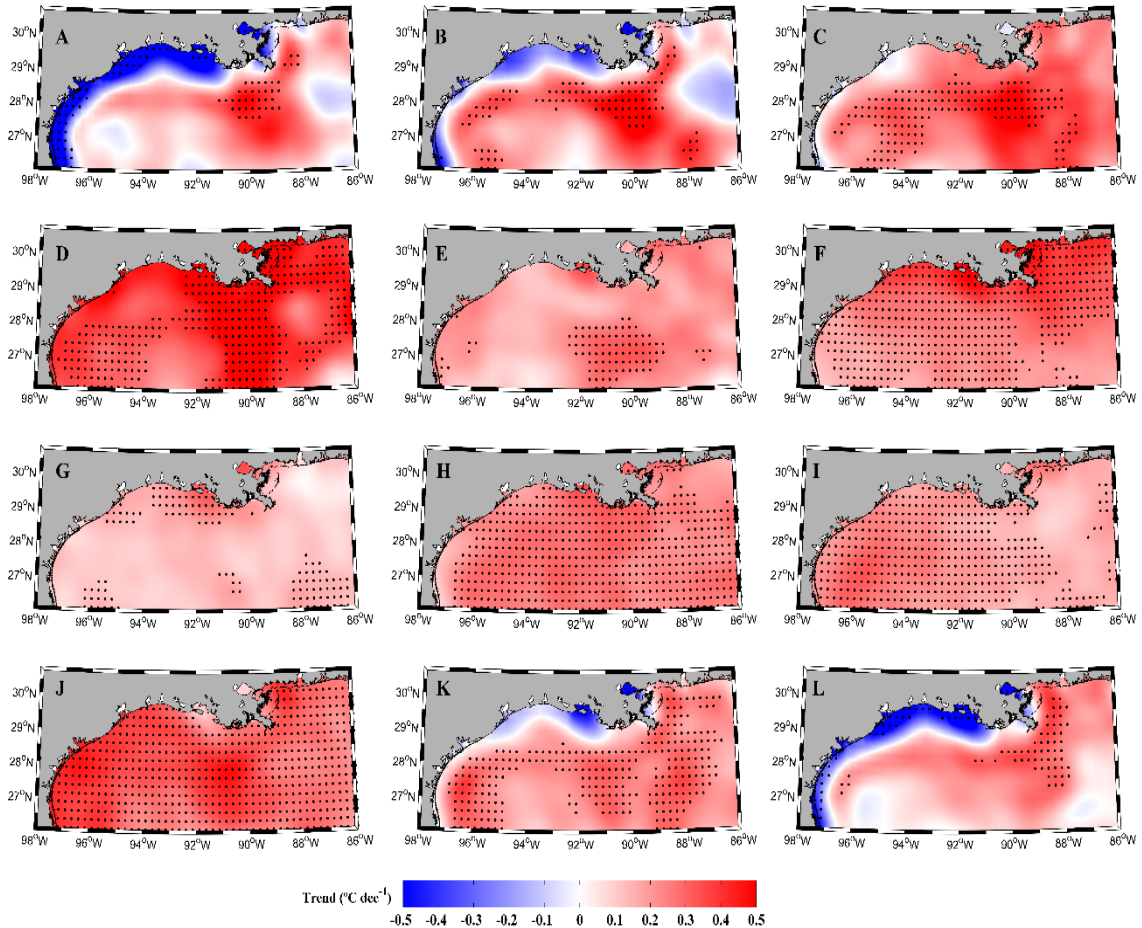


Figure 6.3. Monthly SST trends ($^{\circ}\text{C}$ per decade) along the Texas-Louisiana shelf over the period 1982-2015. Trends were calculated by means of OISST database. Black dots represent the grid points with a significance higher than 95%. (A) January. (B) February. (C) March. (D) April. (E) May. (F) June. (G) July. (H) August. (I) September. (J) October. (K) November. (L) December.

SST trends are averaged over the period November to February (Figure 6.4), which is characterized by a clear contrast between cooling and warming areas as shown in previous figure. A significant cooling trend is detected along the entire Louisiana-Texas shelf with values around -0.5°C per decade. It should be highlighted that cooling widespread to the west of the bird-foot delta but not eastward. A similar SST pattern is obtained using HYCOM data from November to February over the period 1993-2015.

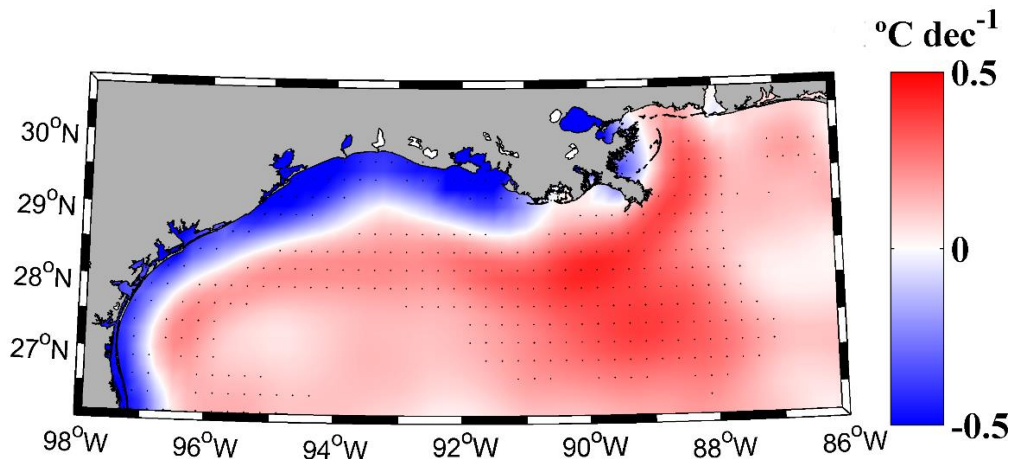


Figure 6.4. Map of SST trend. November-February SST trend ($^{\circ}\text{C}$ per decade) calculated over the period 1982-2015. Black dots represent grid points with significance higher than 95%.

In order to analyze the different warming patterns between coastal and ocean locations, both regions have been delimited (see mini-map in Figure 6.5). White points mark the near coast locations where the highest cooling is observed from November to February. Black dots mark an ocean band where the maximum warming is observed over the same months. A thin band among them, where there is not a clear trend, and the ocean points far from the coast are not considered in this analysis. Points with similar trends (positive or negative) are spatially averaged at monthly scale. Both areas have practically the same warming rate (around 0.25°C per decade) from April to October. Although trends are not exactly equal in March, they are positive both for coast and ocean. In contrast, large differences can be observed from November to February with the coastal area cooling (blue line) and the adjacent oceanic area (red line) warming.

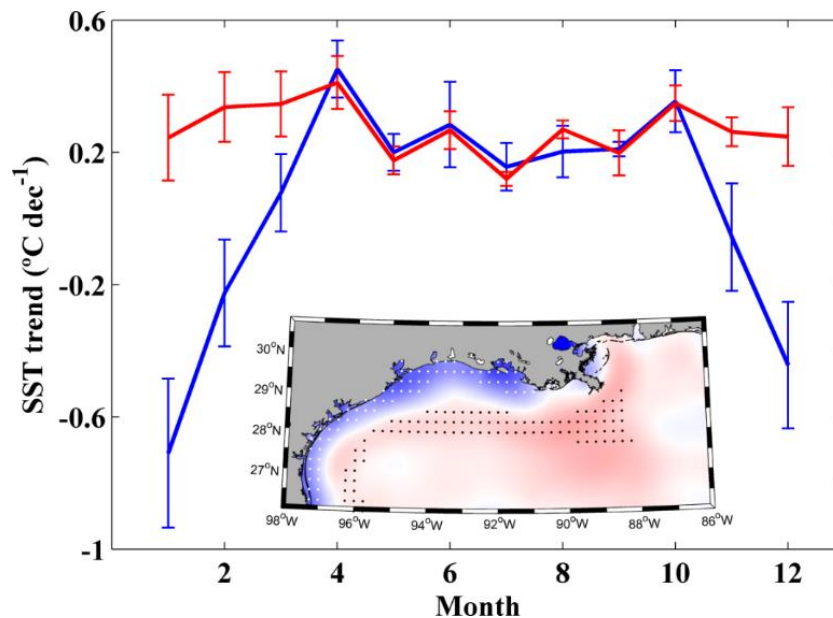


Figure 6.5. Monthly SST trend and its associated variance (bars) for oceanic (red line) and coastal (blue line) areas. The mini-map shows the averaged points selected to calculate monthly trends at coastal (white) and oceanic (black) areas.

The interannual variability of coastal and oceanic SST is shown in Figure 6.6A. Annual SST values are calculated considering only November-February months over the period 1982-2015. In general, coastal SST (blue line) is lower than 20 °C and presents a negative trend and ocean SST (red line) is higher than 21 °C and with a positive trend. The difference between both signals (Figure 6.6B) can be observed to increase progressively throughout most of the studied period with SST differences higher than 4 °C from 2007 on. This increment is even more marked over the last decade ($\sim 0.2^{\circ} \text{C y}^{-1}$), given rise to a difference on the order of 5 °C at present. Previous studies (Wang et al., 1998; Walker et al., 2005) also reported a large cross-shelf SST gradient during winter months due to the fact that Mississippi River is cooler than adjacent shelf waters and also due to the passage of cold fronts along the Northern Gulf of Mexico. To our knowledge, there are no previous studies that analyzed monthly SST trends considering the whole Texas-Louisiana shelf over periods longer than 30 years. Some studies (e.g. Li and Clarke, 2005; Muhling et al., 2012) analyzed the influence of SST variations on different fish populations along the area under scope. Glenn et al., (2015) studied SST trends in the Caribbean and surrounding region, including the whole Gulf of Mexico. Cooling trends in the Mississippi-Atchafalaya area can be observed at their Figure 3C, although they do not mention it explicitly. These authors found that the Atlantic Warm Pool, which flows from the Caribbean Sea into the Gulf of Mexico, has increased in size and intensity affecting the oceanic area considered in this study.

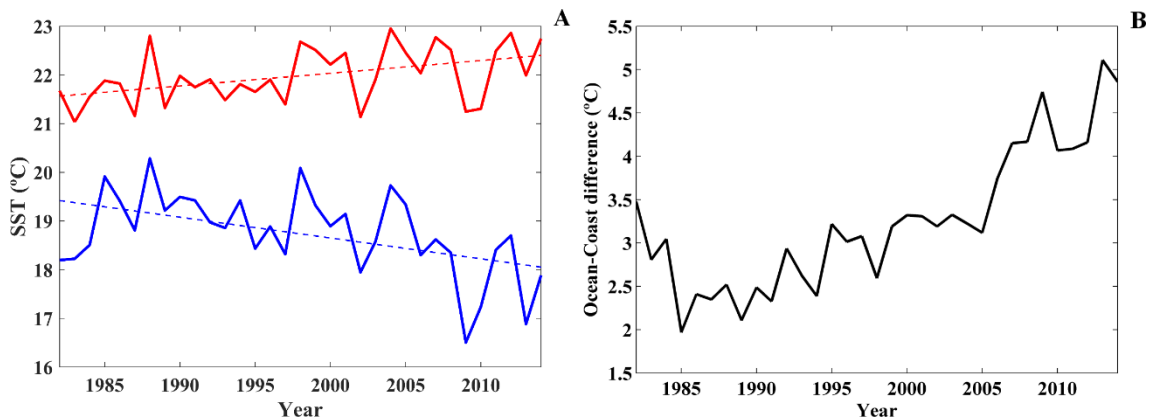


Figure 6.6. Interannual SST. (A) Interannual SST variability in oceanic (red line) and coastal (blue line) areas. Dashed lines show the lineal trend. Both trends have a significance level higher than 95%. (B) Interannual SST difference between both regions over the period 1982-2015. The oceanic and coastal areas were defined in Figure 6.5.

The observed behavior in coastal SST trends can be analyzed in terms of the different drivers that affect surface water. As it was mentioned above, Texas-Louisiana shelf is highly influenced by freshwater inputs, mainly from Mississippi and Atchafalaya Rivers. The river plume formed by these rivers can affect significantly the temperature patterns of seawater because promotes different characteristics that the surrounding ocean water. In order to test if the area occupied by the plume is related with the cooling area, the plume formed by these rivers is obtained from November to February when the different temperature trends are observed. The MA plume (Figure 6.7A) is obtained by means of the high spatial resolution MODIS data following the methodology described in

Fernández-Nóvoa et al., (2015) (see Section 2.2). The MA plume tends to expand westward and its presence is scarce eastward of the bird-foot delta where Mississippi River flows into, coinciding with the cooling area. This coincidence indicates that the river plume plays a key role in the temperature patterns observed. The area affected by Mississippi and Atchafalaya River discharges was also evaluated by means of salinity data from HYCOM (Figure 6.7B). In this image it can be observed how the area characterized by low salinity values, below 35, extends westward along the coast occupying a similar area to than the observed with MODIS, which corroborates that the MA river plume is the main feature promoting the different warming ratios observed between coastal and oceanic locations.

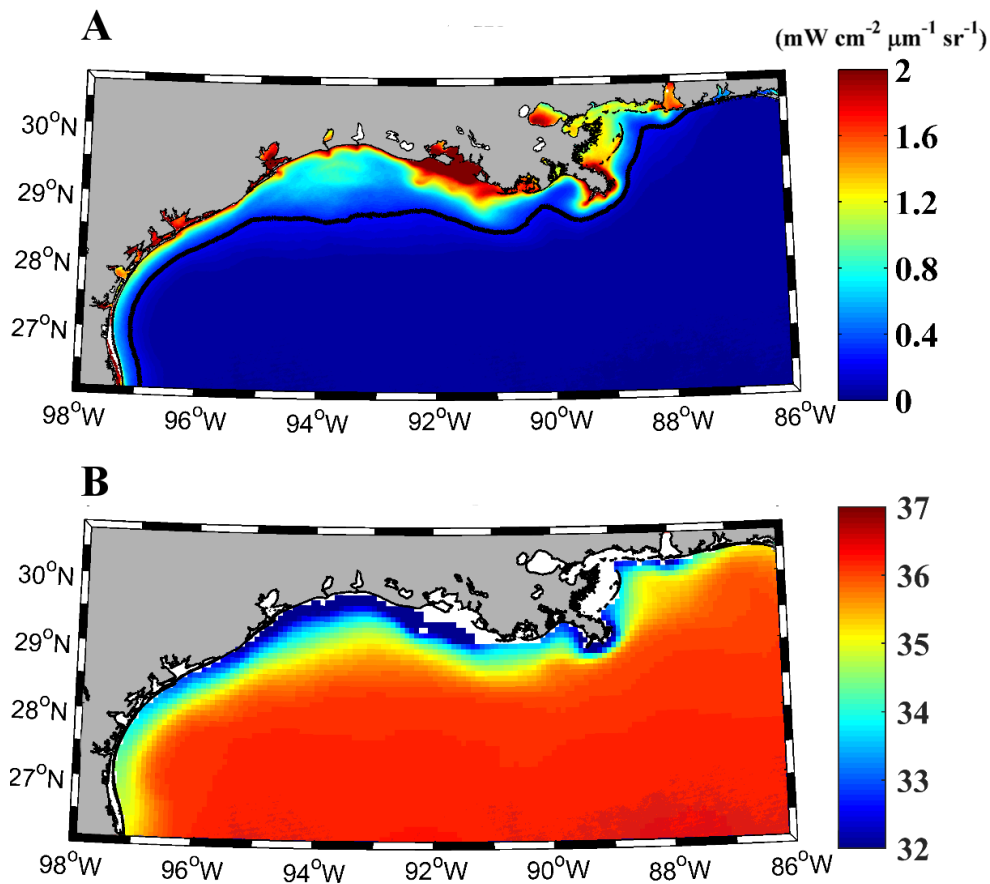


Figure 6.7. Maps of the turbid plume and salinity. (A) Mean turbid plume ($\text{mWcm}^{-2}\mu\text{m}^{-1}\text{sr}^{-1}$) calculated from November to February over the period 2003–2015 using MODIS data. Contour line corresponds to the turbid threshold ($0.25 \text{ mWcm}^{-2}\mu\text{m}^{-1}\text{sr}^{-1}$). (B) Mean salinity calculated from November to February over the period 2003–2015 using HYCOM data.

Therefore, different drivers can be analyzed to better understand changes in the river plume extension and, hence, in coastal warming or cooling. The main drivers that can affect river plumes are river discharge, wind and tides. However, in this particular case, tidal effects are discarded because tidal range is small in the shelf area ($\sim 20\text{--}40 \text{ cm}$) (DiMarco and Reid, 1998; Salisbury et al., 2004) and tidal components have shown a minimal contribution on MA plume development (Walker, 1996).

Regarding river discharge, a seasonal cycle was observed with the maximum river discharge reached in May and the minimum one in September (Figure 6.8A). Large values of river discharge able to sustain different patterns between plume and ocean water masses were also recorded for the period November-February. In addition, a decrease of $1,265 \text{ m}^3\text{s}^{-1}$ per decade is detected considering both rivers from November-February months over the period 1993-2015, whilst a significant ($>99\%$) decrease ($2,117 \text{ m}^3\text{s}^{-1}$ per decade) is observed from 1982 to 2015 (Table 6.3).

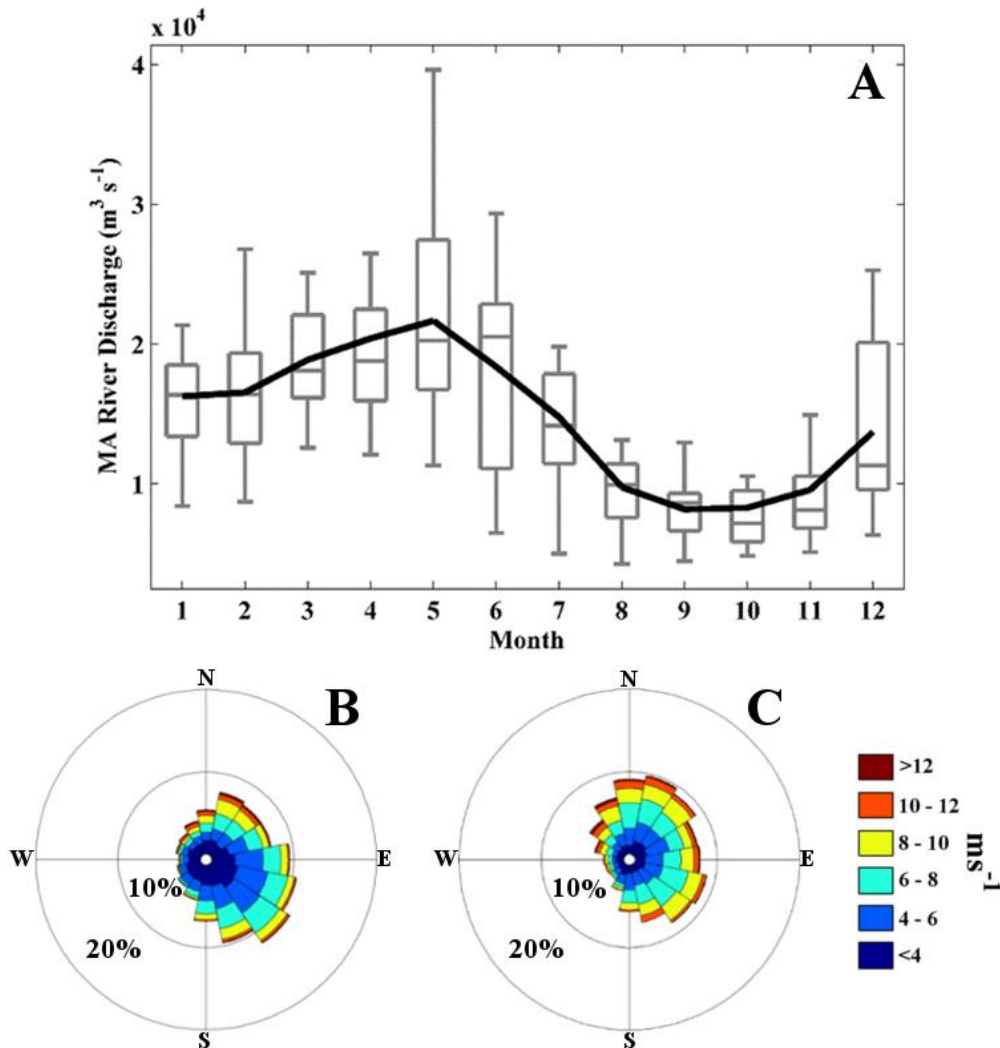


Figure 6.8. MA River discharge and wind roses. (A) Annual hydrologic cycle variability (m^3s^{-1}) for the sum of Mississippi and Atchafalaya runoff over the period 2003–2015. Solid black line represents the monthly average flow and the line inside each box represents the median for each month. Lower and upper whiskers show minimum and maximum river flow, respectively, while lower and upper box indicate first and third quartiles, respectively. (B) Annual wind rose (ms^{-1}) and (C) wind rose from November to February (ms^{-1}) at a location between both river mouths over the period 2003–2015.

River discharge reduction occurs at all months, with the exception of July (results not shown). This fact is important since it is estimated that at least 3 months are necessary to accumulate the freshwater content from Atchafalaya and Mississippi river discharges on the shelf (Zhang et al., 2012).

		1993-2015	1982-2015
Easterly winds	Duration (days per decade)	-4.43*	-2.3*
	Intensity (m s^{-1} per decade)	-	-0.07**
River	Runoff ($\text{m}^3 \text{s}^{-1}$ per decade)	-1,265	-2,117*

Table 6.3. Wind and river discharge values. Trends in wind intensity and wind duration considering winds with an easterly component (ranging between NNE-SSE) and river discharge from November to February. Values with null trends are marked with -. Statistical significance at 95% || 99% is marked with * || ** respectively.

Regarding wind, a clear predominance of winds with an easterly component, both all year long (Figure 6.8B) as from November to February (Figure 6.8C and Figure 9) was observed over a location between both river mouths (see blue dot in Figure 6.1).

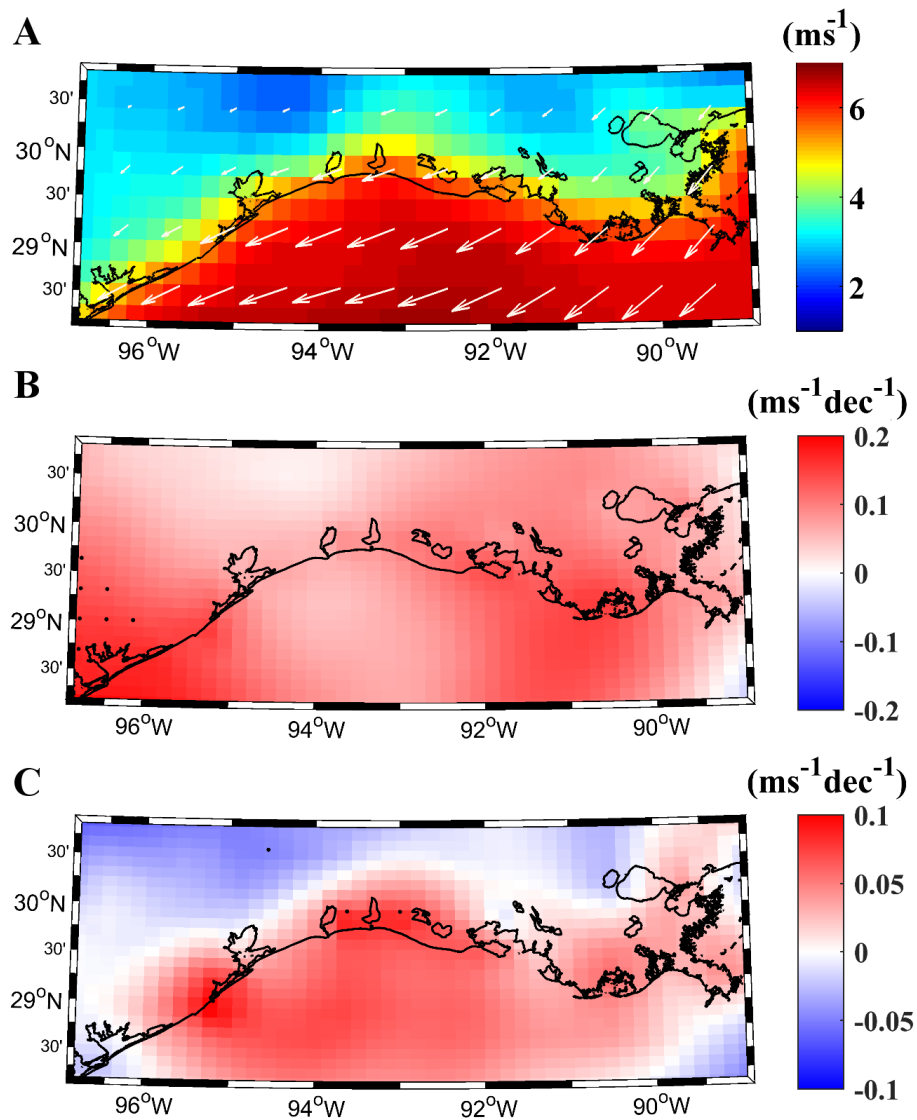


Figure 6.9. Wind pattern from November to February over the period 1982-2015. (A) Monthly mean wind velocity (ms^{-1}) and direction and trends in the (B) meridional and (C) zonal wind components (ms^{-1} per decade). Black dots represent grid points with significance higher than 95%.

These downwelling favorable winds cause the retention of the plume against the coast and its movement downcoast (generating the westward plume development), supported by the effect of the Coriolis force and the coastal current generated in the direction of Kelvin wave propagation. According to Zhang et al. (2012), freshwater transport downcoast along the Texas-Louisiana shelf of Atchafalaya and Mississippi plumes is higher during winter and spring months. In addition, Zhang and Hetland (2012) obtained significant correlations between alongshore flow near surface and alongshore wind during winter months. During summer months, winds are upwelling favorable and push the plume upcoast, trapping the plume over the Louisiana shelf and favoring its offshore displacement and the mixing with ocean waters (Salisbury et al., 2004; Rong et al., 2014; Androulidakis et al., 2015). As we just mentioned, wind is the primary factor influencing circulation along the Texas-Louisiana shelf during winter (Zhang and Hetland, 2012) since winds with easterly component, which are prevalent during these months, mark the westward displacement of the plume. Therefore, changes in the duration and intensity of easterly winds are also analyzed (Table 6.3 and Figure 6.9C, note that positive trends indicate a decrease in the easterly wind component). A significant decrease in the frequency of easterly days is detected for the period 1982-2015 being even larger when the period 1993-2015 is considered. Specifically, most of the days from November-February have an easterly component ranging between NE-SE (53 and 51 days for the periods 1982-2015 and 1993-2015, respectively). Therefore, the obtained trends suppose a reduction of about 4% and 7% in the frequency of easterly winds for the period 1982-2015 and 1993-2015, respectively. Otherwise, not remarkable changes were observed in terms of easterly wind intensity.

Therefore, the reduction of river discharge combined with the decrease in frequency of easterly winds support the idea of buoyancy loss along the Texas-Louisiana shelf conditioned by the reduction of the westward transport of freshwater. With this purpose, changes in the stability of the water column and variations in the freshwater transport along the Texas-Louisiana shelf are analyzed over the period 1993-2015. It is a well-known fact that freshwater inputs strongly influence the stability of the water column (e.g: Kourafalou et al., 1996), conditioning the SST due to variations in the mixed layer depth and the entrainment of colder and deeper water (Alexander et al., 2000).

Temperature and salinity data from HYCOM database are used to analyze the stratification of the water column over the period 1993-2015. The buoyancy frequency (N^2 , also called Brunt-Väisälä frequency squared), which represents the stratification strength at a specified depth (z), was defined as follows:

$$N^2 = -\frac{g}{\rho_z} \frac{\Delta\rho}{\Delta z} \quad (6.1)$$

where g is the gravity constant, ρ_z is the average water density (kg m^{-3}) and the term $\frac{\Delta\rho}{\Delta z}$ accounts for the potential density gradient from surface to the specified depth z . Taking

into account that the Texas-Louisiana shelf is characterized by its shallowness, the first 10 meters of the water column are considered to calculate this frequency.

Mean values of buoyancy frequency from November to February over the period 1993-2015 are shown in Figure 6.10A. The highest values, which denote a higher stratification, are found along the Texas-Louisiana shelf coinciding with the area occupied by the river plume (Figure 6.7A). Within this area, higher values of buoyancy frequency are detected near the Atchafalaya mouth and the Mississippi bird-foot delta. This effect is caused by the haline forcing, which maintains the water column stratified during winter. With the aim of detecting variations in the stratification pattern, changes in Brunt-Väisälä frequency are also calculated (Figure 6.10B). Negative values, which denote buoyancy loss, are observed along the Texas-Louisiana shelf, in the area where the highest mean values are found. On the other hand, the oceanic area shows positive values, which represent a stratification reinforcement in this zone.

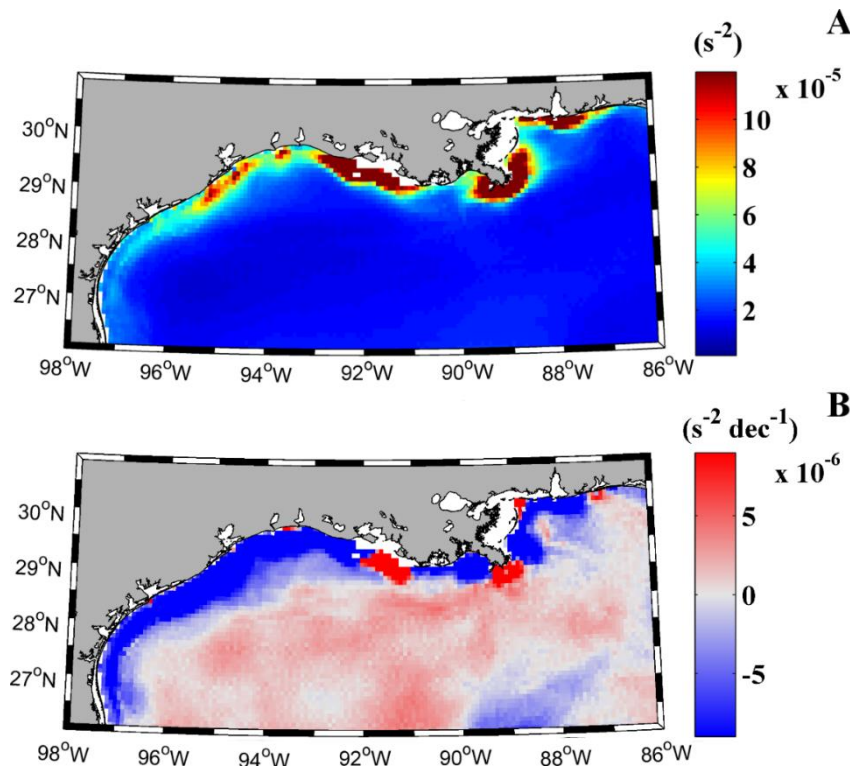


Figure 6.10. Map of the buoyancy frequency and its trend. (A) Squared Brunt-Väisälä frequency (s^{-2}) and (B) trend (s^{-2} per decade) calculated from November to February over the period 1993-2015.

In addition, the stratification along the Texas-Louisiana shelf is also analyzed by means of changes in the mixed layer depth (MLD) from November to February for the period 1993-2015 (Figure 6.11). For this purpose, MLD is calculated using a density threshold criterion of 0.01 kg m^{-3} with respect to the sea surface taking into account the bathymetric features of the Texas-Louisiana shelf. Then, MLD for the first period (1993-2003) is subtracted to the MLD of the second period (2005-2015). MLD tended to be deeper in the area occupied by the river plume, which is the location where a high decrease in the stratification is detected. On the other hand, the MLD tended to decrease in the adjacent

ocean. This means that a larger thickness of the water column is mixed due to buoyancy loss promoting the entrance of deeper and colder water.

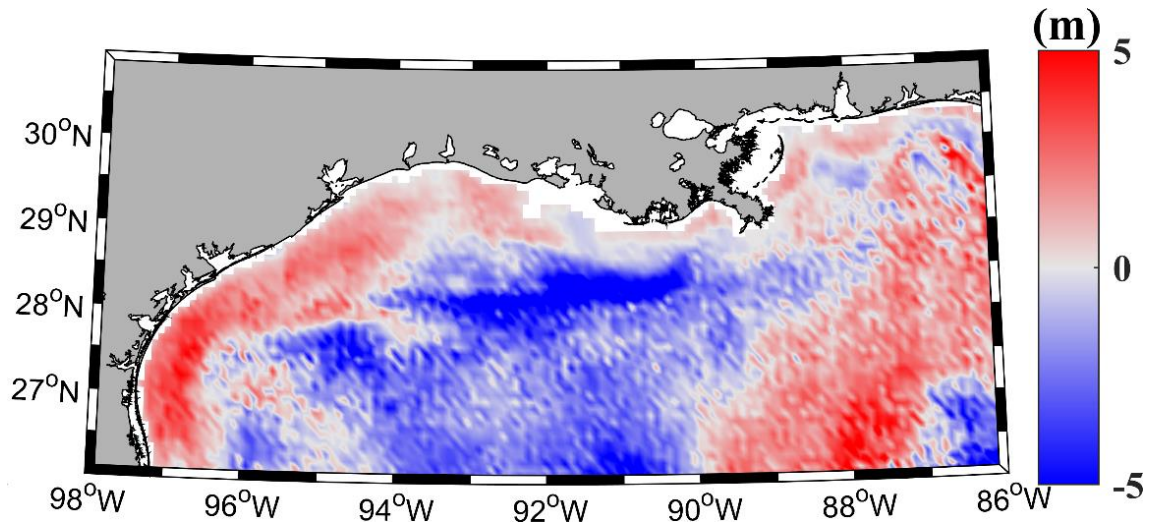


Figure 6.11. Changes in the MLD (m) from November to February over the period 1993-2015 using the HYCOM data. Values for the period 1993-2003 were subtracted to the values for the period 2005-2015. Positive (negative) values mean a deepening (shoaling) of the MLD.

The loss of buoyancy can be explained by the combination of two factors: a decrease in the flow of the MA Rivers and a decrease in the westward transport of freshwater along the Texas-Louisiana shelf (Figure 6.12). Regarding river discharge, its trend (Table 6.3) showed a decrease along the coastal area favoring the buoyancy loss. Regarding freshwater transport, currents along the Texas-Louisiana shelf are also analyzed through Lagrangian simulations of passive particles released at surface layer in the Atchafalaya and Mississippi river mouths. The release date, November to February, is chosen to fit the period when SST cooling is observed (Figure 6.3). First of all, the area is gridded in pixels of $0.08^\circ \times 0.08^\circ$ to calculate the number of times that a particle is found at each pixel during the whole period (1993-2015). Figures 6.12A and 6.12C show the concentration maps (in percentage) for particles released at the Atchafalaya and Mississippi river mouth, respectively. Overall, the patterns fit the area defined by the turbid plume (see Figure 6.7A). In both cases, particles drift mainly westward through the Texas-Louisiana shelf, being the displacement more evident in the case of the Atchafalaya River (Figure 6.12A). Regarding the case of particles released from the Mississippi River mouth (Figure 6.12C), most of the particles move westward, although the percentage of particle moving eastward is not negligible. To detect changes in the current pattern, the percentage of pixel occupancy corresponding to two periods of 11 years (1993-2003 and 2005-2015) is calculated for both river mouths (Figure 6.12B and D). Then, the particle distribution for the first period (1993-2003) is subtracted from the distribution of the second period (2005-2015). In this way, negative (positive) values at a certain pixel indicate the decrease (increase) of riverine water at that pixel. The patterns calculated for both rivers show a clear decrease of riverine water (blue color) at the shelf, except around both release areas. This reduction of westward transport of freshwater on the shelf (see 4

in Figure 6.13) is favored by the reduction in river discharge and the reduction in the frequency of easterly winds. In addition, a reduction in the westward transport favors the retention of river discharge close to river mouths increasing locally the stratification, which explain the positive spots observed when analyzing trends in N^2 (Figure 6.10).

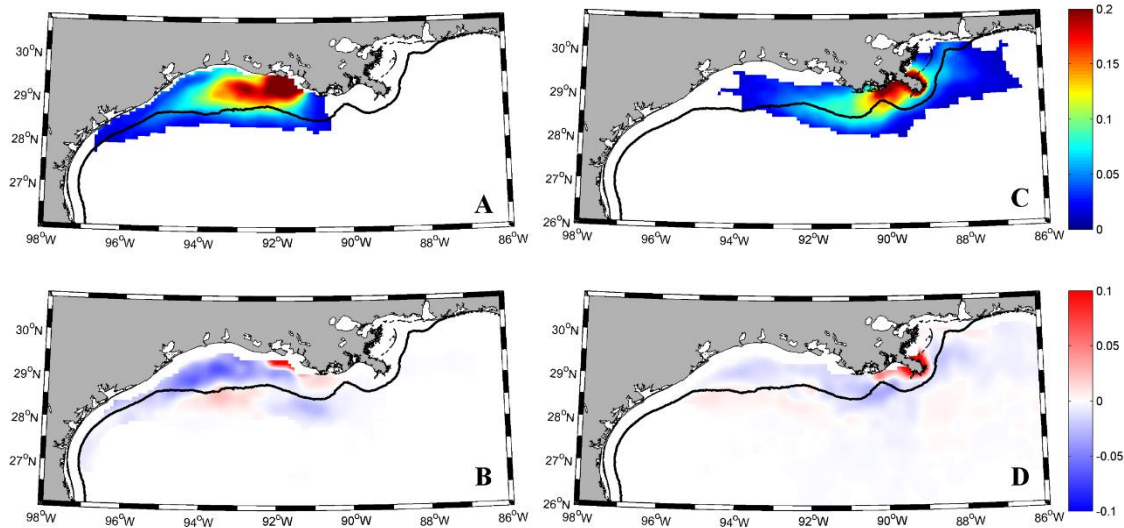


Figure 6.12. Results from the Lagrangian simulation. Percentage of particles after a drift of 2 months after being released at surface layer in the area close to the Atchafalaya River mouth (A) and to the Mississippi River mouth (C) over the period 1993-2016. Contour line corresponds to the turbid threshold ($0.25 \text{ mWcm}^{-2}\mu\text{m}^{-1}\text{sr}^{-1}$) calculated in Figure 6.7A. Changes in the distribution of particles of riverine origin ((B) Atchafalaya River and (D) Mississippi River). The distribution was calculated using HYCOM data for both river mouths for two not overlapping periods of 11 years (1993-2003 and 2005-2015). Then, the distribution corresponding to the first period was subtracted from the distribution of the second period.

In the particular case of the Texas-Louisiana shelf, results obtained from the different analysis carried out in the present study (Figure 6.10 and 6.11) support the idea that coastal cooling is based on a reduction of the stratification and the increase in the MLD. The buoyancy loss, provoked by the reduction of river discharge and the decrease in the frequency of easterly winds, promotes an increase in the density in the area occupied by the plume. In addition, it is observed that the subsurface water is cooler than the surface one (not shown). Therefore, considering these analyses it is hypothesized that the most probable cause of the different SST warming pattern along the Texas-Louisiana shelf, is an increase in the entrainment of cool water from subsurface layers. This is promoted by a reduction in the stratification and the consequence increase in the MLD, which favors the entrainment of deeper and colder water. Figure 6.13 shows a scheme of the proposed mechanism to explain SST cooling due to the influence of the MA river plume. A similar mechanism was previously proposed by [Howden and Murtugudde \(2001\)](#) and by [Seo et al., \(2009\)](#) in some areas of the Bay of Bengal.

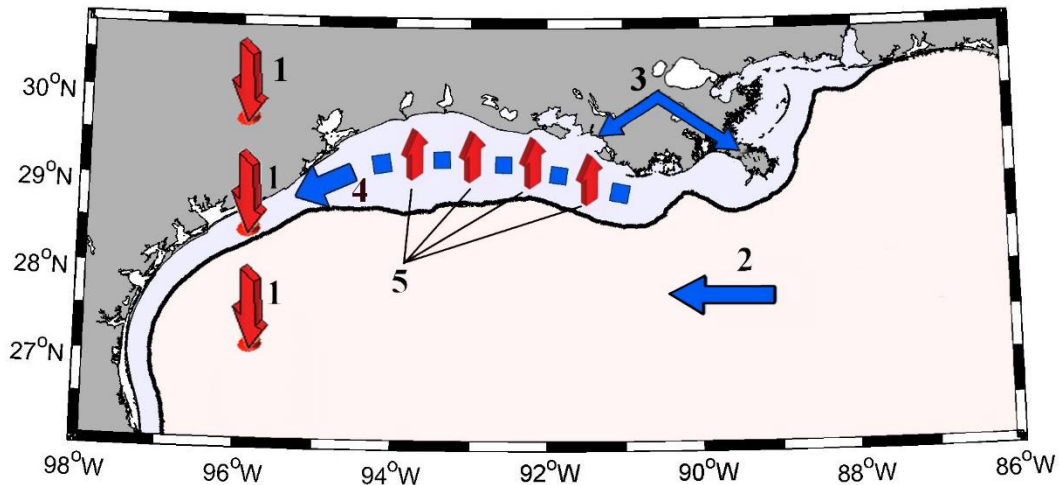


Figure 6.13. Scheme of the proposed mechanism. (1) General warming in the Gulf of Mexico. (2) Decrease in the frequency of easterly wind. (3) Decrease in MA river discharge. (4) Decrease in westward alongshore transport (reduced stratification). (5) Increase in the entrainment of cool water from subsurface layers.

6.4. Conclusions

Sea surface temperature (SST) variability was analyzed at the northwestern part of the Gulf of Mexico from 80s to nowadays.

- a) Different SST warming patterns were observed at coastal and oceanic locations during winter months (November-February). Cooling was detected near shore and warming at ocean locations.
- b) The river plume generated by Mississippi and Atchafalaya freshwater was found to be responsible of near coast cooling. Freshwater inputs, which has decreased over the studied period, condition the stability of the water column during winter months.
- c) A reduction in the frequency of easterly wind (see 2 in Figure 6.13) together with the reduction in river discharge (see 3 in Figure 6.13) and the reduction in westward transport of freshwater along the Texas-Louisiana shelf (see 4 in Figure 6.13), explain the buoyancy loss detected in the area occupied by the turbid plume.
- d) This buoyancy loss causes a higher vertical mixing that favors the entrainment of colder water in the mixed layer (see 5 in Figure 6.13) resulting in SST decrease along the Texas-Louisiana Shelf.

General Conclusions

This thesis represents a step forward in the develop of a particle tracking model able to reproduce the dispersion of particles into ocean currents. In this sense, several study cases like the dispersion of passive tracers in the Atlantic Ocean, the connectivity of species like the European eel in the Atlantic Ocean and the spiny lobster *Panulirus penicillatus* in the Indian Ocean were analyzed. Finally, it was also applied to analyzed the coastal SST cooling measured in the Northwest Gulf of Mexico. The main results obtained are the following:

- First of all, the developed model let us to study different topics related with the dispersion of particles in ocean currents using varied initial release configurations.

Passive tracers in the Atlantic Ocean

- The analysis of the dispersion pattern of particles that succeeded in crossing the Atlantic since the beginning of the twentieth century show results in good agreement with previous research both in the concentration peaks in latitude as in the significant increasing trends obtained in all simulated cases.
- The increase in the chances to cross the Atlantic, deduced from the significant increasing trends, is in agreement with changes in the EKE, which has intensified along the Gulf Stream path.

Connectivity of the European eel in the Atlantic Ocean

- The passive larvae of the European eel need a T_{min} in the order of 8 months to cross the Atlantic.
- The minimum migration time is sensitive to depth, initial distribution of particles and migration strategies. Indeed, larvae travel faster near surface and the values of T_{min} are directly proportional to the initial interparticle spacing. Additionally, migration strategies like the multilayer and the active migration based on the random walk, are, in average, slower than migration at a single layer and purely advective migration, respectively.
- Values of T_{min} , comparables to those obtained from the analysis of the microstructure of eel otoliths, ca be obtained considering the downstream swimming strategy.

*Connectivity among *Panulirus penicillatus* populations in the Indian Ocean*

- The dispersion of passive tracers, that mimic the drift of *Panulirus penicillatus* larvae in the Indian Ocean, shows that the Red Sea area is completely isolated from the rest whilst Maldives, Java, Aceh and Madagascar can potentially exchange genetic information.
- Maldives is the best area for potential genetic exchange since particles released there can reach Aceh and Java through a straightforward migration and probably Madagascar through a migration by stages. In addition, the connectivity between Maldives and Aceh has increased over the period of study.

Sea surface temperature (SST) variability at the NW part of the Gulf of Mexico

- A cooling pattern was detected near shore along the Texas-Louisiana shelf during winter months in contrast with the warming pattern at ocean locations.
- The particle tracking model was applied to the analysis of the freshwater transport from the Mississippi and Atchafalaya river system. Results showed a reduction in the westward transport of freshwater along the Texas-Louisiana shelf during winter months from 80s. This freshwater transport reduction together with a reduction in river discharge and in the frequency of easterly winds explain the buoyancy loss detected in the area occupied by the turbid plume which favors the entrainment of colder water in the mixed layer producing the coastal SST cooling.

Acronym and Abbreviation List

- **AC:** Antilles Current.
- **AMJ:** April-May-June.
- **AMO:** Atlantic Multidecadal Oscillation.
- **AMOC:** Atlantic Meridional Overturning Circulation.
- **AVHRR:** Advanced Very High Resolution Radiometer sensor.
- **AzC:** Azores Current.
- **CC:** Canary Current.
- **CFL:** Courant-Friedrichs- Lewy criterion.
- **CFSR:** Climate Forecast System Reanalysis.
- **Δt :** time step in the numerical simulations.
- **DVM:** Diel Vertical Migration.
- **dx^0 :** initial interparticle spacing in the numerical simulations.
- **E:** Eddies.
- **EAC:** East Arabian Current.
- **EACC:** East African Coast Current.
- **EIC:** East Indian Current.
- **EKE:** Eddy Kinetic Energy.
- **FC:** Florida Current.
- **GS:** Gulf Stream.
- **HYCOM:** Hybrid Coordinate Ocean Model database.
- **LC:** Leewin Current.
- **LpC:** Loop Current.
- **MA River:** Mississippi- Atchafalaya River.
- **MLD:** Mixed layer depth.
- **MODIS:** Moderate Resolution Imaging Spectroradiometer.
- **NAC:** North Atlantic Current.
- **NAO:** North Atlantic Oscillation.
- **NCAR:** National Center for Atmospheric Research.
- **NCODA:** Navy Ocean Data Assimilation.
- **NEC:** North Equatorial Current.

- **NEMC:** Northeast Madagascar Current.
- **NMC:** Northeast Monsoon Current.
- **nLw:** Normalized leaving radiance.
- **NOAA:** National Oceanic and Atmospheric Administration.
- **OGCMs:** Ocean General Circulation Models.
- **OISST_{1/4}:** Daily ¼° Optimum Interpolation Sea Surface Temperature.
- **OND:** October-November-December.
- **PC:** Portugal Current.
- **PLD:** Planktonic larval duration.
- **SC:** Somalia Current.
- **SEC:** South Equatorial Current.
- **SECC:** South Equatorial Countercurrent.
- **SEMC:** Southeast Madagascar Current.
- **SJC:** South Java Current.
- **SL:** Significance level.
- **SMC:** Southwest Monsoon Current.
- **SODA:** Simple Ocean Data Assimilation database.
- **SST:** Sea Surface Temperature.
- **Sv:** Svedrup. Unit of volume transport equivalent to $10^6 \text{ m}^3\text{s}^{-1}$
- **TABS:** Texas Automated Buoy System.
- **T_{inf} :** Infimum time.
- **T_{mean} :** Mean minimum migration time.
- **T_{min} :** Minimum migration time.
- **t_{flying}:** Period of time in which the particles remains active and can be disperse.
- **t_{release}:** Interval between releases in the numerical simulations.
- **t_{rec}:** time between particle positions records in the numerical simulations.
- **UCAR:** University Corporation for Atmospheric Research.
- **U.S.:** United States

List of Figures

- Figure 1.1. Sketch of tidal current.** Source: “Generating Marine Electricity: Transitioning From Subsidies to Commercial Financing” submitted by Alexander Mcphail to The water blog:
<http://blogs.worldbank.org/water/energy/category/tags/tidal> ----- 2
- Figure 1.2. Solar radiation.** The equator receives more radiation than the poles because the vertical incidence of the sun’s rays. Copyrights: 2008 Encyclopaedia Britannica, Inc ----- 3
- Figure 1.3. Global salinity map.** This figure was adapted from the website:
www.sciencelearn.org.nz ----- 4
- Figure 1.4. Sketch of the conveyor belt.** Blue lines represent cold deep water while red line represents warm surface water. This figure was obtained from the NOAA’s National Ocean service website:
https://oceanservice.noaa.gov/education/tutorial_currents/05conveyor2.html.----- 5
- Figure 1.5. The global wind pattern.** Source: This figure was obtained from the National Geographic’s website:
<https://www.nationalgeographic.org/photo/prevaling-winds/>.
 Copyrights: “Prevailing winds” by Kaidor is licensed under CC BY-SA 3.0. ----- 5
- Figure 1.6. Map of the ocean gyres and its associated currents.** The color indicates warm currents (red) and cold currents (blue). Copyrights: 2013 Pearson Education, Inc ----- 6
- Figure 1.7. Map with the locations of worldwide drifters on February 26th, 2018.** This picture was downloaded from The Global Drifter Program’s website:
http://www.aoml.noaa.gov/phod/dac/gdp_maps.php. ----- 7
- Figure 2.1. Sketch of NAO phases and the annual index.** (A) and (B) was obtained from [Bojariu and Gimeno \(2003\)](#). Source: Reprinted from Earth-Science Reviews, Vol. 63 Issues 1-2, Bojariu, R. and Gimeno, L. Predictability and numerical modelling of the North Atlantic Oscillation, 145-168, Copyright (2018). (C) The annual index of NAO is calculated using the monthly data for the period 1899-2010 downloaded from the website:
<https://climatedataguide.ucar.edu/climate-data> ----- 13
- Figure 2.2. Annual index of AMO.** The index is calculated using the monthly data for the period 1899-2010 downloaded from the website:
<https://climatedataguide.ucar.edu/climate-data>. ----- 14

- Figure 3.1. Area under study.** (A) Location of the study area. (B) The color map shows the bathymetry of the Gulf of Mexico and the Straits of Florida. White square represents the release area and green lines correspond to the 100, 500 and 1,000 m isobaths ----- 20
- Figure 3.2. Subtropical gyre of the North Atlantic Ocean.** Abbreviations refer to North Equatorial Current (NEC), Antilles Current (AC), Florida Current (FC), Loop Current (LpC), Gulf Stream (GS), North Atlantic Current (NAC), Azores Current (AzC), Portugal Current (PC) and Canary Current (CC) ----- 21
- Figure 3.3. Analysis to determine the ideal release point.** Percentage of particles that succeeded in crossing the 80.5°W meridian starting for different release points located inside the Gulf of Mexico. Black line in (A) represent the 80.5°W meridian ----- 26
- Figure 3.4. Analysis to determine the number of particles needed in the simulations.** (A) Histogram of the dispersion for 10,000 particles. (B) Maximum difference (%) among histograms in the percentage of particles at any distance, relative to the case with 10,000 particles. (C) Mean difference (%) among histograms for different numbers of particles, relative to the case with 10,000 particles. (D) Percentage of dispersed particles that succeeded in crossing the 25°W meridian for runs with different numbers of particles. All particles were released at 80.836°W 24.754°N in October 2000 at a fixed depth of 100 m, and the final location corresponds to March 2002 ----- 28
- Figure 3.5. Final position of dispersed particles over the period 1996-2009.** Percentage of particles found at the North Atlantic Ocean after a drift of 1.5 years for particles initially released at 5 m in (A) May using SODA. (B) May using HYCOM. (C) October using SODA. (D) October using HYCOM ----- 29
- Figure 3.6. Final position of dispersed particles over the period 1996-2009.** Percentage of particles found at the North Atlantic Ocean after a drift of 1.5 years for particles initially released at 35 m in (A) May using SODA. (B) May using HYCOM. (C) October using SODA. (D) October using HYCOM ----- 29
- Figure 3.7. Final position of dispersed particles over the period 1996-2009.** Percentage of particles found at the North Atlantic Ocean after a drift of 1.5 years for particles initially released at 70 m in (A) May using SODA. (B) May using HYCOM. (C) October using SODA. (D) October using HYCOM ----- 30
- Figure 3.8. Final position of dispersed particles over the period 1996-2009.** Percentage of particles found at the North Atlantic Ocean after a drift of 1.5 years

for particles initially released at 100 m in (A) May using SODA. (B) May using HYCOM. (C) October using SODA. (D) October using HYCOM ----- 30

Figure 3.9. Comparison between the percentage of particles released at 5 m that succeeded in crossing the 25°W meridian using SODA and HYCOM over the period 1996-2009. (A) Particles initially released in May. (B) Particles initially released in October. The numbers represent the year ----- 31

Figure 3.10. Percentage of particles that crossed the North Atlantic Ocean over the period 1996-2009. Time evolution of the percentage of particles released at 5 m depth in (A) May and (B) October that succeeded in crossing the 25°W meridian. Data were obtained with SODA (red) and HYCOM (blue) ----- 31

Figure 3.11. Final position of dispersed particles released in May over the period 1899-2010. Percentage of particles found at the North Atlantic Ocean after a drift of 1.5 years. Particles were initially released in May at a fixed depth of (A) 5 m. (B) 35 m. (C) 70 m. (D) 100 m ----- 33

Figure 3.12. Final position of dispersed particles released in October over the period 1899-2010. Percentage of particles found at the North Atlantic Ocean after a drift of 1.5 years. Particles were initially released in October at a fixed depth of (A) 5 m. (B) 35 m. (C) 70 m. (D) 100 m ----- 33

Figure 3.13. Monthly evolution of dispersed particles over the entire period of study. Percentage of particles that succeeded in crossing the 25°W meridian over the entire period of study for particles initially released in May at a fixed depth (A) 5 m. (B) 35 m. (C) 70 m. (D) 100 m. Errors bars represent the standard deviation of the mean ----- 35

Figure 3.14. Monthly evolution of dispersed particles over the entire period of study. Percentage of particles that succeeded in crossing the 25°W meridian over the entire period of study for particles initially released in October at a fixed depth (A) 5 m. (B) 35 m. (C) 70 m. (D) 100 m. Errors bars represent the standard deviation of the mean ----- 35

Figure 3.15. Percentage of particles that crossed the North Atlantic Ocean over the entire period of study. Time evolution of the percentage of particles released in (A) May and (B) October that succeeded in crossing the 25°W meridian at fixed depths: 5 m (blue), 35 m (red), 70 m (green) and 100 m (yellow) ----- 36

Figure 3.16. Changes in EKE since the beginning of 20th century. (A) Trend in EKE for the North Atlantic Ocean calculated using SODA velocity fields at surface layer. Black dots represent the location where the highest EKE was found.

- (B) Trends at the points marked with black dots in (A). Black circles indicate the confidence limit $\geq 95\%$ ----- 38
- Figure 4.1. Area under scope.** Map of the North Atlantic Ocean and the release area (black rectangle) in the Sargasso Sea divided in 3 subareas (1-red, 2-green and 3-blue). Dotted and dashed line represent the 20°W and 15°W meridians respectively ----- 44
- Figure 4.2. Eddy Kinetic Energy.** Mean surface EKE obtained from HYCOM data with a time resolution of 3 hours over the period 2006-2008 ----- 47
- Figure 4.3. Histogram of the percentage (per latitude) of dispersed particles that have succeeded in crossing the 20°W meridian.** Particles were released at the Sargasso Sea at a layer 50 m deep ----- 48
- Figure 4.4. Minimum duration of migration depending on the depth.** (A) Average of the minimum migration time needed to cross the Atlantic at different depths. Error bars denote the standard deviation of the mean. (B) Comparison between the minimum migration time obtained for a strategy with surface advective movement in the horizontal and no movement in the vertical (X-axis) vs the DVM strategy (Y-axis). The finish line was placed at 20°W ----- 50
- Figure 4.5. Minimum duration of migration depending on the initial distribution.** Dependence of the minimum migration time needed to cross the Atlantic on initial interparticle spacing. The black circle represents the initial interparticle spacing used for the base case. Particles are released in April 1998 and the finishing line is placed at 15°W ----- 51
- Figure 4.6. Minimum duration of migration depending on randomness.** Dependence of the minimum migration time needed to cross the Atlantic on randomness. (A) Fully random process. (B) Downstream swimming strategy. Particles were released in April 1998 and the finishing line was placed at 15°W ----- 52
- Figure 5.1. Region under scope.** The map of the Indian Ocean and the release areas (red) and target areas (blue) are shown ----- 56
- Figure 5.2. Surface system current of the Indian Ocean.** (A) Summer monsoon. (B) Winter monsoon. Abbreviations refer to the Leeuwin Current (LC), South Java Current (SJC), South Equatorial Current (SEC), Northeast and Southeast Madagascar Current (NEMC and SEMC), Somalia Current (SC), East African Coast Current (EACC), South Equatorial Countercurrent (SECC), Southwest and Northeast Monsoon Current (SMC and NMC), The Great Whirl (GW), East

Indian Current (EIC) and East Arabian Current (EAC). This figure was adapted from Tomczak and Godfrey (2003) -----	56
Figure 5.3. Seasonal average velocity of Indian Ocean surface and 100 m currents. The velocity field of Indian Ocean currents is averaged by seasons over the period of study 1958-2008 at surface layer (A, C, E, and G) and at 100 m (B, D, F and H). Colors only apply to the zonal component of velocity. (A and B) Winter (January to March). (C and D) Spring (April to June). (E and F) Summer (July to September). (G and H) Autumn (October to December) -----	60
Figure 5.4. Distribution of particles released from Madagascar. The percentage of particles dispersed is shown for those particles released from Madagascar in December over the period of study (1958-2008) -----	62
Figure 5.5. Distribution of particles released from Java. The percentage of particles dispersed is shown for those particles released from Java in December over the period of study (1958-2008) -----	62
Figure 5.6. Distribution of particles released from Maldives. The percentage of particles dispersed is shown for those particles released from Maldives over the period of study (1958-2008). (A) June. (B) September -----	63
Figure 5.7. Distribution of particles released from Aceh. The percentage of particles dispersed is shown for the particles released from Aceh over the period of study (1958-2008). (A) June. (B) September -----	65
Figure 5.8. Sketch of migration paths. Solid color lines represent the connection between areas due to a direct migration. The dashed line represents the possible connection between Maldives and Madagascar due to a migration by stages. The circular arrow over the Red Sea represents the isolation of this area -----	66
Figure 6.1. Bathymetry of the region under scope. Green dots mark the location where river discharge was sampled. Blue triangles mark the location of the main mouth of Atchafalaya and Mississippi Rivers. Blue dot marks the location where wind data were acquired -----	69
Figure 6.2. Sketch of the surface currents in the Gulf of Mexico. Abbreviations refer to Loop Current (LpC) and eddies (E). The figure was adapted from NOAA: (https://flowergarden.noaa.gov/image_library/regionmaps.html) -----	70
Figure 6.3. Monthly SST trends (°C per decade) along the Texas-Louisiana shelf over the period 1982-2015. Trends were calculated by means of OISST database. Black dots represent the grid points with a significance higher than 95%.	

- (A) January. (B) February. (C) March. (D) April. (E) May. (F) June. (G) July. (H) August. (I) September. (J) October. (K) November. (L) December ----- 73
- Figure 6.4. Map of SST trend.** November-February SST trend ($^{\circ}\text{C}$ per decade) calculated over the period 1982-2015. Black dots represent grid points with significance higher than 95% ----- 74
- Figure 6.5. Monthly SST trend and its associated variance (bars) for oceanic (red line) and coastal (blue line) areas.** The mini-map shows the averaged points selected to calculate monthly trends at coastal (white) and oceanic (black) areas - ----- 74
- Figure 6.6. Interannual SST.** (A) Interannual SST variability in oceanic (red line) and coastal (blue line) areas. Dashed lines show the lineal trend. Both trends have a significance level higher than 95%. (B) Interannual SST difference between both regions over the period 1982-2015. The oceanic and coastal areas were defined in Figure 6.5 ----- 75
- Figure 6.7. Maps of the turbid plume and salinity.** (A) Mean turbid plume ($\text{mWcm}^{-2}\mu\text{m}^{-1}\text{sr}^{-1}$) calculated from November to February over the period 2003–2015 using MODIS data. Contour line corresponds to the turbid threshold ($0.25 \text{ mWcm}^{-2}\mu\text{m}^{-1}\text{sr}^{-1}$). (B) Mean salinity calculated from November to February over the period 2003-2015 using HYCOM data ----- 76
- Figure 6.8. MA River discharge and wind roses.** (A) Annual hydrologic cycle variability (m^3s^{-1}) for the sum of Mississippi and Atchafalaya runoff over the period 2003–2015. Solid black line represents the monthly average flow and the line inside each box represents the median for each month. Lower and upper whiskers show minimum and maximum river flow, respective, while lower and upper box indicate first and third quartiles, respectively. (B) Annual wind rose (ms^{-1}) and (C) wind rose from November to February (ms^{-1}) at a location between both river mouths over the period 2003-2015 ----- 77
- Figure 6.9. Wind pattern from November to February over the period 1982-2015.** (A) Monthly mean wind velocity (ms^{-1}) and direction and trends in the (B) meridional and (C) zonal wind components (ms^{-1} per decade). Black dots represent grid points with significance higher than 95% ----- 78
- Figure 6.10. Map of the buoyancy frequency and its trend.** (A) Squared Brunt-Väisälä frequency (s^{-2}) and (B) trend (s^{-2} per decade) calculated using the HYCOM data from November to February over the period 1993-2015 ----- 80
- Figure 6.11. Change in the MLD (m) from November to February over the period 1993-2015 using the HYCOM data.** Values for the period 1993-2003

were subtracted to the values for the period 2005-2015. Positive (negative) values mean a deepening (shoaling) of the MLD ----- 81

Figure 6.12. Results from the Lagrangian simulation. Percentage of particles after a drift of 2 months after being released at surface layer in the area close to the Atchafalaya River mouth (A) and to the Mississippi River mouth (C) for the period 1993-2016. Contour line corresponds to the turbid threshold ($0.25 \text{ mWcm}^{-2} \mu\text{m}^{-1} \text{sr}^{-1}$) calculated in Figure 6.7A. Changes in the distribution of particles of riverine origin ((B) Atchafalaya River and (D) Mississippi River). The distribution was calculated using HYCOM data for both river mouths for two not overlapping periods of 11 years (1993-2003 and 2005-2015). Then, the distribution corresponding to the first period was subtracted from the distribution of the second period ----- 82

Figure 6.13. Scheme of the proposed mechanism. (1) General warming in the Gulf of Mexico. (2) Decrease in the frequency of easterly wind. (3) Decrease in MA river discharge. (4) Decrease in westward alongshore transport (reduced stratification). (5) Increase in the entrainment of cool water from subsurface layers ----- 83

List of Tables

Tabla 1. Resumen de los datos usados en esta tesis. La resolución temporal hace referencia a los periodos usados en los diferentes casos de estudio -----	ii-iii
Table 3.1. Summary of data used in the study. Additional information is included in the observation column and the data source -----	22
Table 3.2. Initial conditions. Summary of the conditions used to run the simulations -----	24-25
Table 3.3. Distribution of the maximum number of particles by longitude and latitude. The longitude column indicates the longitude position where the maximum number of particles was found considering all latitudes. The latitude column is divided into two peaks corresponding to the latitude position where the highest percentage of particles that succeeded in crossing the 25°W meridian was found -----	34
Table 3.4. Statistical analysis of the number of particles crossing the 25°W meridian for all simulated cases. Mean indicates the average percentage of particles that have succeeded in crossing the 25°W for each simulation. Trend indicates the increase in the percentage of particles that succeeded in crossing the 25°W. Values are expressed in percentage per decade. The significance level was calculated using the Spearman correlation -----	36
Table 3.5. Statistical analysis of the minimum travel period for all simulated cases. T_{inf} indicates the minimum migration time needed for the first particles that crossed the 25°W meridian. T_{mean} indicates the minimum migration time, in average, to cross the 25°W meridian being the error the standard deviation. Trend indicates changes in the time needed to cross the 25°W meridian. Values are expressed in months per decade. The significance level was calculated using the Spearman correlation -----	37
Table 3.6. Statistical analysis of the teleconnection patterns performed for all simulated cases. Mean indicates the average of the percentage of particles that have succeeded in crossing the 25°W meridian of the four depths. Only values of $R \geq 0.10$ are shown in the table for the correlation between the percentage of particles that have succeeded in crossing the 25°W meridian for each simulation and the teleconnection patterns. (A) The AMO index. (B) The NAO index. The significance level (SL) was calculated using the Spearman correlation -----	39

Table 4.1. Migration duration of European eel larvae. Summary of previous estimations of the migration duration of European eel based on different methods -----	42
Table 4.2. Summary of data used in the study. Additional information is included in the observation column and the data source -----	43
Table 4.3. Initial conditions. Summary of the conditions used to run the simulations -----	45-46
Table 4.4. Analysis of the origin of successful particles. Values indicate the origin (in percentage) of successful particles. The analysis covers the period 1996-2012. Particles were released at the Sargasso Sea in April of each year and followed for 18 months. The finish line was placed at 20°W -----	49
Table 5.1. Summary of data used in the study. It was included some information in the observation column and the source of the data -----	57
Table 5.2. Initial conditions. Summary of the conditions used to run the simulations -----	58-59
Table 5.3. Mean and standard deviation performed for all simulated cases. Mean indicates the percentage of particles that have remained in the release areas and/or have succeeded in reach the target areas over the period of study (1958-2008). Only mean values > 5% are shown -----	61
Table 5.4. Statistical analysis performed for particles released from Maldives and Aceh. Trend indicates the increase (in percentage per decade) in the number of particles that have succeeded in reaching the target areas. The significance level was calculated using the Spearman correlation -----	65
Table 6.1. Summary of data used in the study. Additional information is included in the observation column and the data source -----	71
Table 6.2. Initial conditions. Summary of the conditions used to run the simulations -----	72
Table 6.3. Wind and river discharge values. Trends in wind intensity and wind duration considering winds with an easterly component (ranging between NE-SE) and river discharge from November to February. Statistical significance at 95% and 99% is marked with * and **, respectively -----	78

Bibliography

- [Abdullah et al., 2014] Abdullah, M.F., Alimuddin, Muththalib, M., Salama, A.J., Imai, H. 2014. Genetic isolation among the Northwestern, Southwestern and Central-Eastern Indian Ocean populations of the pronghorn spiny lobster *Panulirus penicillatus*. *International Journal of Molecular Sciences*, 15(6): 9242-9254.
- [Alexander et al., 2000] Alexander, M. A., Scott, J.D., Deser, C. 2000. Processes that influence sea surface temperature and ocean mixed layer depth variability in a coupled model, *Journal of Geophysical Research Oceans*, 105(C7), 16823-16842.
- [Allahdadi et al., 2017] Allahdadi, M.N., Jose, F., D'Sa, E.J., Ko. D.S. 2017. Effect of wind, river discharge, and outer-shelf phenomena on circulation dynamics of the Atchafalaya Bay and Shelf. *Ocean Engineering*, 129, 567-580.
- [Allison et al., 2012] Allison, M.A., Demas, C.R., Ebersole, B.A., Kleiss, B.A., Little, C.D., Meselhe, E.A., Poweill, N.J., Pratt, T.C., Vosburg, B.M. 2012. A water and sediment budget for the lower Mississippi–Atchafalaya River in flood years 2008–2010: Implications for sediment discharge to the oceans and coastal restoration in Louisiana, *Journal of Hydrology* 432–433(0), 84–97.
- [Androulidakis et al., 2015] Androulidakis, Y.S., Kourafalou, V.H., Schiller, R.V. 2015. Process studies on the evolution of the Mississippi River plume: Impact of topography, wind and discharge conditions, *Continental Shelf Research* 107, 33-49.
- [Arai et al., 2000] Arai, T., Otake, T., Tsukamoto, K. 2000. Timing of metamorphosis and larval segregation of the Atlantic eels *Anguilla rostrata* and *A. Anguilla*, as revealed by otolith microstructure and microchemistry. *Marine Biology* 137: 39-45.
- [Arellano and Young, 2009] Arellano S.A., Young C.M. (2009). Spawning, Development, and the Duration of Larval Life in a Deep-Sea Cold-Seep Mussel. *Biological Bulletin* 216: 149–162.
- [Awaji et al., 1980] Awaji, T., Imasato, N., Kunishi, H. 1980. Tidal exchange through a strait: a numerical experiment using a simple model basin. *Journal of Physical Oceanographic* 10(10): 1499-1508.
- [Balseiro et al., 2003] Balseiro, C.F., Carracedo, P., Gómez, B., Leitaó, P.C., Montero, P., Naranjo, L., Penabad, E., Pérez-Muñuzuri, V. 2003. Tracking the Prestige oil spill: An operational experience in simulation at MeteoGalicia. *Weather*, 58(12): 452-458.

- [Beal and Donahue, 2013] Beal, L.M., Donahue, K.A. 2013. The Great Whirl: Observations of its seasonal development and interannual variability. *Journal of Geophysical Research* 118: 1-13.
- [Behara and Vinayachandran, 2016] Behara, A., Vinayachandran, P.N. 2016. An OGCM study of the impact of rain and river water forcing on the Bay of Bengal, *Journal of Geophysical Research Oceans* 121(4), 2425-2446.
- [Blanke et al., 2012] Blanke B., Bonhommeau S., Grima N., Drillet Y. 2012. Sensitivity of advective transfer times across the North Atlantic Ocean to the temporal and spatial resolution of model velocity data: Implication for European eel larval transport. *Dynamics of Atmospheres and Oceans* 55-56: 22-44.
- [Blanke and Raynaud, 1997] Blanke B., Raynaud S. 1997. Kinematics of the Pacific Equatorial Undercurrent: An Eulerian and Lagrangian approach from GCM results. *Journal of Physical Oceanographic* 27: 1038-1053.
- [Blanke et al., 2001] Blanke B., Speich S., Madec G., Doos K. 2001. A global diagnostic of interocean mass transfer. *Journal of Geophysical Research* 31: 1623-1632.
- [Boëtius and Harding, 1985] Boëtius, J., Harding, E.F. 1985. A re-examination of Johannes Schmidt's Atlantic eel investigations. *Dana* 4: 129- 162.
- [Bojariu and Gimeno, 2003] Bojariu, R., Gimeno, L. 2003. The role of snow cover fluctuations in multiannual NAO persistence. *Geophysical Research Letters* 30(4): 1156.
- [Bonhommeau et al., 2009a] Bonhommeau S., Blanke B., Tréguere A.M., Grima N., Rivot E., Vermard Y., Greiner E., Le Pape O. 2009a. How fast can the European eel (*Anguilla Anguilla*) larvae cross the Atlantic Ocean?. *Fisheries Oceanography* 18: 371-385.
- [Bonhommeau et al., 2008] Bonhommeau, S., Chassot, E., Rivot, E. 2008. Fluctuation in European eel (*Anguilla anguilla*) recruitment resulting from environmental changes in the Sargasso Sea. *Fisheries Oceanography* 17: 32-44.
- [Bonhommeau et al., 2009b] Bonhommeau S., Le Pape O., Gascuel D., Blanke B., Tréguier A-M., Gima N., Verinat Y., Castonguay M., Rivot E. 2009b. Estimates of the mortality and the duration of the trans-Atlantic migration of European eel *Anguilla anguilla* leptocephali using a particle tracking model. *Journal of Fish Biology* 74: 1891-1914.

- [Böning and Cox, 1988] Böning, C.W., Cox, M.D. 1988. Particle dispersion and mixing of conservative properties in an eddy-resolving model. *Journal of Physical Oceanographic* 18: 320-338.
- [Booth, 1986] Booth, J.D. 1986. Recruitment of packhorse rock lobster *Jasus verreauxi* in New Zealand. *Canadian Journal of Fisheries and Aquatic Sciences*, 43(11): 2212–2220.
- [Booth and Phillips, 1994] Booth, J.D., Phillips, B.F. 1994. Early life history of spiny lobster. *Crustaceana* 66(3): 271-294.
- [Bowditch, 2017] Bowditch, N. Ed. 2017. American Practical Navigator. National Geospatial-Intelligence Agency. ISBN: 9781942388562.
- [Bradford et al., 2005] Bradford, R.W., Bruce, B.D., Chiswell, S.M., Booth, J.D., Jeffs, A., Wotherspoon, S. 2005. Vertical distribution and diurnal migration patterns of *Jasus edwardsii* phyllosomas off the east coast of the North Island, New Zealand. *Journal of Marine and Freshwater Research* 39: 593-604.
- [Brown et al., 2001] Brown, E., Colling, A., Park, D., Phillips, J., Rothery, D., Wright, J. 2001. Ocean Circulation. 2nd edn. Ed. by Butterworth-Heinemann, in association with the Open University, Boston. 286 pp.
- [Bull and van Sebille, 2016] Bull C.Y.S., van Sebille E. 2016. Sources, fate, and pathways of Leeuwin Current water in the Indian Ocean and Great Australian Bight: A Lagrangian study in an eddy-resolving ocean model. *Journal of Geophysical Research Oceans* 121: 1626-1639.
- [Butler et al., 2011] Butler, M.J., Paris, C.B., Goldstein, J. S., Matsuda, H., Cowen, R.K. 2011. Behavior constrains the dispersal of long-lived spiny lobster larvae. *Marine Ecology Progress Series* 422: 223-237.
- [Carlson et al., 2017] Carlson, D.F., Suaria, G., Aliani, S., Fredj, E., Fortibuoni, T., Griffa, A., Russo, A., Melli, V. 2017. Combining litter observations with a regional ocean model to identify sources and sinks of floating debris in a semi-enclosed basin: The Adriatic Sea. *Frontiers in Marine Science*, 4: 78.
- [Carton et al., 2000a] Carton J.A., Chepurin G., Cao X., Giese B. 2000a. A Simple Ocean Data Assimilation analysis of the global upper ocean 1950-1995. Part 1: methodology. *Journal of Physical Oceanography* 30(2): 294-309.
- [Carton et al., 2000b] Carton J.A., Chepurin G., Cao X. 2000b. A Simple Ocean Data Assimilation analysis of the global upper ocean 1950-1995. Part 2: results. *Journal of Physical Oceanography* 30(2): 311-326.

- [Carton et al., 2005] Carton J.A., Giese B.S., Grodsky S.A. 2005. Sea level rise and the warming of the oceans in the SODA ocean reanalysis. *Journal of Geophysical Research* 110(C9): 2156-2202.
- [Carton and Giese, 2008] Carton J.A., Giese B.S. 2008. A Reanalysis of Ocean Climate Using Simple Ocean Data Assimilation (SODA). *Monthly Weather Review* 136(8): 2999-3017.
- [Casey et al., 2010] Casey, K.S., Brandon, T.B., Cornillon, P., Evans, R. 2010. The past, present, and future of the AVHRR Pathfinder SST program, in *Oceanography from Space*, edited by J. F. R. Gower, V. Barale and L. Alberotanza, pp. 273–287, Springer, Netherlands.
- [Castonguay and McCleave, 1987] Castonguay, M., McCleave, J.D. 1987. Vertical distributions, diel and ontogenetic vertical migrations and net avoidance of leptocephali of *Anguilla* and other common species in the Sargasso Sea. *Journal of Plankton Research* 9: 195–214.
- [Chang et al., 2007] Chang, Y-J., Sun, C-L., Chen, Y., Yeh, S-Z., Chiang, W. 2007. Reproductive biology of the spiny lobster, *Panulirus penicillatus*, in the southeastern coastal waters of Taiwan. *Marine Biology* 151(2): 553-564.
- [Charria et al., 2013] Charria, G., Lazure, P., Le Cann, B., Serpette, A., Reverdin, G., Louazel, S., Batifoulier, F., Dumas, F., Pichon, A., Morel, Y. 2013. Surface layer circulation derived from Lagrangian drifters in the Bay of Biscay. *Journal of Marine Systems* 109-110: 560-576.
- [Chen et al., 2007] Chen, Z., Chuanmin, H., Muller-Karger, F. 2007. Monitoring turbidity in Tampa Bay using MODIS/Aqua 250-m imagery, *Remote Sensing Environment* 109: 207-220.
- [Chenillat et al., 2015] Chenillat, F., Blanke, B., Grima, N., Franks, P.J.S., Capet, X., Rivi re, P. 2015. Quantifying tracer dynamics in moving fluids: a combined Eulerian-Lagrangian approach. *Frontiers in Environmental Science* 3: 1-5.
- [Chiswell and Booth, 2017] Chiswell S.M., Booth J.D. 2017. Evolution of long larval life in the Australasian rock lobster *Jasus edwardsii*. *Inter-Research Marine Ecology Progress Series* 576: 69-87.
- [Church et al., 2011] Church, J.A., White, N.J., Kokikow, L.F., Domingues, C.M., Cogley, G.J., Rignot, E., Gregory, J.M., van den Broeke, M.R., Monaghan, A.J., Velicogna, I. 2011. Revisiting the earth’s sea-level and energy budgets from 1961 to 2008, *Geophysical Research Letters* 38(18): L18601.

- [Chykek et al., 2006] Chylek, P., Dubey, M.K., Lesins, G. 2006. Greenland warming of 1920–1930 and 1995–2005. *Geophysical Research Letters* 33: L11707.
- [Chylek et al., 2014] Chylek, P., Klett, J.D., Lesins, G., Dubey, M.K., Hengartner, N. 2014. The Atlantic Multidecadal Oscillation as a dominant factor of oceanic influence on climate. *Geophysical Research Letters* 41(5): 1689-1697.
- [Cornillon, 1992] Cornillon P. Gulf Stream. 1992. In: Encyclopedia of earth system science, vol. 2. Academic Press Inc. pp 465-480.
- [Costoya et al., 2015] Costoya, X., deCastro, M., Gómez-Gesteira, M., Santos, F. 2015. Changes in sea Surface temperature seasonality in the Bay of Biscay over the last decades (1982–2014), *Journal of Marine Systems* 150, 91–101.
- [Costoya et al., 2016] Costoya, X., Fernández-Nóvoa, D., deCastro, M., Santos, F., Lazure, P., Gómez-Gesteira, M. 2016. Modulation of sea surface temperature warming in the Bay of Biscay by Loire and Gironde Rivers, *Journal of Geophysical Research Oceans*, 120, 966-979.
- [Courant et al., 1928] Courant, R., Friedrichs, K., Lewy, H. 1928. Über die partiellen Differenzgleichungen der mathematischen Physik, *Mathematische Annalen (in german)*, 100(1): 32-74.
- [Courant et al., 1967] Courant, R., Friedrichs, K., Lewy, H. 1967. On the partial difference equations of mathematical physics. *IBM Journal of Research and Development*, 11(2): 215-234.
- [Coutures, 2003] Coutures, E. 2003. The biology and artisanal fishery of lobsters of American Samoa. DMWR Biological Report Series, 103.
- [Cowen et al., 2000] Cowen, R.K., Iwiza, K.M., Sponaugle, S., Paris, C.B., Olson, D.B. 2000. Connectivity of marine population: open or closed?. *Science* 2887(5454): 857-859.
- [Cowen and Sponaugle, 2009] Cowen, R.K., Sponaugle, S. 2009. Larval dispersal and marine population connectivity. *Annual Review of Marine Science* 1, 443-466.
- [Cummings, 2005] Cummings J.A. 2005. Operational multivariate ocean data assimilation. *Quarterly Journal of the Royal Meteorological Society Part C.*, 131(613): 3583-3604.
- [Cummings and Smedstad, 2013] Cummings J.A., Smedstad O.M. 2013. Variational Data Assimilation for the Global Ocean. Data Assimilation for Atmospheric, Oceanic and Hydrologic Applications vol. II, chapter 13, 303-343.

- [deCastro et al., 2009] deCastro, M., Gómez-Gesteira, M., Álvarez, I., Gesteira, J.L.G. 2009. Present warming within the context of cooling–warming cycles observed since 1854 in the Bay of Biscay, *Continental Shelf Research* 29: 1053–1059.
- [Dekker et al., 2003] Dekker, W., Casselman, J.M., Cairns, D.K., Tsukamoto, K., Jellyman, D., Lickers, H. 2003. Worldwide decline of eel resources necessitates immediate action. Québec Declaration of Concern. *Fisheries* 28(12): 28-30.
- [Dennis et al., 2001] Dennis, D.M., Pitcher, C.R., and Skewes, T.D. 2001. Distribution and transport pathways of *Panulirus ornatus* (Fabricius, 1776) and *Panulirus* spp. larvae in the Coral Sea, Australia. *Marine and Freshwater Research* 52(8): 1175-1185.
- [Dias et al. 2001] Dias, J.M., Lopes, J.F., Dekeyser, I. 2001. Lagrangian transport of particles in Ria de Aveiro Lagoon, Portugal. *Physics and Chemistry of Earth, Part B: Hydrology, Oceans and Atmosphere*, 26(9): 721-727.
- [Díaz et al., 2008] Díaz B., Pavón A., Gómez-Gesteira M. 2008. Use of a probabilistic particle tracking model to simulate the Prestige oil spill. *Journal of Marine Systems* 72(1): 159-166.
- [Dima and Lohman, 2007] Dima, M., Lohman, G. 2007. A hemispherical mechanism for the Atlantic Multidecadal Oscillation, *Journal of Climate* 20: 2706–2719.
- [DiMarco and Reid, 1998] DiMarco, S. F., Reid, R.O. 1998. Characterization of the principal tidal current constituents on the Texas-Louisiana Shelf, *Journal of Geophysical Research* 103(C2): 3093–3109.
- [Döös, 1995] Döös, K. 1995. Inter-ocean exchange of water masses. *Journal of Geophysical Research* 100: 13499-13514.
- [Drijfhout et al., 1996] Drijfhout, S.S., Maier-Reimer, E., Mikolajewicz, U. 1996. Tracing the conveyor belt in the Hamburg large-scale geostrophic ocean general circulation model. *Journal of Geophysical Research* 101: 22563-22575.
- [Elliot et al., 1992] Elliot, A.J., Dale, A.C., and Proctor, R. 1992. Modelling the movement of pollutants in the UK Shelf Seas. *Marine Pollution Bulletin*, 24(12): 614-619.
- [Enfield et al., 2001] Enfield D.B., Mestas-Nuñez A.M., Trimble P.J. 2001. The Atlantic Multidecadal Oscillation and its relation to rainfall and river flows in the continental U.S. *Geophysical Research Letters* 28: 2077-2080.

- [Etter and Bower, 2015] Etter R.J, Bower A.S. 2015. Dispersal and population connectivity in the deep North Atlantic estimated from physical transport processes. *Deep Sea Research Part I* 104: 159-172.
- [Feng et al., 2011] Feng, M., Caputi, N., Penn, J., Slawinski, D., de Lestang, S., Weller, E., Pearce, A. 2011. Ocean circulation, Stokes drift and connectivity of western rock lobster (*Panulirus Cygnus*) population. *Canadian Journal of Fisheries and Aquatic Sciences* 68: 1182-1196.
- [Fernández-Nóvoa et al., submitted manuscript, 2018] Fernández-Nóvoa, D., Costoya, X., **Rodríguez-Díaz, L.**, deCastro, M., Gómez-Gesteira, M. [Under Review]. Modulation of SST warming in the Northwestern Gulf of Mexico due to Mississippi and Atchafalya Rivers. Submitted to *Journal of Geophysical Research*.
- [Fernández-Nóvoa et al., 2015] Fernández-Nóvoa, D., Mendes, R., deCastro, M., Dias, J.M., Sánchez-Arcilla, A., Gómez-Gesteira, M. 2015. Analysis of the influence of river discharge and wind on the Ebro turbid plume using MODIS-Aqua and MODIS-Terra data, *Journal of Marine Systems* 142: 40–46.
- [Fujio and Imasato, 1991] Fujio, S., Imasato, N. 1991. Diagnostic calculation for circulation and water mass movement in the deep pacific. *Journal of Geophysical Research* 96 (C1): 759-774.
- [Gargano et al., 2017] Gargano F., Garofalo G., Fiorentino F. 2017. Exploring connectivity between spawning and nursery areas of *Mullus barbatus* (L. 1758) in the Mediterranean through a dispersal model. *Fisheries and Oceanography* 26:4: 476-497.
- [Glenn et al., 2015] Glenn, E., Comarazamy, D., Gonzalez, J.E., Smith, T. 2015. Detection of recent regional sea Surface temperatura warming in the Caribbean and surrounding region. *Geophysical Research. Letters* 42, 6785-6792.
- [Gómez-Gesteira et al., 1999] Gómez-Gesteira, M., Montero, P., Prego, R., Taboada, J.J., Leitao, P., Ruiz-Villarreal, M., Neves, R., Perez-Villar, V. 1999. A two-dimensional particle tracking model for pollution dispersion in A Coruña and Vigo Rias (NW Spain). *Oceanologica Acta* 22 (2): 167-177.
- [Gordon and Giulivi, 2014] Gordon, A.L., Giulivi, C.F. 2014. Ocean eddy freshwater flux convergence into the North Atlantic subtropics. *Journal of Geophysical Research* 119(6), 3327-3335.

- [Govinden and Hollanda, 2013] Govinden, R., Hollanda, S. 2013. The Seychelles Spiny Lobster Fishery: Fishery and Stock Status: 2010-2013. Seychelles Fishing Authority, Victoria, Seychelles, 25 pp.
- [Gouretski et al., 2012] Gouretski, V., Kennedy, J., Boyer, T., Köhl, A. 2012. Consistent near-surface ocean warming since 1900 in two largely independent observing networks, *Geophysical Research Letters*, 39 (19).
- [Griffin et al., 2001] Griffin, D.A., Wilkin, J.L., Chubb, C.F., Pearce, A.F., Caputi, N. 2001. Ocean currents and the larval phase of Australian western rock lobster, *Panulirus cygnus*. *Marine and Freshwater Research* 52: 1187–1199.
- [Hakkinen and Rhines, 2009] Hakkinen S., Rhines P.B. 2009. Shifting surface currents in the northern North Atlantic Ocean, *Journal of Geophysical Research-Oceans* 114(20): C04005.
- [Hancke et al., 2014] Hancke, L., Roberts, M.J., Ternon, J.F. 2014. Surface drifter trajectories highlight flow pathways in the Mozambique Channel. *Deep- Sea Research II* 100: 27-37.
- [Hare et al., 2002] Hare J.A., Churchill J.H., Cowen R.K., Berger T.J., Cornillon P.C., Dragos P., Glen S.M., Govoni J.J., Lee T.N. 2002. Routes and rates of larval fish transport from the southeast to the northeast United States continental shelf. *Limnology and Oceanography* 47(6): 1774-1789.
- [Hellweger et al., 2014] Hellweger, F.L., van Sebille, E., Fredrick, N.D. 2014. Biogeographic patterns in ocean microbes emerge in a neutral agent-based model. *Science* 345: 1346-1349.
- [Hetland and Dimarco, 2012] Hetland, R.D., Dimarco, S.F. 2012. Skill assessment of a hydrodynamic model of circulation over the Texas-Louisiana continental shelf, *Ocean Model.*, 43, 64-76.
- [Heywood et al., 1994] Heywood, K.J., Mconagh, E.L., White, M.A. 1994. Eddy kinetic energy of the North Atlantic subpolar gyre from satellite altimetry. *Journal of Geophysical Research Oceans* 99: 22525-22539.
- [Hogg and Johns, 1995] Hogg N.G., Johns W.E. 1995. Western boundary currents. *Reviews of Geophysics* 33(S2): 1311-1334.
- [Howden and Murtugudde, 2001] Howden, S.D., Murtugudde, R. 2001. Effects of river inputs into the Bay of Bengal, *Journal of Geophysical Research* 106(C9), 19,825–19,843.

- [Hsu et al., 2017] Hsu, A.C., Xue, H., Chai, F., Xiu, P., Han, Y-S. 2017. Variability of the Pacific North Equatorial Current and its implications on Japanese eel (*Anguilla japonica*) larval migration. *Fisheries Oceanography*, 23(3): 251-267.
- [Hu et al., 2005] Hu, C., Nelson, J.R., Johns, E., Chen, Z., Weisberg, R.R., Müller-Karger, F.E. 2005. Mississippi River water in Florida Straits and in the Gulf Stream off Georgia in summer 2004, *Geophysical Research Letters* 32: L14606.
- [Hurrell, 1995] Hurrell J.W. 1995. Decadal Trends in the North Atlantic Oscillation: Regional temperatures and precipitation. *Science* 269: 676-679.
- [Imasato et al., 1980] Imasato, N., Awaji, T., Kunishi, H. 1980. Tidal exchange through naruto, akashi and kitan straits. *Journal of Oceanography Society Japan* 36(3): 151-162.
- [Imasato and Qiu, 1987] Imasato, N., Qiu, B. 1987. An event in water exchange between continental shelf and the kuroshi off southern Japan: Lagrangian tracking of a low-salinity water mass on the kuroshi. *Journal of Physical Oceanographic* 17(7): 953-968.
- [IPCC, 2013] IPCC 2013. Climate Change 2013: The Physical Science Basis. Contribution of Working Group I to the Fifth Assessment Report of the Intergovernmental Panel on Climate Change. In: Stocker, T.F., D. Qin, G.K. Plattner, M. Tignor, S.K. Allen, J. Boschung, A. Nauels, Y. Xia, V. Bex, and P.M. Midgley (Eds.), Cambridge University Press, Cambridge, United Kingdom and New York, NY, USA (1535 pp.).
- [Jespersen, 1942] Jespersen, P. 1942. Indo-Pacific leptocephalids of the genus *Anguilla*. Dana Rep. 22:1-128.
- [Johnson, 1968] Johnson, M.W. 1968. Palinurid phyllosoma from the Hawaiian archipelago (Palinuridae) *Crustaceana, Supplement*, 2: 59-79.
- [Joung and Shiller, 2014] Joung, D., Shiller, A.M. 2014. Dissolved barium behavior in Louisiana Shelf waters affected by the Mississippi/Atchafalaya River mixing zone, *Geochim. Cosmochim. Acta*, 141, 303-313.
- [Juinio, 1987] Juinio, M.A. 1987. Some aspects of the reproduction of *Panulirus penicillatus* (Decapoda: Palinuridae). *Bulletin of Marine Science* 41(2): 242-252.
- [Kawada et al., 2013] Kawada, A., Ruiz-Barradas, A., Nigam, S. 2013. AMO's structure and climate footprint in observations and IPCCAR5 climate simulations. *Climate Dynamics* 41: 1345–1364.

- [Kawase, 1993] Kawase, M. 1993. Topographic effect on the bottom water circulation of the western tropical North Atlantic Ocean. *Deep-Sea Research I*: 40(6): 1259-1283.
- [Kelly, 1991] Kelly K.A. 1991. The meandering Gulf Stream as seen by the Geosat altimeter: surface transport, position and velocity variance from 73° to 46°W. *Journal of Geophysical Research* 96(C9): 16721-16738.
- [Kerr, 2000] Kerr, R.A. 2000. A North Atlantic climate pacemaker for the centuries, *Science* 288: 1984–1986.
- [Kettle and Haines, 2006] Kettle A.J, Haines K. 2006. How does the European eel (*Anguilla anguilla*) retains its population structure during its larval migration across the North Atlantic Ocean?. *Canadian Journal of Fisheries and Aquatic Sciences* 63(1), 90-106.
- [Kim et al., 2014] Kim, T-H, Yang, C-S., Oh, J-H., Ouchi, K. 2014. Analysis of the contribution of wind drift factor to oil slick movement under strong tidal condition: Hebei Spirit Oil Spill case. *PLoS ONE* 9(1): e87393.
- [Kittaka et al., 2005] Kittaka, J., Ono, K., Booth, J.D., Webber, W.R. 2005. Development of the red rock lobster, *Jasus edwardsii*, from egg to juvenile. *New Zealand Journal of Marine and Freshwater Research*, 39(2): 263–277.
- [Kleckner and McCleave, 1988] Kleckner, R.C., McCleave, J.D. 1988. The northern limit of spawning by Atlantic eel (*Anguilla* spp.) in the Sargasso Sea in relation to thermal fronts and surface water masses. *Journal of Marine Research* 46: 647-667.
- [Kolker et al., 2014] Kolker, A.S., Li, C., Walker, N.D., Pilley, C., Ameen, A.D., Boxer, G., Ramatchandirane, C., Ullah, M., Williams. K.A. 2014. The impacts of the great Mississippi/Atchafalaya River flood on the oceanography of the Atchafalaya Shelf, *Continental Shelf Research* 86: 17-33.
- [Kourafalou et al., 1996] Kourafalou, V.H., Oey, L.Y., Wang, J.D., Lee, T.N. 1996. The fate of river discharge on the continental shelf: 1. Modeling the river plume and the inner shelf coastal current, *Journal of Geophysical Research* 101(C2), 3415-3434.
- [Kozlov et al., 2014] Kozlov, I., Dailidienè, I., Korosov, A., Klemas, V., Mingèlaitè, T. 2014. MODIS-based sea surface temperature of the Baltic Sea Curonian Lagoon, *Journal of Marine Systems* 129: 157–165.
- [Kubryakov et al., 2016] Kubryakov, A., Stanichny, S., Zatseping, A. 2016. River plume dynamics in the Kara Sea from altimetry-based lagrangian model, satellite salinity and chlorophyll data. *Remote Sensing of Environment*, 176: 177-187.

- [Kuroki et al., 2008] Kuroki, M., Momoko, K., Jónsson, B., Aoyama, J., Miller, M.J., Noakes, D.L.G., Tsukamoto, K. 2008. Inshore migration and otolith microstructure/microchemistry of anguillid glass eels to Iceland. *Environmental Biology Fishes* 83: 309-325.
- [Lavin et al., 2003] Lavin, A.M., Bryden, H.L., Parrilla, G. 2003. Mechanisms of heat, freshwater, oxygen and nutrient transports and budgets at 24.5 °N in the subtropical North Atlantic. *Deep-Sea Research I* 50(9): 1099-1128.
- [Lebreton et al., 2012] Lebreton L.C.M., Greer S.D., Borrero J.C. 2012. Numerical modelling of floating debris in the world's oceans. *Marine Pollution Bulletin* 64: 653-661.
- [Lecomte-Finiger, 1992] Lecomte-Finiger, R. 1992. Growth history and age at recruitment of European glass eels (*Anguilla Anguilla*) as revealed by otolith microstructure. *Marine Biology* 114: 205-210.
- [Leonard and Summers, 1976] Leonard, J.B., Summers, R.G. 1976. The ultrastructure of the integument of the American eel, *Anguilla rostrata*. *Cell and Tissue Research* 171: 1-30.
- [Levitus et al., 2012] Levitus, S., Antonov, J.I., Boyer, T.P., Branova, O.K., Garcia, H.E., Locarnini, R.A., Mishonov, A.V., Reagan, J.R., Seidov, D., Yarosh, E.S., Zweng, M.M. 2012. World ocean heat content and thermosteric sea level change (0-2000 m), 1955-2010, *Geophysical Research Letters*, 39, L01603.
- [Li and Clarke, 2005] Li, J., Clarke, A.J. 2005. Sea surface temperature and the brown shrimp (*Farfantepenaeus aztecus*) population on the Alabama, Mississippi, Louisiana and Texas continental shelves. *Estuarine, Coastal and Shelf Science* 64, 261-266.
- [Lillibridge and Mariano, 2012] Lillibridge, J. L., Mariano, A.J. 2012. A statistical analysis of Gulf Stream variability from 181 years of altimetry data. *Deep-Sea Research II*, 85, 1–20.
- [Lima and Wethey, 2012] Lima, F.P., Wethey, D.S. 2012. Three decades of high-resolution coastal sea surface temperature reveal more than warming. *Nature Communications* 3, article 704.
- [MacDonald, 1979] MacDonald, C.D. 1979. Management aspects of the biology of the spiny lobsters, *P. marginatus*, *P. penicillatus*, *P. versicolor* and *P. longipes femoristriga* in Hawaii and the Western Pacific. Final Report to the Western Pacific Regional Fishery Management Council, Honolulu, Hawaii, 46 pp.

- [MacDonald, 1988] MacDonald, C.D. 1988. Fecundity and reproductive rates in Indo-West Pacific spiny lobsters. *Micronesica* 21: 103-114.
- [Mansui et al., 2015] Mansui, J., Molcard, A., Ourmières, Y. 2015. Modelling the transport and accumulation of floating marine debris in the Mediterranean basin. *Marine Pollution Bulletin*, 91: 249-257.
- [Marta-Almeida et al., 2013] Marta-Almeida, M., Hetland, R.D., Zhang, X. 2013. Evaluation of model nesting performance on the Texas-Louisiana continental shelf, *Journal of Geophysical Research Oceans* 118: 2476–2491.
- [Materia et al., 2012] Materia, S., Gualdi, S., Navarra, A., Terray, L. 2012. The effect of Congo River freshwater discharge on Eastern Equatorial Atlantic climate variability, *Climate Dynamincs* 39: 2109–2015.
- [Matsuda et al., 2006] Matsuda, H., Takenouchi, T., Goldstein, J.S. 2006. The complete larval development of the pronghorn spiny lobster *Panulirus penicillatus* (Decapoda: Paniluridae) in culture. *Journal of Crustacean Biology* 26(4): 579-600.
- [Marancik et al., 2011] Marancik, K.E, Richardson, D.E, Lyczkowski-Shultz, J., Cowen, R.K., Konieczna, M. 2011. Spatial and temporal distribution of group larvae (Serranidae: Epinephelinae: Epinephelini) in the Gulf of Mexico and Straits of Florida. *Fishery Bulletin* 110: 1-20.
- [Mayer et al., 2010] Mayer, B., Damm, P.E., Pohlmann, T., Rizal, S. 2010. What is driving the ITF? An illumination of the Indonesian throughflow with a numerical nested model system. *Dynamics of Atmosphere and Oceans*, 50(2): 301-312.
- [McClain and Hardy, 2010] McClain C.R., Hardy S.M. 2010. The dynamics of biogeographic ranges in the deep sea. *Proceedings of the Royal Society B Biological Sciences* 277(1700): 3533-3546.
- [McCleave et al., 1998] McCleave, J.D., Brickley, P.J., O'Brien, K.M., Kistner, D.A. 1998. Do leptocephali of the European eel swim to reach continental water? Status of the question. *Journal of Marine Biology Association of the United Kingdom* 78: 285-306.
- [Menard, 1983] Menard, Y. 1983. Observations of eddy fields in the northwest Atlantic and northwest Pacific by SEASAT altimeter data. *Journal of Geophysical Research Oceans* 88: 1853-1866.

- [Miller and McKee, 2004] Miller, R.L., McKee, B.A. 2004. Using MODIS Terra 250 m imagery to map concentrations of total suspended matter in coastal waters, *Remote Sensing Environmental* 93: 259–266.
- [Milliman and Meade, 1983] Milliman, J. D., Meade, R.H. 1983. World-wide delivery of river sediment to the ocean, *Journal of Geology* 91(1), 1–21.
- [Milton et al., 2014] Milton, D.A, Satria, F., Proctor, C.H., Prasetyo, A.P., Utama, A.A., Fauzi, M. 2014. Environmental factors influencing the recruitment and catch of tropical *Panulirus* lobsters in southern Java, Indonesia. *Continental Shelf Research*, 91: 247-255.
- [Minami et al., 2001] Minami, H., Inoue, N., Sekiguchi, H. 2001. Vertical distribution phyllosoma larvae in the western North Pacific. *Journal of Oceanography* 57: 743-748.
- [Montero et al., 1999] Montero, P., Gómez-Gesteria, M., Taboada, J.J., Ruiz-Villarreal, M., Santos, A.P., Neves, R.R., Prego, R., Pérez-Villar, V. 1999. On residual circulation of the Ria of Vigo, using a 3-D baroclinic model. *Boletín Instituto Español de Oceanografía*, 15(1-4): 31-38.
- [Montero et al., 1996] Montero, P., Prego, R., Gómez-Gesteiro, M., Neves, R., Taboada, J.J., Pérez-Villar, V. 1996. Aplicación de un modelo 2D al transporte de partículas en la bahía de la Coruña. In *Actas del VIII Seminario Ibérico de Química Marina (Prego, R. and Fenández, J.m. eds)*, 131-136.
- [Morris, 2010] Morris R.A. 2010. A bioeconomic analysis of the jamaican industrial Spiny lobster (*panulirus argus*) fishery. United Nations University: Fisheries Training Programme.
- [Muhling et al., 2012] Muhling, B.A., Lamkin, J.T., Richards, W.J. 2012. Decadal-scale responses of larval fish assemblages to multiple ecosystem processes in the northern Gulf of Mexico, *Marine Ecology Progress Series* 450, 37-53.
- [Muller et al., 2013] Muller, R.A., Curry, K., Groom. D., Jacobsen, R., Perlmutter, S., Rohde, R., Rosenfeld, A., Wickham, C., Wurtele, J. 2013. Decadal variations in the global atmospheric land temperatures, *Journal of Geophysical Research Atmospheres* 118, 5280–5286
- [Neumann et al., 2014] Neumann, D., Callies, U., Matthies, M. 2014. Marine litter ensemble transport simulations in the southern North Sea. *Marine Pollution Bulletin*, 86, 219-228.

- [Ogata and Masumoto, 2011] Ogata, T., Masumoto, Y. 2011. Interannual modulation and its dynamics of the mesoscale eddy variability in the southeastern tropical Indian Ocean. *Journal of Geophysical Research*, 116, C05005.
- [Osadchiev and Zaviolov, 2013] Osadchiev, A.A., Zaviolov, P.O. 2013. Lagrangian model of a surface-advected river plume. *Continental Shelf Research*, 58: 96-106.
- [Pacariz et al., 2014] Pacariz S., Westerberg H., Björk G. 2014. Climate change and passive transport of European eel larvae. *Ecology of Freshwater Fish* 23(1): 86-94.
- [Pakoa et al., 2012] Pakoa, K., Kabu, R., Nimitia, T. 2012. Status of pronghorn spiny lobster fishery in Aneityum Island, Vanuatu, and management advice. *SPC Fisheries Newsletter* 138: 31-36.
- [Paris et al., 2013] Paris C.B., Helgers J., van Sebille E., Srinivasan A. (2013). Connectivity Modeling System: A probabilistic modeling tool for the multi-scale tracking of biotic and abiotic variability in the ocean. *Environmental Modelling & Software* 42: 47-54.
- [Park et al., 2011] Park, T., Jand, C.J., Jungclaus, J.H., Haak, H., Park, W., Oh, I.S. 2011. Effects of the Changjiang river discharge on sea surface warming in the Yellow and East China Seas in summer, *Continental Shelf Research* 31, 15–22.
- [Phillips et al., 2006] Phillips, B.F., Booth, J.D., Cobb, J.S., Jeffs, A.G., McWilliam, P. 2006. Chapter 7. Larval and postlarval ecology, in *Lobsters: Biology, Management Aquaculture and Fisheries*, Ed. by B.F. Phillips, Blackwell Publishing Ltd, Oxford, 506 pp.
- [Pitcher, 1993] Pitcher, C.R. 1993. Chapter 17. Spiny lobster, in *Nearshore Marine Resources of the South Pacific. Information for Fisheries Development and Management*, Ed. by A. Wright and L. Hill, Institute of Pacific Studies, Suva, Forum Fisheries Agency, Honiara, International Centre for Ocean Development, Canada, 710 pp.
- [Plaut, 1993] Plaut, I. 1993. Sexual maturity, reproductive season and fecundity of the spiny lobster *Panulirus penicillatus* from the Gulf of Eilat (Aqaba), Red Sea, Australian. *Journal of Marine and Freshwater Research* 44(4): 527-535.
- [Politikos et al., 2017] Politikos, D.V., Loakeimidis, C., Papatheodorou, G., Tsiaras, K. 2017. Modeling the fate and distribution of floating litter particles in the Aegean Sea (E: Mediterranean). *Frontiers in Marine Science*, 4:191.
- [Polyako and Johnson, 2000] Polyako, I.V., Johnson, M.A. 2000. Artic decadal and interdecadal variability. *Geophysical Research Letters* 27(24): 4097-4100.

- [Pous et al., 2010] Pous, S., Feunteu E., Ellien C. 2010. Investigation of tropical eel spawning area in the South-Western Indian Ocean: Influence of the oceanic circulation. *Progress in Oceanography* 86(3-4): 396-413.
- [Putman and He, 2013] Putman, N.F., He R.Y. 2013. Tracking the long-distance dispersal of marine organisms: sensitivity to ocean model resolution. *Journal of the Royal Society Interface* 10(81): 20120979.
- [Qin et al., 2014] Qin X., van Sebille E., Sen Gupta A. 2014. Quantification of errors induced by temporal resolution on Lagrangian particles in an eddy-resolving model. *Ocean Modelling* 76: 20-30.
- [Relvas et al., 2009] Relvas, P., Luis, J., Santos, A.M.P. 2009. Importance of the mesoscale in the decadal changes observed in the northern Canary upwelling system, *Geophys. Res. Lett.*, 36, L22601.
- [Reynolds, 2009] What's New in Version 2, NOAA/NCDC Rep., 10 pp., Asheville. [Available at http://www.ncdc.noaa.gov/oa/climate/research/sst/papers/whats_new_v2.pdf.]
- [Reynolds and Chelton, 2010] Reynolds, R.W., and Chelton, D.W. 2010. Comparisons of daily sea surface temperature analysis for 2007–08, *Journal of Climate*, 23, 3545–3562, doi:10.1175/2010JCLI3294.1.
- [Reynolds et al., 2007] Reynolds, R.W., Smith, T.M., Liu, C., Chelton, D.B., Casey, K.S. Schlax, M.G. 2007. Daily high-resolution-blended analyses for sea surface temperature, *Journal of Climate* 20(22): 5473–5496.
- [Richardson, 2001] Richardson P.L. 2001. Florida Currents, Gulf Stream, and Labrador Current. Steel J., Turekian K., Thorpe S. (Eds.), *Encyclopedia of Ocean Sciences*, Elsevier, vol. 2, pp 1054-1064.
- [Rodríguez-Díaz et al., submitted manuscript, 2018] **Rodríguez-Díaz, L.**, Álvarez, I., Gómez-Gesteira, M., Santos, F. [Under Review]. Changes in the probability of larvae crossing the North Atlantic over the twentieth century. Submitted to *Marine and Freshwater Research*.
- [Rodríguez-Díaz and Gómez-Gesteira, 2017] **Rodríguez-Díaz, L.**, Gómez-Gesteira, M. 2017. Can lagrangian models reproduce the migration time of European eel obtained from otolith analysis? *Journal of Sea Research* 130: 17-23.
- [Rodríguez-Díaz et al., submitted manuscript] **Rodríguez-Díaz, L.**, Gómez-Gesteira, M., Santos, F. [Under Review]. Can the connectivity among spiny lobster *Panulirus*

Penicillatus populations in the Indian Ocean be explained in terms of currents?
Submitted to *ICES Journal of Marine Science*.

- [Rong et al., 2014] Rong, Z., Hetland, R.D., Zhang, W., Zhang, X. 2014. Current–wave interaction in the Mississippi–Atchafalaya river plume on the Texas–Louisiana shelf, *Ocean Model.*, 84, 67-83.
- [Rudorff et al., 2009] Rudorff, A.A.G., Lorenzetti, J.A., Gherardi, D.F.M., Lins-Oliveira, J.E. 2009. Modeling spiny lobster larval dispersion in the Tropical Atlantic. *Fisheries Research* 96: 206-215.
- [Sabatini et al., 2008] Sabatini, G., Salley, S., Ramanamanjato, J.B. 2008. A review of the spiny lobster fishery in the Tolagnaro (Fort-Dauphin) Region. *Biodiversity, ecology and conservation of littoral ecosystems in Southeastern Madagascar, Tolagnaro*, 299-308
- [Saha et al., 2010] Saha, S., Moorthi, S., Pan, H., Wu, X., Wang, J., Nadiga, S., Tripp, P., Kistler, R., Woollen, J., Behringer, D., Liu, H., Stokes, D., Grumbine, R., Gayno, G., Wang, J., Hou, Y., Chuang, H., Juang, H. H., Sela, J., Iredell, M., Treadon, R., Kleist, D., Van Delst, P., Keyser, D., Derber, J., Ek, M., Meng, J., Wei, H., Yang, R., Lord, S., Van Den Dool, H., Kumar, A., Wang, W., Long, C., Chelliah, M., Xue, Y., Huang, B., Schemm, J., Ebisuzaki, W., Lin, R., Xie, P., Chen, M., Zhou, S., Higgins, W., Zou, C., Liu, Q., Chen, Y., Han, Y., Cucurull, L., Reynolds, R. W., Rutledge, G., Goldberg, M. 2010. The NCEP climate forecast system reanalysis, *Bulletin of the American Meteorological Society* 91(8): 1015–1057.
- [Sala et al., 2013] Sala I., Caldeira R.M.A., Estrada-Allis S.N., Froufe E., Couvelard X. 2013. Lagrangian transport pathways in the northeast Atlantic and their environmental impact. *Limnology and Oceanography Fluids and Environments* 3(1): 40-60.
- [Sala et al., 2016] Sala I., Harrison C.S., Caldeira R.M.A. 2016. The role of the Azores Archipelago in capturing and retaining incoming particles. *Journal of Marine Systems* 154: 146-156.
- [Salisbury et al., 2004] Salisbury, J.E., Campbell, J.W., Linde, r E., Meeker, L.D., Muller-Karger, F.E., Vorosmarty, C.J. 2004. On the seasonal correlation of surface particle fields with wind stress and Mississippi discharge in the northern Gulf of Mexico, *Deep Sea Research Part II* , 51, 1187–1203.
- [Santos et al., 2012a] Santos, F., Gómez-Gesteira, M., deCastro, M., Alvarez, I. 2012a. Variability of coastal and ocean water temperature in the upper 700 m along the Western Iberian Peninsula from 1975 to 2006, *PLoS One*, 7(12), 1–7.

- [Santos et al., 2012b] Santos, F., Gómez-Gesteira, M., deCastro, M., Alvarez, I. 2012b. Differences in coastal and oceanic SST trends due to the strengthening of coastal upwelling along the Benguela current system, *Continental Shelf Research* 34: 79–86.
- [Santos et al., 2012c] Santos, F., deCastro, M., Gómez-Gesteira, M., Alvarez, I. 2012c. Differences in coastal and oceanic SST warming rates along the Canary upwelling ecosystem from 1982 to 2010, *Continental Shelf Research* 47: 1–6.
- [Santos et al., 2015] Santos, F., Gómez-Gesteira, M., deCastro, M., Dias, J.M. 2015. A dipole-like SST trend in the Somalia region during the monsoon season, *Journal of Geophysical Research Oceans* 120: 597–607.
- [Schiller et al., 2010] Schiller, A., Wijffels, S.E., Sprintall, J., Molcard, R., Oke, P.R. 2010. Pathways of intraseasonal variability in the Indonesian Flowthrough region. *Dynamics of Atmosphere and Oceans* 50(2): 174-200.
- [Schmidt, 1922] Schmidt, J. 1922. The breeding places of the eel. *Philosophical Transactions of the Royal Society B London* 211:179–211.
- [Schmidt, 1923] Schmidt, J. 1923. Breeding places and migration of the eel. *Nature* 111:51–54.
- [Schmidt, 1925] Schmidt, J. 1925. The breeding places of the eel. *Annual Report of the Smithsonian Institution for 1924*, 279–316.
- [Schmidt, 1932] Schmidt, J. 1932. Danish eel investigations during 25 years (1905-1930). Nordisk Forl. Kobenhavn, 16pp.
- [Schoth and Tesh, 1982] Schoth, M., Tesh, F.W. 1982. Saptial distribution of 0-group eel larvae (*Anguila* sp.) in the Sargasso Sea. *Helgolander Meeresuntersuchungen* 35: 309-320.
- [Schott and McCreary, 2001] Schott, F., McCreary, J.P. 2001. The monsoon circulation of the Indian Ocean. *Progress in Oceanography*, 51(1): 1-123.
- [Schott et al., 2009] Schott, F.A., Stramma, L., Giese, B.S., Zantopp, R. 2009. Labrador Sea convection and subpolar North Atlantic Deep Water export in the SODA assimilation model. *Deep Sea Research Part 1: Oceanography* 56(6), 926-938.
- [Seo et al., 2009] Seo, H., Xie, S.P., Murtugudde, R., Jochum, M., Miller, A.J. 2009. Seasonal effects of Indian ocean freshwater forcing in a regional coupled model, *Journal of Climate* 22(24): 6577–6596.

- [Shenoi et al., 1999] Shenoi, S.S.C., Saji, P.K., Almeida, A.M. 1999. Near-surface circulation and kinetic energy in the tropical Indian Ocean derived from Lagrangian drifters. *Journal of Marine Research*, 57: 885-907.
- [Shi and Wang, 2009] Shi, W., Wang, M. 2009. Satellite observations of flood-driven Mississippi River plume in the spring of 2008, *Geophysical Research Letters* 36, L07607.
- [Silvestre and Pauly, 1997] Silvestre, G., and Pauly, D. 1997. Status and management of tropical coastal fisheries in Asia. ICLARM Conference Proceedings, 53, 208 pp.
- [Sofian, 2007] Sofian, I. 2007. Simulation of the Java Sea using an oceanic general circulation model. *Jurnal Ilmiah Geomatika*, 13(2).
- [Steinberg et al., 2002] Steinberg, D.K., Goldthwait, S.A., Hansell, D.A. 2002. Zooplankton vertical migration and the active transport of dissolved organic and inorganic nitrogen in the Sargasso Sea. *Deep-Sea Research Part I*, 49: 1145-1461.
- [Sutton and Hodson, 2005] Sutton, R.T., Hodson, D.L.R., 2005. Atlantic Ocean forcing of North American and European summer climate. *Science* 290: 2133-2137.
- [Tesch, 1977] Tesch, F.W. 1977. *The Eel - Biology and Management of Anguillid Eels*. Chapman & Hall, London.
- [Tesch, 1980] Tesch, FW. 1980. Occurrence of eel, *Anguilla anguilla*, larvae west of the European continental shelf, 1971-1977. *Environmental Biology Fisheries* 5: 185-190.
- [Tett et al., 2014] Tett, S. F. B., Sherwin, T. J., Shrivastava, A. and Browne, O. 2014. How much has the North Atlantic Ocean overturning circulation changed in the last 50 years? *Journal of Climate* 27, 6325–6342.
- [Timmermann et al., 1998] Timmermann, A., Latif, M., Voss, R., Grötzner, A. 1998. Northern Hemisphere interdecadal variability: A coupled air–sea mode. *Journal of Climate* 11: 1906–1931.
- [Tomczak and Godfrey, 2003] Tomczak M, Godfrey JS. 2003. *Regional oceanography: An Introduction*. 2nd ed. Delhi: Daya Publishing House.
- [Trenberth and Caron, 2001] Trenberth, K.E., Caron, J.M. 2001. Estimates of meridional atmosphere and ocean heat transports. *Journal of Climate* 14: 3433-3443.

- [van Ginneken and Maes, 2005] van Ginneken, V.J.T. and Maes, G.E. 2005. The European eel (*Anguilla anguilla*, Linnaeus), its lifecycle, evolution and reproduction: a literature review. *Reviews in Fish Biology Fisheries* 15: 367-398.
- [van Sebille et al., 2012] van Sebille E., England M.H., Zika J.D., Sloyan B.M. 2012. Tasman leakage in a fine-resolution ocean model. *Geophysical Research Letters* 39: L06601.
- [van Sebille et al., 2018] van Sebille E., Griffies, S.M., Abernathey, R., Adams, T.P., Berloff, P., Biastoch, A., Blanke, B., Chassignet, E.P., Cheng, Y., Cotter, C.J., Dellersnijder, E., Döös, K., Drake, H.F., Drijfhout, S., Gary, S.F., Heemink, A.W., Kjellsson, J., Koszalka, I.M., Lange, M., Lique, C, MacGilchrist, G.A., Marsh, R., Mayorga Adame, C.G., McAdam, R., Nencioli, F.M., Paris, C.B., Piggott, M.D., Polton, J.A., Rühls, S., Shah, S.H.A.M., Thomas, M.D., Wang, J., Wolfram, P.J., Zanna, L., Zika, J.D. 2018. Lagrangian ocean analysis: Fundamentals and practices. *Ocean Modelling* 121: 49-75.
- [van Utrecht and Holleboom, 1985] van Utrecht, W.L., Holleboom, M.A. 1985. Notes on eel larvae (*Anguilla Anguilla* Linnaeus, 1758) from the central and eastern North Atlantic and on glass eels from European continental shelf. *Bijdragen Tot de Dierkunde*, 55(2): 249-262.
- [Varela et al., 2015] Varela, R., Álvarez, I., Santos, F., and Gómez-Gesteira, M. 2015. Has upwelling strengthened along worldwide coasts over 1982-2010?, *Scientific Reports*, 5, article 10016.
- [Vizy and Cook, 2010] Vizy, E.K., Cook, K.H. 2010. Influence of the Amazon/Orinoco Plume on the summertime Atlantic climate, *Journal of Geophysical Research* 115, D21112.
- [Walker, 1996] Walker, N.D. 1996. Satellite assessment of Mississippi River plume variability: Causes and predictability, *Remote Sensing Environmental* 58, 21–35.
- [Walker et al., 2005] Walker, N.D., Wiseman Jr., W.J., Rouse Jr., L.J., Babin, A. 2005. Effects of river discharge, wind stress, and slope eddies on circulation and satellite-observed structure of the Mississippi River plume, *Journal of Coastal Research* 216, 1228–1244.
- [Wang and Tzeng, 2000] Wang C.H., Tzeng W.N. 2000. The timing of metamorphosis and growth rates of American and European eel leptocephali: A mechanism of larval segregative migration. *Fisheries Research* 46(1): 191–205.

- [Wang et al., 1998] Wang, W., Nowlin, W.D., Reid, R.O. 1998. Analyzed surface meteorological fields over the northwestern Gulf of Mexico for 1992–94: Mean, seasonal, and monthly patterns, *Monthly Weather Review*, 126(11), 2864–2883.
- [White and Heywood, 1995] White, M.A and Heywood, K.J. 1995. Seasonal and interannual changes in the North Atlantic subpolar gyre from Geosat and TOPEX/POSEIDON altimetry. *Journal of Geophysical Research Oceans* 100: 100, 24931-24941.
- [White and Toumi, 2014] White, R.H., Toumi, R. 2014. Riverflow and ocean temperatures: The Congo River, *Journal of Geophysical Research Oceans*, 119: 2501–2517.
- [Williams et al., 2011] Williams, R.G., McDonagh, E., Roussenov, V.M., Torres-Valdes, S., King, B., Sanders, R., Hansell, D.A. 2011. Nutrients streams in the North Atlantic: Advective pathways of inorganic and dissolved organic nutrients. *Global Biogeochemical Cycles*, 25, GB4008.
- [Yeung et al., 2000] Yeung C., Criales M.M., Lee T.N. 2000. Unusual larval abundance of *Scyllarides nodifer* and *Albunea* sp. in the Florida Keys during the intrusion of low salinity Mississippi flood water in September, 1993. *Journal of Geophysical Research* 105(C12): 28741–28758.
- [Young et al., 2012] Young C.M., He R., Emlet R.B. Li Y., Qian H., Arellano S.M., Van Gaest A., Bennett K.C., Wolf M., Smart T.I., Rice M.E. 2012. Dispersal of Deep-Sea Larvae from the Intra-American Seas: Simulations of Trajectories using Ocean Models. *Integrative and Comparative Biology* 52(4), 483-496.
- [Xu et al., 2011] Xu, K., C.H. Harris, R.D. Hetland, J. N. Kaihatu 2011. Dispersal of Mississippi and Atchafalaya sediment on the Texas-Louisiana shelf: Model estimates for the year 1993, *Cont. Shelf Res.*, 31, 1558-1575.
- [Zhang and Hetland, 2012] Zhang, Z., Hetland, R.D. 2012. A numerical study on convergence of alongshore flows over the Texas-Louisiana shelf, *Journal of Geophysical Research* 117, C11010.
- [Zhang et al., 2012] Zhang, X., Hetland, R.D., Marta-Almeida, M., DiMarco, S.F. 2012. A numerical investigation of the Mississippi and Atchafalaya freshwater transport, filling and flushing times on the Texas-Louisiana Shelf, *Journal of Geophysical Research* 117, C11009.
- [Zlotnicki, 1991] Zlotnicki V. (1991). Sea level differences across the Gulf Stream and Kuroshio Extension. *Journal of Physical Oceanography* 21(4): 599-609.